Ultra-High-Throughput Single-Cell Functional Screening by Combination of Microfluidics and GMD-FACS

Yanakieva, Desislava

(2020)

Ultra-high-throughput single-cell functional screening by combination of microfluidics and GMD-FACS

TECHNISCHE UNIVERSITÄT DARMSTADT

Vom Fachbereich Chemie
der Technischen Universität Darmstad

zur Erlangung des akademischen Grades eines
Doctor rerum naturalium (Dr. rer. nat)

genehmigte

Dissertation

von

M.Sc. Desislava Georgieva Yanakieva
aus Varna, Bulgarien

Referent:	Prof. Dr. Harald Kolmar
Korreferent:	Prof. Dr. Siegfried Neumann

Darmstadt 2020

Yanakieva, Desislava: Ultra-High-Throughput Single-Cell Functional Screening by Combination of Microfluidics and GMD-FACS

Darmstadt, Technische Universität Darmstadt,

Jahr der Veröffentlichung der Dissertation auf TUprints: 2020

URN: urn:nbn:de:tuda-tuprints-134645

Tag der mündlichen Prüfung: 27.07.2020

Die vorliegende Arbeit wurde unter der Leitung von Herrn Prof. Dr. Harald Kolmar am Clemens-Schöpf-Institut für Organische Chemie und Biochemie der Technischen Universität Darmstadt von Oktober 2016 bis Juni 2020 angefertigt.

„Die Wissenschaft versucht ständig, die Natur zu entzaubern –

sie merkt nicht, dass dieser Zauber Realität ist."

Klaus Ender, 1939

Publications derived from this work:

Yanakieva D*, Elter A, Bratsch J, Friedrich KH, Becker S, Kolmar H (2020). FACS-Based Functional Protein Screening via Microfluidic Co-encapsulation of Yeast Secretor and Mammalian Reporter Cells. *Scientific Reports* 10(1),10182.

Further publications during PhD thesis:

Bogen JP*, Storka J*, **Yanakieva D**, Fiebig D, Grzeschik J, Hock B, Kolmar H (2020). Isolation of common light chain antibodies from immunized chickens using yeast biopanning and fluorescence-activated cell sorting. Submitted at *Biotechnology Journal*

Grzeschik J*, **Yanakieva D*,** Roth L, Krah S, Hinz SC, Elter A, Zollmann T, Schwall G, Zielonka S, Kolmar H (2019). Yeast surface display in combination with fluorescence-activated cell sorting enables the rapid isolation of antibody fragments derived from immunized chickens. *Biotechnology Journal*, *14*(4), 1800466.

Schneider H*, **Yanakieva D**, Macarrón A, Deweid L, Becker B, Englert S, Avrutina O, Kolmar H (2019). TRAIL-Inspired Multivalent Dextran Conjugates Efficiently Induce Apoptosis upon DR5 Receptor Clustering. *ChemBioChem*, *20*(24), 3006-3012.

Schneider H*, Deweid L, Pirzer T, **Yanakieva D**, Englert S, Becker B, Avrutina O, Kolmar, H. (2019). Dextramabs: A Novel Format of Antibody-Drug Conjugates Featuring a Multivalent Polysaccharide Scaffold. *ChemistryOpen*, *8*(3), 354-357.

Hilberg V*, Avrutina O, Ebenig A, **Yanakieva D**, Meckel T, Biesalski, M, Kolmar H. (2019). Light-Controlled Chemoenzymatic Immobilization of Proteins towards Engineering of Bioactive Papers. *Chemistry–A European Journal*, *25*(7), 1746-1751.

Deweid L*, Neureiter L, Englert S, Schneider H, Deweid J, **Yanakieva D**, Sturm J, Bitsch S, Christmann A, Avrutina O, Fuchsbauer HL, Kolmar H (2018). Directed Evolution of a Bond-Forming Enzyme: Ultrahigh-Throughput Screening of Microbial Transglutaminase Using Yeast Surface Display. *Chemistry–A European Journal*, *24*(57), 15195-15200.

Könning D*, Rhiel L, Empting M, Grzeschik J, Sellmann C, Schröter C, Zielonka S, Dickgießer S, Pirzer T, **Yanakieva D**, Becker S, Kolmar H (2017). Semi-synthetic vNAR libraries screened against therapeutic antibodies primarily deliver anti-idiotypic binders. *Scientific reports*, *7*(1), 1-13.

*first authors are marked with an asterisk.

Table of Content

Zusammenfassung und wissenschaftlicher Erkenntnisgewinn

Biopharmazeutika sind potente Medikamente, welche häufig in zielgerichteten Therapien eingesetzt werden. Sie weisen bemerkenswerte Spezifitäten und geringe Nebenwirkungen auf, Aspekte, die unter anderem für die Behandlung von Autoimmunkrankheiten und Krebs von großer Relevanz sind. Allerdings stellen die Generierung und die aufwendige funktionelle Validierung von neuen Molekülen heutzutage immer noch einen Engpass in dem Entwicklungsprozess von neuen biopharmazeutischen Medikamenten dar. Die Durchführung von funktionellen Assays in einem frühen Entwicklungsstadium wäre von großem Vorteil für die Identifizierung von neuen potenten Medikamenten und möglicherweise neuartigen Therapieansätzen. Dennoch sind klassische phänotypische Screens in Zusammenhang mit Proteinbibliotheken mit hoher Diversität limitiert durch den niedrigen Durchsatz der Funktionalitätsbestimmung und der erforderlichen Expression und Aufreinigung jedes einzelnen Wirkstoffkandidaten.

Ziele dieser Arbeit waren die Etablierung und Validierung eines neuen generischen Verfahrens für die direkte Selektion funktioneller Proteinvarianten mit vorgeschriebener biologischer Wirkweise in einem Ultra-Hoch-Durchsatz Prozess. Für diesen Zweck wurden *S. cerevisiae* Hefezellen als Sekretionswirt eingesetzt, da deren hohe Transformationseffizienz und Kompatibilität zu hoch-diversen Protein Bibliotheken ein wichtiges Merkmal darstellt. In Kombination mit den Hefezellen wurden Säugertier Reporterzellen verwendet, um aktivitätsabhängige fluoreszente Signale, welche auf einen erwünschten Wirkmechanismus hinweisen, zu erhalten. Diese Strategie bildet die Grundlage einer neuen Selektionsplattform, welche die Dursuchung einer hohen Anzahl verschiedener Proteine nach gewünschter biologischer Funktion ermöglicht. Die Kompartimentierung eines Gemisches aus Hefe- und Reporterzellen resultiert in Mikroreaktoren, in denen eine Phänotyp-Genotyp Kopplung gewährleistet ist. Durch das geringe Volumen, welches sich im Picoliter Maßstab bewegt, findet eine schnelle und effiziente Akkumulation von sekretierten bioaktiven Molekülen statt. Durch den Einsatz mikrofluidischer Verfahren können beide Zelltypen schnell und hoch-präzise in Mikrotröpfchen verpackt werden. Hydrogel-bildendende Polymere ermöglichen die Erzeugung von uniformen kugelähnlichen Mikroreaktoren, welche sowohl Hefe- als auch Reporterzellen in sich tragen. Diese Strategie macht das System kompatibel mit Ultra-Hoch-Durchsatz Fluoreszenz-aktivierter Zellsortierung und ermöglicht den Einsatz von herkömmlichen kommerziell erhältlichen Sortiergeräten zur Durchmusterung von Protein-Bibliotheken mit hoher Diversität.

Der erste Teil dieser Arbeit befasst sich mit der Generierung von Hydrogel-Mikroreaktoren. Drei verschiedene Hydrogel-bildende Matrizes und Polymere wurden getestet und die Mikroreaktoren-Generierung sowie die Gellierungs-Konditionen wurden optimiert. Darauffolgend wurden die Lebensfähigkeit und die Aktivierung der Säugertier Reporterzellen unter diversen Bedingungen und unter Verwendung der drei verschiedenen Polymere untersucht. Kultivierungsbedingungen wie das verwendete Zellkulturmedium, die Kultivierungstemperatur und die Rotationsgeschwindigkeit während der Kultivierung wurden umfassend getestet und miteinander verglichen um optimale Bedingungen für beide Zellspezies (Hefe und Säugerzellen) zu identifizieren.

Der zweite Teil der Forschungsarbeit fokussierte sich auf die Validierung des Konzepts. Immortalisierte Maus B-Zellen wurden zusammen mit Zytokin-sekretierenden Hefezellen als Modell für erste funktionelle Selektionsversuche eingesetzt. In einer Reihe von Mischungsexperimenten wurden Hefezellen, welche ein

biologisch aktives Zytokin sekretierten in verschiedenen Verhältnissen mit einem Überschuss an Hefezellen gemischt, welche eine nicht-funktionelle Zytokin-Mutante sekretierten. Durch den Einsatz von Ultra-Hoch-Durchsatz Fluoreszenz-aktivierter Zellsortierung konnten Mikroreaktoren isoliert werden, welche eine durch ein biologisch funktionelles Zytokin aktivierte Reporterzelle beinhalteten. Dieser Prozess führte zu einer schnellen und effizienten Anreicherung von Hefezellen, die das biologisch aktive Zytokin sekretieren. Diese ersten Erfolge gewährten einen Einblick in die Stärken und Schwächen dieses Verfahrens und warfen Licht auf die vielen verschiedenen ausschlaggebenden Faktoren, welche unumgänglich sind, um eine robuste und zuverlässige Selektionsplattform zu etablieren.

Der letzte Abschnitt der Arbeit ist der Implementierung des Verfahrens zur Selektion agonistischer Antikörper gewidmet. Dazu wurde die T-Zell Aktivierung durch anti-CD3 Antikörper mithilfe einer immortalisierten T-Zell Reporterzelllinie nach Verkapselung in Mikroreaktoren untersucht. Im Zuge der Arbeiten hatte sich die Menge an durch die *S. cerevisiae* Hefezellen sekretiertem anti-CD3 Antikörper als zu niedrig herausgestellt. Dies resultierte in einer unzureichenden T-Zell Aktivierung, sowohl unter Standard-Zellkulturbedingungen, als auch in den miniaturisierten Mikroreaktoren. Aus diesem Grund wurde eine Adaptierung des Systems vorgenommen, um den Einsatz eines alternativen Sekretionswirtes, welcher besser für die Sekretion von großen und komplexen Molekülen wie Volllängen Antikörpern geeignet ist, zu ermöglichen. Dies wird als Teil eines Postdoktoralen Forschungsprojektes weiterbearbeitet.

Diese Arbeit liefert eine methodische und konzeptionelle Grundlage für die weitere Entwicklung und möglicher Etablierung einer generischen Plattform zur Identifizierung und Selektion von Biomolekülen mit angestrebten biologischen Funktionen. Das bearbeitete Konzept hat sich als geeignet für die funktionale Durchmusterung Hefe-basierter Bibliotheken erwiesen und besitzt das Potential, die Entwicklung von neuen maßgeschneiderte Biopharmazeutika mit definiertem biologischem Wirkmechanismus, wie z.B. Zytokine, zell-penetrierende oder agonistische Antikörper, zu beschleunigen.

Scientific Novelty and Significance

Biologics in targeted therapies often demonstrate remarkable safety and specificity, especially in case of autoimmune diseases and cancer. However, the discovery of novel molecules and the necessary functional validation still represent a bottleneck in the development of novel biopharmaceuticals. Implementation of functional assays in an early drug-discovery stage appears highly beneficial for the discovery of new potent biologic drugs or even first-in class medicines. Nevertheless, the low throughput and the need of individual expression and purification of the tested candidates, limit the applicability of the classical phenotypic screens for high-diversity protein libraries.

Aim of this work was the establishment and validation of a novel generic functional screening approach for selection of protein variants with desired biological function in an ultra-high-throughput manner. This new process is based on the combination of a *S. cerevisiae* secretion host, capable of high transformation efficiencies and compatible with high-diversity protein libraries, with a mammalian-based reporter system for activity-dependent fluorescence readout of functional molecules. This strategy represents the base of a straightforward selection platform for testing a high number of different protein molecules for desired biological function. Compartmentalization of the secretor and reporter cells in distinct microreactors enables phenotype-genotype coupling while miniaturization of the test assays to volumes in the picolitre range brings the advantage of rapid biochemical reactions by fast accumulation of secreted molecules. Microfluidic-assisted encapsulation of the two cell types supports the generation of microdroplets with high speed and precision and implementation of hydrogel-forming polymers enables the recovery of uniform hydrogel microbeads surrounding the encapsulated cells. This strategy makes the system compatible to ultra-high throughput fluorescence-activated cell sorting on a commercially available device and enables the screening of high diversity protein libraries.

The first part of the work assessed the generation of hydrogel microbeads using different emulsification techniques. Three different hydrogel-forming matrixes and polymers were tested and droplet generation, as well as gelation conditions were optimised. Next, mammalian reporter cell viability and activation were examined under diverse conditions in hydrogel microbeads consisted of the three different polymers. Cocultivation conditions like culture medium, culture temperature, and rotation speed, were extensively tested and compared in order to identify conditions compatible with both species (*S. cerevisiae* and mammalian cells).

The second part of the research was focused on validating the concept by conducting a proof-of-concept functional screening using a model secretor-reporter system. By means of mixing experiments of yeast cells secreting a biologically active cytokine with an excess of yeast cells secreting a non-functional mutant variant, the successful and efficient enrichment of biologically active variants following our novel functional selection approach was proven. These experiments gave insights into the strengths and limitations of the method and revealed which factors play a decisive role for a robust and reliable selection platform.

The last part of the work was dedicated to implementation of the functional screening approach for selection of agonistic antibodies. By utilizing an immortalized T cell reporter cell line, T cell activation by anti-CD3 antibodies was examined after compartmentalization into microdroplets. However, the amount of secreted full-length anti-CD3 antibody from *S. cerevisiae* cells was too low and was insufficient to induce reporter cell activation both in

standard cell culture and in miniaturized microdroplets. Therefore, adaptation of the system towards an alternative secretion host, more appropriate for secretion of large and complex molecules like full-length immunoglobulins, was envisaged and will be performed in the scope of a post-doctoral research.

In summary, this work provides a methodical and conceptional basis for the development of a generic platform for discovery and selection of biomolecules with desired biological function. A comprehensive investigation of the effects of microfluidic co-encapsulation of living organisms from two distinct kingdoms was performed, giving insides into critical aspects like culturing conditions, which determine limiting factors like cell viability and protein expression and secretion. The strategy has proven suitable for functional screening of yeast-based libraries and has the potential to enable and accelerate the discovery of new functional biologics, including cytokines, agonistic or internalizing antibodies.

1. Introduction

Historically, drug discovery and development dates back to the juvenility of human civilization. In ancient times, remedies were derived mainly from plant or animal products in form of ointments or potions and were most probably discovered through a trial-and-error experimentation[1]. Centuries of development and refinement led to the development of medicinal substances[2], but it was not until the 1800s when the drug discovery started to follow scientific techniques[3], beginning with the chemical isolation of active ingredients from plants (morphine from opium[4], quinine from cinchona bark[5], cocaine from coca leaves[6] and many more). While in the 20th century, diseases were mainly controlled by small molecule-based medicines, with antibiotics being in the forefront[2], the discovery of the DNA structure and function by Watson and Crick in 1953[7] set a new milestone in the pharmaceutical research and gave rise to modern molecular biology[8]. Combined scientific progress in the fields of biochemistry and molecular biology in the late 20th century enabled the development of the first biological drug - recombinant human insulin (Humilin®), which reached the pharmaceutical marked in 1982[9]. Since then, the development of biologics (also called biopharmaceuticals) has become a focus of interest, opening the door to novel treatments with superior safety and specificity especially in case of autoimmune diseases[10] and cancer[11]. Nowadays, the biologics represent a significant part of the medical arsenal with 17 novel biopharmaceuticals approved in 2018 by the FDA (US Food and Drug Administration) from a total of 59 new drugs[12] and a continuous growth of the biologics market, predicted to reach nearly 400 billion USD/year by 2025[13].

1.1. Biologics: Definition and Classification

Biological medicines represent a heterogenous class of drugs, which according to EMA's (European Medicines Agency) definition "contain active substances from a biological source, such as living cells or organisms (human, animals, and microorganisms such as bacteria or yeast)"[14]. Vaccines, antitoxins, somatic cells, blood products, gene therapy, tissues, peptides and a broad range of recombinant therapeutic proteins (hormones, enzymes, cytokines, antibodies) represent the main entities which fall in the category of biopharmaceuticals up to date[15]. Due to their biological origin, those medicines often represent complex mixtures consisting of sugars, proteins, or nucleic acids or combinations of all those, making the characterization of the final product not trivial. Further characteristics, differing biologics from conventional small molecule drugs, are the higher molecular size, light and heat sensitivity, aggregation and degradation behaviour, which could affect the shelf life time of the products and, thus, often increase the final price of the medicines[16]. Nevertheless, together with higher complexity, the biologics bring advantages over conventional drugs, by exhibiting higher selectivity and potent therapeutic efficacy, paired with limited side effects. Today, biopharmaceuticals represent the cutting-edge of biomedical research and have the potential to offer not only novel treatment but also cure for a variety of challenging diseases.

1.2. Discovery and Development of Biologics

The biologics market is up to date dominated by monoclonal antibodies (mAbs) and other recombinant proteins (Fig. 1). Generation of monoclonal antibodies was first established in 1975 by Köhler and Milstein by hybridoma technology[17], enabling for first time *in vivo* antibody application as therapeutics. In the past decades, variety of antibody discovery platforms have been developed, which can be broadly divided into three categories: *in vivo*, *in vitro*, and *in silico* technologies.

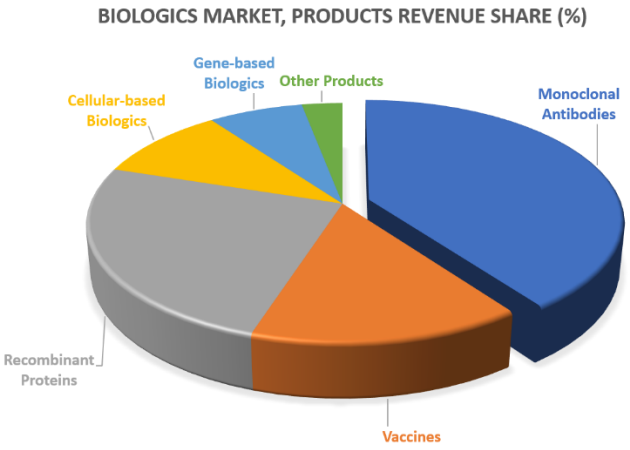

Figure 1. Global biologics market share of different biopharmaceutic products in 2018[18]. Graph modified from https://www.mordorintelligence.com/industry-reports/biologics-market, accessed on 23.03.2020.

1.2.1. *In vivo* antibody discovery technologies

Hybridoma technology opened up the field of therapeutic antibody development. In the process of hybridoma generation, mice are immunized with the target molecule. Based on the *in vivo* humoral immune response of the animals, followed by natural antibody maturation processes in lymphoid organs, B cells producing highly specific and affine murine antibodies are stimulated to expand and differentiate to plasma cells, which represent the antibody-secreting reactors of the organism[19]. After sufficient immunogenic response, the maturated B cells are isolated from the spleen of the host animal and fused with myeloma cancer cells to generate immortalized hybridoma cell lines. Important factor in this step is to ensure monoclonality of the resulting cell lines, which is crucial for the following selection process. Generated hybridomas are then subjected to multiple rounds of screening and selection for isolation of mAbs with desired target specificity and affinity[20, 21]. Standard screening procedure is microplate-based antigen-immobilized enzyme-linked immunosorbent assay (indirect-ELISA)[22]. In this approach, the target molecule (antigen) is immobilized on the surface of a microtiter plate, culture supernatant of the different hybridoma cell lines is incubated in the wells in different dilutions and after washing steps, the antigen-bound monoclonal antibodies are detected using enzyme-conjugated (e.g. peroxidase) detection antibodies, where a chemical substrate is converted to a chromophore (a molecule with specific colour and absorption). Although this procedure has been successfully implemented, delivering the first approved mAb on the market – muromonab[23], direct use of murine antibodies for human therapy resulted in immune response

against the drug (human anti-mouse antibodies or HAMAs) leading to rapid clearance of the murine antibodies[24]. This shortcoming of murine antibodies shifted the focus into the development of less immunogenic biologics by genetic engineering humanization strategies, giving rise to second-generation chimeric (rituximab[25]) and humanized (trastuzumab[26]) mAbs. In order to surpass the need of additional humanization of the isolated murine mAbs (resulting often in much lower antibody affinity than the parental antibody[27]) , the current state-of-the art is to use transgenic host animals for the immunization, where the rodent immunoglobulin genes are replaced with those from human repertoire, leading to formation of fully human antibodies[28].

1.2.2. *In vitro* antibody discovery technologies

Another approach for the production of fully human antibodies representing alternative to animal immunization, is implementation of *in vitro* display platforms like phage display[29], yeast surface display[30], bacterial[31], or ribosome display[32] for generation and screening of combinatorial antibody libraries. These libraries can be derived from immune human individuals, or contain the complete naïve human repertoire. For this purpose, the antibody heavy and light chain repertoire is obtained from mRNA from B lymphocytes, reverse transcribed to cDNA and the variable domains (for heavy (VH) and light (VL) chains) are randomly recombined to form antibodies or antibody fragments (single chain variable domain (scFv) or fragment antigen binding (Fab))[33]. Additionally, combinatorial libraries can be selectively mutated or randomized, generating semi-synthetic antibody libraries with diversity beyond the scope of the immune system, which enhances the probability of isolating antibodies with desired properties significantly[34]. While immune libraries usually have sizes in the range of 10^8 clones, naïve libraries must be bigger than 10^9 in order to compensate for the fact that no affinity maturation and expansion of antigen-specific clones has occurred[35]. Nowadays, antibody libraries with sizes of over 5 x 10^{10} for phage display[34-36] and up to 10^9 for yeast surface display[37] are standard.

In case of phage display, antibodies or antibody fragments are expressed and presented on the surface of phage particles by genetic fusion to one of the coat proteins of filamentous bacteriophage. The most common screening strategy is based on biopanning in multiple rounds, where in similar to ELISA manner, the target molecules are immobilized on the surface of 96-well polystyrene microtiter plates. Subsequently, the phage library is incubated in the microplate wells and the non-binding phages are washed away. Bound phages are eluted and amplified by infection of bacteria (mostly *E. coli*) and the cycle is repeated several times with increased selection stringency by more extensive washing steps to enable isolation of high-affinity phages. At the end, enriched clones are analysed by DNA sequencing, reformatted for mammalian expression as full-length antibodies and target binding and functionality are further characterized[38, 39].

Cloning of variable antibody genes could also easily be performed for the generation of yeast surface display (YSD) libraries. For this purpose, antibody genes are genetically fused N- or C-terminally to a cell wall anchor protein (e.g. Aga2p). Commonly, homologous recombination in *S. cerevisiae* yeast is implemented as cloning strategy, resulting in generation of large YSD libraries[40]. Following protein expression induction, the Aga2p-fused library is secreted by the yeast cells and displayed on the cell surface through a disulfide bond formation between Aga2p and Aga1p domains of the α-agglutinin mating system[41]. In comparison with other display formats, YSD offers several advantages like comparability to fluorescence-activated cell sorting (FACS), where real time selection monitoring and quantitative measurements of equilibrium binding constants, stability and

specificity is possible, without soluble protein expression necessary[42]. Furthermore, yeast cells represent a eukaryotic expression system capable of incorporation of post-translational modifications like glycosylation. Implementation of protein tags on the displayed molecules enables normalization of the ligand binding to the surface expression levels, thus selection of variants exhibiting simultaneously high expression levels and high affinity is possible[41].

Common in all *in vitro* surface display platforms is the phenotype-genotype coupling, ensured by the display host which carries either the DNA (phage, yeast, bacteria) or the mRNA (ribosome) code of the enriched variants. This feature enables high-throughput selection of the display hosts either by biopanning (phage, ribosome) or by FACS (yeast) and has resulted in the generation of numerous diagnostic and therapeutic antibodies[43-45].

1.2.3. *In silico* antibody discovery technologies

The youngest category antibody discovery approaches (third generation), is based on *in silico* computational antibody analysis and design. Computational antibody design is a complex process and involves different methods and approaches like structure and energy-based modelling, combinatorial design and machine learning. Among optimization of antibody affinity and/or physicochemical properties, these techniques enable also *de novo* antibody design, where structure and antigen-antibody complexes are modelled using a set of different algorithms (e.g. OPTCDR, AbDesign, RosettaAntibodyDesign)[46]. Current advances in next generation sequencing (NGS) of whole immunoglobulin repertoires (Ig-seq), enabled the generation of huge databases containing multiple Ig-seq datasets, representing enormous diversity of naturally occurring antibody variants. These databases build the base of antibody model libraries, where *in silico* high-throughput screenings with different targets can be performed and binding interactions (docking) between the antigen of interest and antibody variants is predicted. Furthermore, these antibody model libraries are used also for developability prediction by assessment of residues charge, hydrophobicity, or loops length[47]. Although *in silico* antibody design has emerged as essential part of the discovery and development process of novel antibodies, computational methods are unlikely to replace the entire experimental process. Nevertheless, they represent cost-efficient analysis and optimization tools for guiding the experimental procedures and development of the lead antibodies[48].

1.3. Functional Antibodies

In the context of disease therapy, antibodies exhibit diverse mechanisms of action. Natural antibody functions like neutralization, antibody-dependent cell-mediated cytotoxicity (ADCC), complement-dependent cytotoxicity (CDC), and antibody-dependent cellular phagocytosis (ADCP) involve a complex interplay of the immune system for defence against pathogens and toxins, and are exploited by the majority of marketed therapeutic antibodies[49]. Additionally, antibodies have emerged as suitable tools for regulation of cellular processes by modulation of signalling pathways[50]. Inhibition of overactivated growth factor pathways in cancer cells can limit tumour progression and angiogenesis, and prevent metastasis[51-53]. However, in many cases cancer resistance against neutralizing and blocking antibodies can be observed, due to signal compensation by alternative cellular pathways[54]. Next generation antibody therapeutics (antibody-drug conjugates, radioimmunoconjugates bispecifics, multispecifics, BiTEs etc.) aim at surpassing the limitations of a conventional antibody format, either by combination of the antibody target specificity with tumour killing by potent chemotherapeutics[55] or radioisotopes[56], or by immune system modulation by T cell engagement[57].

1.3.1. Blocking antibodies for therapy

Neutralizing antibodies intercept antigens like allergens, viruses, and toxins and thereby negate downstream cellular effects like cell infection, chemotaxis or cell death. This mode of action has been exploited for therapy of infectious viral diseases (palivizumab[58]), cancer (bevacizumab[59], durvalumab[60]), and autoimmune diseases (adalimumab[61], infliximab[62]).

On the other side, antagonistic antibodies inhibit directly the function of its target like receptor-ligand interaction or receptor activation by multimerization and block or dampen its biological function. Multiple disease-relevant receptors have been identified and targeted by antagonistic antibodies. Examples of approved therapeutic antibodies for various indications, targeting different receptors are listed in Table 1.

Table 1. Examples for approved antagonistic antibodies used for therapy [63].

Antibody	*Target*	*Indication*
*Ipilimumab (*Yervoy®*)*	Cytotoxic T-lymphocyte-associated Protein 4 (CTLA4)	Melanoma
*Cetuximab (*Erbitux®*)*	Epidermal Growth Factor Receptor (EGFR)	Colorectal cancer, head and neck cancer
*Pertuzumab (*Perjeta®*)*	Human Epidermal Growth Factor Receptor 2 (ERBB2/HER2)	Breast cancer
*Nivolumab (*Opdivo®*)*	Programmed Cell Death Protein 1 (PD1)	Melanoma, Hodgkin lymphoma, NSCLC and others
*Olaratumab (*Lartruvo®*)*	Platelet-Derived Growth Factor Receptor A (PDGFRα)	Soft tissue sarcoma
*Natalizumab (*Tysabri®*)*	Integrins ($\alpha_4\beta_1$ and $\alpha_4\beta_7$)	Multiple sclerosis and Crohn's disease
*Daclizumab (*Zinbryta®*)*	Interleukin 2 Receptor (IL-2R)	Multiple sclerosis

1.3.2. Agonistic antibodies for therapy

Opposite to receptor blocking, agonistic antibodies induce cellular pathway cascades by interaction with its target receptor in a manner that mimics binding of the native ligand. Generation and development of agonistic antibodies against co-stimulatory immune cell receptors (secondary signal for activation of immune cell response) has emerged as promising strategy to target cancer cells which otherwise remain "hidden" from the immune system[64, 65]. Numerous co-stimulatory agonistic antibodies are currently undergoing clinical trials as combination therapies for diverse cancer indications mostly in advanced-stage malignancies. Promising and well-characterized targets are TNF receptor superfamily members (e.g. CD40, OX40, GITR)[66-68] and co-stimulatory B7-CD28 superfamily members (e.g. CD28 and ICOS)[69, 70]. However, scientists are facing new challenges during discovery and characterization of new agonistic molecules, due to the complexity of immune checkpoint activation mechanisms, which often demand extensive antibody structure design and novel biophysical profiles, not been necessary for other antibody therapies[65].

1.3.3. Cell-penetrating antibodies – future tools for regulation of intracellular targets

Monoclonal antibodies have empowered targeted disease therapy due to their high specificity and excellent pharmacokinetic properties. However, despite their huge success, antibodies are generally confined to the extracellular space remaining unable to penetrate cellular membranes. With a limited number of validated tumour-specific or disease-associated cell surface or soluble antigens, the target repertoire for novel mAbs is shrinking and the competition in the field is becoming very tough[71, 72]. At the same time, intracellular proteins such as enzymes, transcription factors, or proteins involved in signal pathways, are becoming attractive drug targets. Although the intracellular space has been so far reserved by small molecule drugs, which in most cases are capable of free diffusion through cellular membranes, many intracellular targets have been considered undruggable by small molecules due to large flat contact areas in the active centres or protein interaction sites where specific inhibition by chemical molecules is not possible[73]. Oncoproteins like c-Myc and Ras[74, 75] or intracellular immune checkpoints[76] represent some examples for promising intracellular antibody targets. Diverse strategies for intracellular antibody delivery have been extensively studied, however the majority of them have not passed the proof-of-principle or preclinical research stage, yet[77].

Whereas cellular internalization can be achieved by specific binding of antibodies to cell surface receptors (receptor-mediated endocytosis), in this case the antibodies remain entrapped in enclosed intracellular vesicles (endosomes) where they are either subjected to degradation (lysosomes), recycling, or transcytosis (transport to the other side of the cell)[78]. Since the majority of potential therapeutic targets are located either in the cytoplasm or in the nucleus (e.g. transcription activators), cytosolic antibody delivery represents a high in-demand branch in antibody development and engineering. Chemical modification of antibodies (e.g. conjugation of membrane transport peptides[79] and cell-penetrating peptides (CPPs)[80] or conjugation of phosphorothioated DNA oligonucleotides[81]), as well as utilization of lipid-based[82], polymer-based[83], inorganic[84], or virus-like nanocarriers[85] are examples for some of the most extensively studied intracellular antibody delivery approaches up to date. Additionally, natural autoantibodies occurring in some autoimmune diseases like systemic lupus erythematosus[86] and multiple sclerosis[87] have been observed to penetrate cytoplasm of living cells and even accumulate in the nucleus[88]. Such autoantibodies have been used as vehicles for the delivery of

different payloads like nanoparticles[89] and proteins[90]. Nevertheless, natural anti-DNA autoantibodies lack cell specificity and often have cytolytic or cytotoxic effects. In order to address these problems, engineered cytosol-penetrating antibodies (cytotransmabs) were generated by substitution of the variable domains (VL) of two approved therapeutic antibodies (adalimumab and bevacizumab) by a humanized VL from a mouse-derived lupus autoantibody (hT4)[91]. Both engineered antibodies demonstrated cytosolic penetration, however the antigen specificity of the parental therapeutic antibodies was lost. Instead, the cytotransmabs interacted with ubiquitously expressed heparan sulfate proteoglycans (HSPGs) on the cell surface and following endocytosis, dissociated from HSPG in the acidified endosomes. In the endosomal escape mechanism, proposed by the authors, conformational changes in the cytotransmab structure take place upon endosome acidification (pH 5.5-6.5) and lead to formation of endosomal pores, enabling the release of the cytotransmabs in the cytoplasm[92]. Further engineering of the cell-penetrating antibody moiety (hT4) reduced the interaction of the cytotransmabs with HSPGs (which previously has rendered the cytotransmabs unspecific) and grafting of the endosomal escape motif $W_{92}Y_{93}W_{94}$ on the VH resulted in enhanced endosomal escape efficiency[93].

With recent advances in the development of multispecific antibody formats[94], grafting of endosomal escape motifs from autoantibodies and/or their combination with antibody domains addressing intracellular targets becomes more attractive. However, a reliable high-throughput selection system for both efficient cytosolic penetration and functional intracellular target engagement is required for successful screening and validation of engineered cytosol-penetrating antibody formats[95].

1.4. Functional Antibody Screening

Affinity-based antibody discovery techniques (described in 1.2) stand out with high probability of finding a specific and highly affine binder and, hence, represent the approach-of-choice (also called “target-based approach”) in most antibody discovery campaigns nowadays. However, antibody discovery in this case often stumble upon the problem of limited validated therapeutic targets, leading to extensive generation of follow-up drugs which differentiate only in the addressed epitopes, mechanisms of action, or simply are characterized by one improved property (“me better” antibodies)[96]. Alternatively, novel drugs can be identified based on their effects upon a disease-relevant model system (animal models, tissues, or cell models) in so called phenotypic or functional approach[97]. In this case no profound knowledge of the molecular target and mode of action are initially required and candidates leading to desired effects (e.g. cell death, pathway activation or inhibition) are further characterized as hit molecules. Function-based antibody discovery has the potential of engendering the development of first-in class antibody therapeutics against novel targets[72], nevertheless bottleneck in this approach represents the last step of the discovery process - target deconvolution, where the molecular target and the mode of action are identified. Furthermore, in this case extensive clinical validation of the novel targets is required, which brings along high development risk and prolonged research time frames[98]. Comparison of the discovery process following either function-based, or target-based approach is illustrated in Figure 2. : phenotypic (function-based) screening starts with the establishment of accurate disease model. Here personalized medicine can be engaged by utilizing patient-derived primary cancer cells[99]. Library screening is performed in most cases in microtiter plate formats, where high-content microscopy plays often a significant

role in the assay analysis[100]. After identification of the hits and leads with desired properties and effects, the molecular target is deconvoluted and identified using proteomics and mass spectrometry techniques[101].

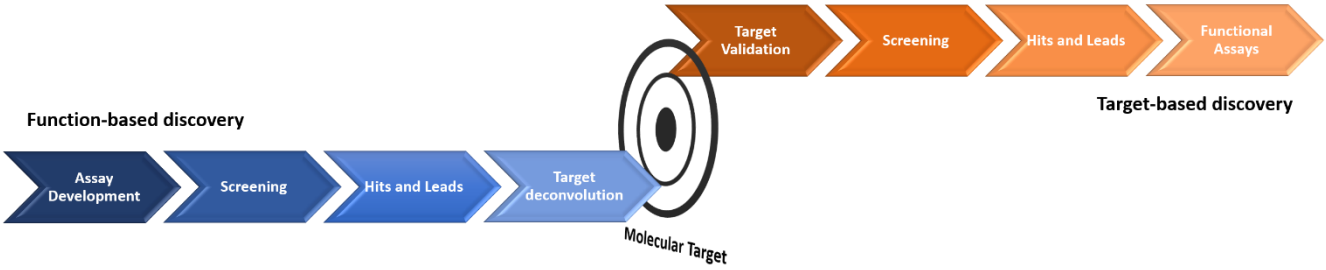

Figure 2. Function-based vs. target-based antibody discovery. Figure modified from Terstappen *et al.* 2007 [102]

The target-based discovery approach begins with the identification and validation of disease-relevant drug target. Affinity-based screening of high-diversity antibody libraries can be performed in an ultra-high-throughput manner resulting in the generation of hits which specifically recognize the target antigen. However, often secondary and tertiary screens are necessary for examination and validation of desired functions (e.g. agonistic or antagonistic properties). For this purpose, isolated antibody molecules are subjected to various functional assays, where the lead molecules are individually tested in soluble form (after expression and purification)[103]. Although target-based antibody discovery often leads to isolation of highly affine and specific antibodies against various targets, in context of *in vivo* antibody functionality (e.g. agonism) antibodies with moderate affinities sometimes demonstrate superior agonist potencies than higher-affinity molecules[104, 105]. Thus, implementation of functional screens in an earlier selection phase could be beneficial for more precise isolation of lead molecules with desired functionalities. For this purpose, new more holistic approaches need to be established which, depending on the existing experimental models and disease information, incorporate both discovery models.

1.5. High-Throughput Functional Screening

Since the size of antibody libraries almost always extends those of chemical small-molecule libraries by multiple orders of magnitude[106, 107], screening techniques with huge success in small-molecule phenotypic screening (e.g. high-content microscopy, multiplexed flow cytometry[108]) face limitations regarding the throughput of the phenotypic assays. As functionality of biologics is mediated by complex protein-protein interactions[109], cell internalization[110], receptor clustering[111], or effector cell interactions (CDC, ADCC)[112], functional validation of antibody variants derived by target-based screening is similarly mainly conducted *in vitro* in multi-well plate formats using mammalian cell cultures. This assays often require individual expression and purification of all candidates in soluble form. The following section describes and compares the most promising strategies up to date for increasing the throughput of *in vitro* cell-based functional assays.

1.5.1. High-content screening technologies

Multicolour fluorescence microscopy is one of the most powerful tools to analyse spatiotemporal events in biological systems[113]. Image-based analysis of intracellular events and cellular morphology has been broadly implemented for defining the functions of genes, proteins and other biomolecules and for the early drug discovery in the context of high content screening (HCS) of small molecules[114]. Modern HCS platforms integrate automated cell-sample preparation, fluorescent labelling, image acquisition, image processing and image analysis by a combination of sophisticated hardware and software components. Automated microscopes with improved auto-focusing and sample positioning, together with artificial intelligence (AI)-based algorithms (machine learning, neural networks) enable the generation and management of huge image data sets[113]. Big advantage of the latest HCS platforms is that they permit quantitative analysis of the phenotypes of single living cells by cell segmentation algorithms, simultaneously combining observations of multiple parameters like cellular morphology, protein expression, localization and post-translational modifications[115]. The dramatic progress in the software field enabled the handling and analysis of huge data sets, as well as advanced data mining, modelling and prediction. Nonetheless, the bottleneck of HCS platforms remains the throughput of the image acquisition and processing which is performed by the hardware components (confocal microscopes). Up to date most of the commercially available devices support only 96- and 384-well plate formats[116], which are not suitable for screening of high diversity libraries within the scope of phage or yeast surface display.

1.5.2. High-throughput microtiter plate formats

Since functional validation of hit molecules, derived from various screening campaigns, is a crucial step for the generation of new drug candidates, high-throughput screening (HTS) in microtiter plate formats has undergone a developmental revolution[117]. Adopted from standard methods for screening of small-molecule libraries where extensive robotics optimization enabled assay miniaturization in 384- and 1536-well formats, HTS approaches are now combined with new molecular biology methods and protein-expression technologies increasing the applicability for screening of biopharmaceuticals from protein libraries[118]. Sole HTS protein screening consists of three main stages: generation of cDNA library encoding all protein variants, expression of the DNA library to individual functional proteins, and screening for therapeutically relevant molecules in a suitable assay[117]. Furthermore, HTS is often applied as subsequent secondary and tertiary screens after ultra-high-throughput screening *via* phage or yeast surface display[119]. In contrast to high-content phenotypic screening (described above), HTS is a target-based approach which precisely focuses on single mechanism of action (biochemical or cell-based assays). Biochemical assays can be based on enzyme/substrate reactions, protein-protein interactions, or more complex *in vitro* transcription systems[120]. Substituting cell-based systems by biochemical assays permits in some setups sample miniaturization to assay volumes of 1-2 µL (3456-well microplates), which complies to screening of >100,000 variants per day in an ultra-high-throughput manner. However technical hurdles like liquid dispensing and sample evaporation often compromise the validity and reproductivity of such assays[121].

1.5.3. Assay miniaturization techniques

Miniaturization of functional assays for drug discovery and validation is highly desirable in order to accelerate the screening process and to reduce the associated costs. Reduced quantity of biological and chemical reagents used per sample enables higher assay throughput without massive increase of the material costs and at the same time sample parallelization permits the implementation of multiple detection modes. However, important for all miniaturization strategies is to ensure the stability of all assay components over the time course of the reactions and to exclude impact by the implemented automation devices (e.g. dispensers or readers)[122]. Miniaturization processes can be divided in three different scales:

(1) mini-scale: several mm, corresponding to volumes in the µL range;
(2) micro-scale: 50 µm to a few mm with sample volumes in the range of 10 nL to few µL;
(3) nano-scale: 1 µm – 50 µm, sample size < 10 nL[123].

Assay development has split up in two main miniaturization approaches: batch-based systems (microplate, microarray, and nanoarray formats) and continuous, flow-based systems (lab-on-a-chip, microfluidic devices, and lab-on-valve (LOV))[122].

Microplate assays remain the most frequently used format, due to their easier handling, low costs, and simpler assay adaptation. However, as commercially available microtiter plates range from 96- to a maximum of 3456-wells[124], micro- and nanoarrays has emerged as novel analytical tools which overcome the scale and density limitations of microtiter plates by reaching densities of thousands of spots per cm^2. In the past, microarrays have been extensively used for gene expression studies *via* cDNA or RNA analysis, additionally, modern applications include protein or small-molecule library screening[125]. Microarray assays are based on immobilization of biomolecules in high density and in a defined order on glass or silicon slides, alternative materials like aluminium and gold surfaces, as well as hydrophilic polymers are also being implemented[126]. Protein microarrays have been successfully used for identification, quantitation and functional analysis of a variety of proteins, such as biomarkers and potential target molecules[127]. While earlier microarray setups were mainly based on readout by colour change (chromophores) or fluorescence (fluorophores), recently label-free detection techniques have been broadly applied. Label-free detection methods are based on measurement of changes in molecular biophysical properties like molecular weight (mass spectrometry or microcantilevers), refractive index (e.g. surface plasmon resonance), and molecular charge which occur during a biochemical reaction or interaction between the molecules in the assay. The main advantage of the label-free detection strategies is that the involved methods use only native proteins and ligands, thus, unspecific cross-reactions with detection molecules are excluded[128]. Nanoarrays are further miniaturized microarrays and have been used for highly sensitive and selective detection of molecules in trace quantities (e.g. pathogens)[129]. Although micro- and nanoarray devices can dramatically increase the throughput (over 10,000 samples per single microarray), they demonstrate several weaknesses regarding the reliability of the assays, resulting from low accuracy and precision of the automated dispensing and detection devices[122].

1.6. Microfluidic Technologies

Technical progress over the past decades in the field of microfluidics[130] has stimulated the development of a second branch of miniaturization techniques – flow-based systems. Microfluidic systems enable the control and manipulation of fluids that are geometrically constrained to the sub-millimetre scale in microchannels with wight/height dimensions between 100 nm and 10 μm[131]. Microscaling has several advantages in the context of fluidics, which have allowed one to screen for novel functionalities that were elusive for macroscale devices. By miniaturizing fluidic devices, a laminar flow regime is achieved, which is highly predictable and simpler to control than turbulent flow in macroscale devices. As surface tension, interfacial tension, and capillary forces dominate the physics of microfluidics, faster diffusion of molecules, due to smaller fluid volumes leads to much shorter reaction times[130]. Although the microfluidic discipline is still considered in its adolescence[132], it has opened new possibilities for cell-based drug screening like simultaneous testing of compounds on different cell types[133] (continuous-flow microfluidics), more accurate tissue models for disease studies and drug testing[134, 135] (3D cell culture on microchips and organ-on-a-chip), and facile generation of millions of individual microreactors with volume in the picolitre range[136] (droplet-based microfluidics).

1.6.1. Droplet microfluidics for high-throughput biological assays

Droplet microfluidics enables the encapsulation of reactants in discrete compartments by using an inert carrier fluid (usually oil) for the generation of small-volume aqueous droplets in a water-in-oil (w/o) emulsion. In contrast to continuous-flow microfluidic systems, where entire reactions take place on a microfluidic chip, droplet microfluidics allows large number of reactions without increasing the size or complexity of the microfluidic device. Thus, droplet microfluidics offers greater potential for increased throughput and scalability than other microfluidic approaches[137]. Droplet-based microfluidic devices are capable of producing monodisperse droplets with volumes in the range 0.05 pL – 1 nL (diameter 5-120 μm), which can encapsulate cells, DNA, and diverse other molecules, dissolved (or suspended) in the inner aqueous phase of the droplet[136].

Huge influence on the generation of stable aqueous droplets plays the carrier fluid (oil phase) which surrounds the droplets. The oil phase should prevent coalescence (fusion) of the droplets, it must not influence the reaction in the droplets, and should be biocompatible and permit sufficient gas permeability. Surfactants, mixed to the oil phase, stabilize the droplets and prevent coalescence by adsorbing to the oil-water interface and lowering the interfacial tension between the two immiscible phases[138]. Fluorocarbon oils are commonly preferred for biological applications using microfluidics, because they are characterized by low-viscosity and high gas permeability, which is essential for the viability of the encapsulated cells[139]. Additionally, fluorocarbon oils are biologically inert and, due to their simultaneous hydrophobicity and lipophobicity, exhibit excellent retention of reagents inside the droplets preventing cross-contamination between the drops[140, 141]. Alternatively, silicone, hydrocarbon, or mineral oils can be used, but all of them bring certain disadvantages either with respect to the viscosity of the oil or to the swelling properties of the microfluidic chip[142]. In accordance to the oil-of-choice, the appropriate surfactant should be selected. In the case of fluorocarbon oil, commercially available fluorosurfactants consist of mixtures of perflurinated polyethers (PFPE) or further modified (PEGylated) PFPE

derivatives and facilitate generation of "highly stable over a wide range of temperatures and biological conditions picodroplets"[143].

For the generation of monodispersed droplets, three different microchannel geometries (co-flow, T-junction, and flow-focusing) are most commonly used (Fig. 3).

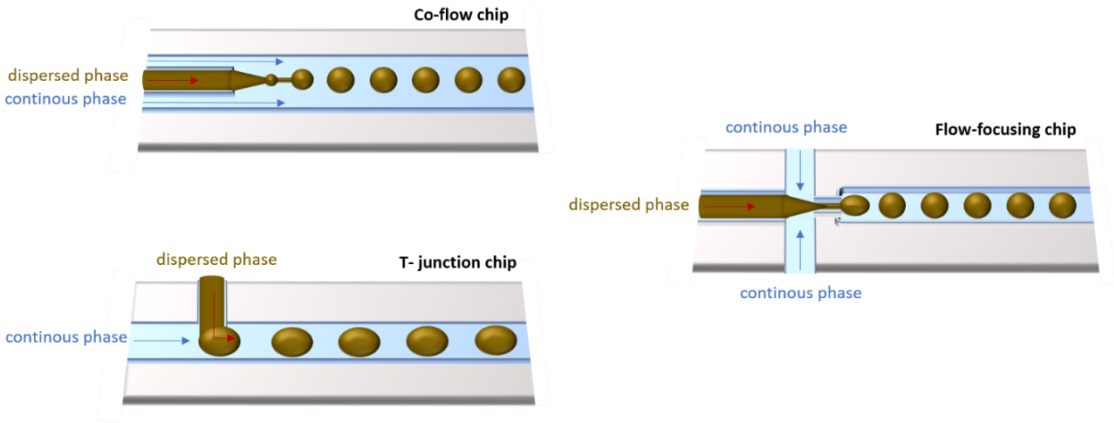

Figure 3. Microfluidic chip geometries commonly used for droplet formation. Figure modified from Damiati *et al.* 2018 [144].

In case of co-flow microfluidic chips, a small capillary for the aqueous phase (dispersed phase) is centered within a larger microfluidic channel in which the oil phase (continuous phase) is flowing. Thus, both phases are flowing in parallel directions and droplets are formed by the viscous shear of the continuous phase over the dispersed phase[142, 145]. Alternatively, the dispersed phase can be injected from a channel, which is placed perpendicularly to the continuous phase channel (T-junction). By T-junction geometry, in the majority of cases drop-formation is carried out at low capillary number (Equation 1) (surface forces >> viscous forces) of the continuous phase by a mechanism of plugging and squeezing. In this case, the pressure in the continuous phase is increased each time the tip of the dispersed phase emerges from the input channel, this leads to squeezing and pinching off droplets from the dispersed phase[146]. Due to the pressure fluctuations, which occur in the continuous and dispersed phases, the generated drops are larger than the downstream channel, hence they look spherical[142]. The third drop formation geometry is the flow-focusing device. Here, the dispersed phase is injected through one channel, while the continuous phase flows from two orthogonal directions. Similar to the T-junction, when the capillary number is low, a mechanism of plugging and squeezing takes place, resulting in big droplets. At high capillary numbers (surface forces << viscous forces) drop-formation is facilitated by viscous drag and interfacial tension[147]. Common to all three geometries is that the size of the generated droplets and the speed of droplet formation (frequency) depend on the ratio of the flow rates of the continuous and dispersed phases.

Equation 1. Capillary number [148].

$$Ca = \mu \times \frac{U}{\gamma}$$

μ (Pa s) = viscosity of the continuous phase

U (m s-1) = characteristic velocity of the continuous phase

γ (N m-1) = surface tension of the water-oil interface

Droplet microfluidics offers an efficient high throughput technology for compartmentalization of single cell populations. Single-cell analysis provides information related to differences between individual cells in a

population[149]. Since heterogeneity of individual cells in genetically identical cell populations has been an issue limiting drug response and survival by cancer treatment[150], single-cell analysis and screening has emerged as strategy to unmask differences in the responses of individual cells and to obtain deeper knowledge over the processes induced by a given compound[151]. The most common way to achieve single-cell droplet encapsulation is to use limiting dilution, where the cell density is adjusted in a way that statistically only one of ten droplets contains a single cell. The statistical distribution of the cells in the droplets follows the Poisson distribution (Equation 2). Parameters which influence the Poisson statistics in microfluidics are cell size, cell density and droplet size[148].

Equation 2. Poisson statistics [148].

$$p(k,\lambda) = \frac{\lambda^k e^{-\lambda}}{k!};$$

p = probability
k = number of particles in a droplet
λ = average number of cells per droplet

$$\lambda = \frac{\Phi_s}{\Phi_d}; \qquad \Phi_d = \frac{\bar{V}_c}{\bar{V}_d}$$

Φ_s = volume fraction of cells in the pre-encapsulation solution
Φ_d = volume fraction of a droplet containing one cell
$\bar{V}_c$ = average cell volume
$\bar{V}_d$ = average droplet volume

In case of limiting dilution λ is adjusted to 0.1 (1 of 10 droplets contains a cell), resulting statistically in a small fraction (< 0.5 %) of droplets containing more than one cell, ~9 % containing exactly one cell and over 90 % empty droplets. The trade-off of minimal droplets occupied with more than one cell, with a huge amount of useless empty droplets is in most cases not a big issue due to the fast generation of a high number of droplets. However, depending on the capability of downstream droplet sorting and assay analysis, increasing λ to 1, can be favourable, since this elevates significantly the fraction of cell-containing droplets (~37 % droplets with single cells and ~26 % droplets with more than one cell).

1.6.1. Fluorescence-activated droplet sorting (FADS)

Once encapsulated in water-in-oil droplets, the cells/reagents can be either further incubated and processed off-chip (in microtubes) or this can be performed directly on-chip by integration of delay lines[152]. Sophisticated microfluidic geometries allow for further post-emulsification manipulations, like droplet splitting[153] or addition of new reagents by droplet fusion, electrocoalescence, or picoinjection[154-157]. Together with high-throughput analysis of the assays in the microdroplets, droplet sorting enables the selection of a subset of reactions for additional manipulation[158]. Fluorescence-activated droplet sorters are custom-made microfluidic devices which incorporate fluorescence detection and a dielectrophoretic sorting unit[159]. For droplet sorting, the w/o emulsion is re-injected in the FADS device (Fig. 4) where the re-injection inlet facilitates spacing of the individual droplets by intersection with a channel for the continuous phase. The spacing junction is followed by a Y-shaped sorting junction, where droplet separation is facilitated *via* dielectrophoresis. With the help of the detection unit, passing droplets are irradiated and emitted fluorescence is recorded. The sorting electric filed is turned on only in case the droplet has fluorescence intensity above a preselected threshold, resulting in a vertical electric gradient. A dielectrophoretic force attracts the droplets toward the region of high electric gradient on the side of the electrodes and they are diverted into the collection channel. When no electric field is applied, the

collection channel possesses higher fluidic resistance than the waste channel, leading to flow of all droplets into the waste channel[159].

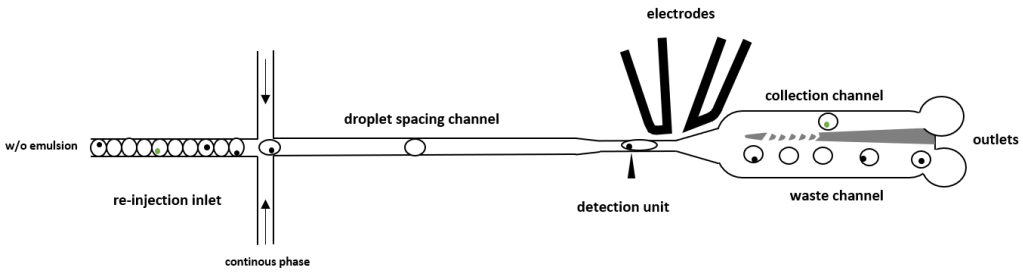

Figure 4. Scheme of a custom-made FADS microfluidic device. Figure modified from Mazutis *et al.* 2013 [159].

Dielectrophoretic FADS devices can perform droplet sorting with a maximal speed of 2 kHz[160, 161], alternatively, surface acoustic waves can be used for droplet deflection, reaching sorting rates of maximal 3 kHz[162]. Due to the Y-form of the sorting junction, flow rates need to be kept under a capillary number (Ca) of 0.1, which limits the throughput of the device. At faster flow rates, surface tension is dramatically reduced and the drops split at the divider between the collection and waste channels, contaminating the collection reservoir[158]. In order to overcome these shortcomings, new channel divider architectures have been developed, which prevent splitting of the droplets at very high flow rates and thus permit sorting rates of up to 30 kHz[158].

1.7. Fluorescence-Activated Cell Sorting (FACS)

The first fluorescence-activated cell sorter (FACS) was introduced in the late 1960s by Herzenberg and co-workers. It was developed as an instrument for separation of specific cell types from a complex biological sample (e.g. lymph nodes, bone narrow, or liver) based on fluorescence signal from a cell-specific fluorescent marker[163]. While significant improvements over the decades have taken place, enabling specific detection of 8-12 fluorophores and sorting rates up to 200 kHz[164], the analysis and sorting essentials of the FACS remain unchanged[165]:

Living cells are treated with specific fluorescent markers (e.g. cell type-specific antibody-fluorophore conjugates). The stained cell suspension is placed into a pressurized cell reservoir, from where it is injected through an inner nozzle, while cell-free sheath fluid flows around the inner nozzle, resulting in acceleration and narrowing of the stream and generation of a cylindrical liquid stream emerging from an outer nozzle. The stream breaks up into identical droplets (jet stream). The liquid stream is illuminated directly after emerging from the nozzle (before breaking into droplets) by a laser beam with distinct wavelengths. When a cell crosses a laser beam, it is illuminated for several microseconds and emits a fluorescence signal which is collected by a detector and directed to a row of photomultipliers and filters. In case the fluorescent signal of a cell meets the sort criteria, the drop occupied by the positive cell is specifically charged at the moment of formation. The charged droplets are sorted as they pass through a transverse electrostatic field generated by two parallel deflection plates and are collected in a separate tube[166].

FACS technology has revolutionized many areas of biology, biotechnology, and medicine. Starting by separation of mixed cell populations, through antibody screening and single-cell hybridoma cloning[167], to modern clinical

diagnostics[168], the application area of flow cytometry and FACS has rapidly expanded, giving rise to automated, robust, and exceptionally specific FACS instruments. However, since standard FACS devices work with aqueous buffers as sheath fluid, direct implementation of w/o droplet emulsions for flow cytometric analysis and sorting is not possible. Thus, the advantages of FACS over FADS regarding the significantly higher throughput and multichannel detection, has so far not been fully exploited for analysis and processing of w/o emulsions.

1.7.1. FACS of double emulsions (w/o/w)

One strategy for combining droplet-based compartmentalization with FACS represents the generation of water-in-oil-in-water (w/o/w) emulsions, also called double emulsions. In this case, the aqueous microdroplets containing cells and reagents are surrounded by a thin oil shell (oil and surfactant mix) and are dispersed in an aqueous phase (buffer), which makes them compatible with FACS processing[169-171] (Fig. 5). For this purpose, the primary w/o emulsion, produced by droplet-based microfluidics (described in 1.6.1) is emulsified in a second step using an aqueous buffer as a continuous phase. The second emulsification can be performed as bulk emulsification by mixing with a carrier aqueous phase and applying shear stress by pipetting or vortexing[172]. Although this technique is time saving, the resulting double emulsion is highly polydisperse and consists of a huge fraction of very small empty oil droplets and oil droplets with multiple aqueous cores[173, 174], which hampers the FACS selection. For controlled generation of monodispersed double emulsions, droplet microfluidics is favored[175]. Following initial w/o emulsification using a microfluidic chip with fluorophilic or lipophilic wall coating (depending on the oil-of-choice), the w/o emulsion is injected in a second droplet microfluidic chip with a hydrophilic coating and an aqueous continuous phase[176]. Stabilization of double emulsions necessitates addition of hydrophilic non-ionic surfactants to the outer aqueous phase like Tween 20[170], Tween 80[174], and sodium dodecyl sulfate (SDS)[177]. However, these agents have the ability to break lipid bilayers, inducing membrane damage in mammalian cells and thus exhibit cytotoxic effects even at very low concentrations[178, 179]. Since cell viability is a critical parameter in the context of mammalian cell – based assays, implementation of double emulsions is still mainly limited to cell-free assays[170, 174], screening of enzymes in cell lysates[180] or encapsulation of robust organisms with cell wall, like bacteria[171, 181].

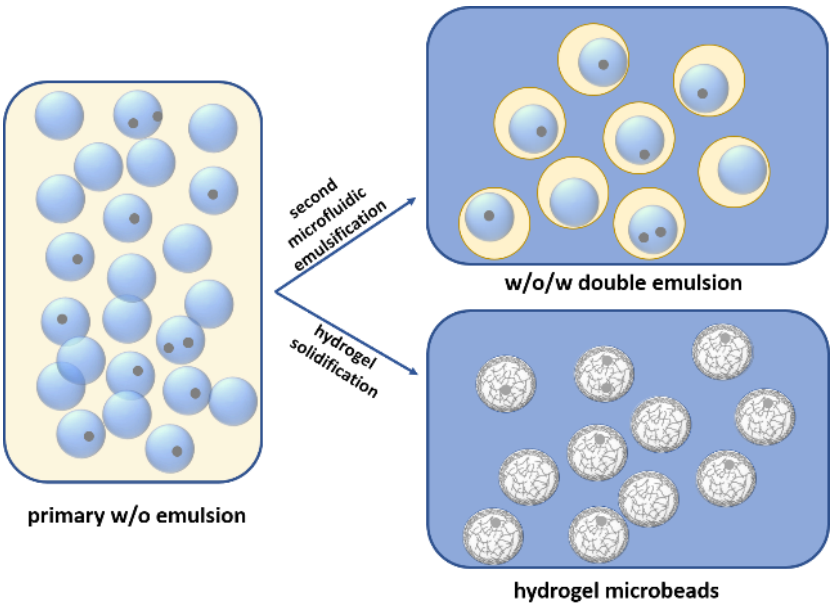

Figure 5. Strategies for combination of droplet micro-compartmentalization and FACS. Primary w/o emulsion with encapsulated cells consists of aqueous droplets in an oil phase. After second microfluidic emulsification using an aqueous buffer as a continuous phase, the aqueous droplets are surrounded by an oil shell and are dispersed in the aqueous buffer. When hydrogel forming molecules are initially mixed to the cell-containing encapsulation solution, the droplets in the primary emulsion can be solidified to hydrogel microbeads and after emulsion breakage can be recovered and resuspended in an aqueous buffer. (Image modified from Sukhorukov *et al.* 2004[182]).

1.7.2. Gel microdroplet – FACS

Gel microdroplets (GMDs) are aqueous microdrops containing a biocompatible matrix (hydrogel)[183]. GMDs can either be dispersed in a nonaqueous fluid as emulsion ("closed" GMDs), or they can be transferred to an aqueous medium ("open" GMDs). The big advantage of the GMDs over double emulsions is the easier handling and the option to switch from "closed" GMD system, where all reagents are retained and accumulated in the droplets, to "open" GMD system (Fig. 5), where rapid molecular exchange with the surrounding medium takes place, enabling manipulation of the encapsulated cells and simple addition of assay components[183]. Since GMDs can be readily recovered in an aqueous solution, they are compatible with an ultra-high-throughput flow cytometric analysis and sorting. GMD-FACS expands the types of assays compatible with flow cytometry, which is technically limited to measuring intracellular or cell-membrane-associated fluorescence[184]. Additionally, hydrogel matrixes structurally resemble extracellular matrix (ECM) and retain cell viability and growth. Hence, ECM-like gels have extensively been implemented in 3D cell culturing[185] and hydrogel microbeads have emerged as promising technique for the generation of multicellular spheroids, as they combine high-throughput generation with efficient transport of oxygen, nutrients, and metabolites[186-188].

1.8. Hydrogel Microbeads

Hydrogels are by definition macromolecular networks swollen in water or biological fluids[189]. Nowadays, hydrogel materials are implemented in different fields like drug delivery, tissue engineering, optics, diagnostics, and imaging[190]. Building blocks for hydrogels can be of natural or synthetic origin. Natural polymers like chitosan, alginate, collagen, agarose, cellulose, and gelatine, as well as synthetic polymers e.g. polyethylene glycol (PEG), hydroxyethyl methacrylate (HEMA) and derivatives of those are commonly used in the pharmaceutical filed[190]. Hydrogels can be classified in different categories depending on diverse parameters like physical structure (e.g. amorphous or semi-crystalline), ionic charge (anionic, cationic, neutral, or ampholytic), size (macro-, micro-, or nanogels), and bond formation (chemical or physical)[191]. These parameters dictate the functions of the different hydrogels and determine properties like swelling, elasticity, pore size, stability, and biocompatibility and degradation. For the purposes of this work, three different biopolymers with different crosslinking mechanisms have been exploited for encapsulation of viable cells in hydrogel microbeads.

1.8.1. Alginate

Alginic acid and its salts (commonly referred to as alginates) are derived from marine brown algae, where they play a role as a structure-giving element of the cell wall. Alginates are anionic, linear polysaccharides, composed of blocks of (1-4)-linked α-L-guluronic or β-D-mannuronic acid monomers (Fig. 6)[192]. Solubilized, they build large water-soluble polymers (hydrocolloids) enhancing the viscosity of the fluid dramatically[193]. Alginate forms soluble salts with monovalent metal ions, with sodium alginate being most commonly used. In presence of divalent cations, especially Ca^{2+}, strong ionotropic hydrogels are formed (Fig. 6)[193]. Sodium alginate and Ca^{2+}-alginate gels are considered as generally non-toxic, biocompatible, and biodegradable and find wide application in the pharmaceutical, cosmetic, and food industries[194]. Encapsulation of different bioactive substances and

living cells in alginate beads have been largely exploited, due to the inert environment within the polymer network and the mild gelation conditions[195, 196].

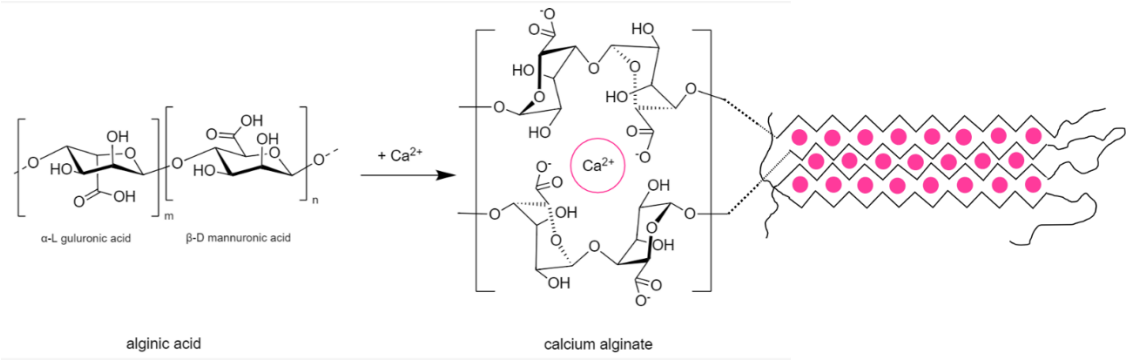

Figure 6. Chemical structure of alginic acid and calcium alginate hydrogel. Figure was modified from Liang *et al.* (2015)[192] and Lee *et al.* (2012)[193].

Different approaches for the generation of alginate beads and different gelation strategies have been published[197]. Utilizing a droplet-based microfluidic system for the generation of alginate beads has proven efficient for formation of discrete and uniform hydrogel structures[198]. However, on-chip gelation of alginate represents a significant challenge since rapid gelation can cause clogging of the chip. Gelation techniques can differ in the source of calcium ions and are broadly separated into external and internal gelation[199]. External gelation by dripping into a calcium-containing solution has been broadly applied[200-202] since in this way chip clogging is prevented. Nonetheless, this often results in aggregation of alginate beads and non-spherical form of the hydrogels[203]. For internal gelation, non-soluble $CaCO_3$ nanoparticles can be mixed to the dispersed phase and used as a crosslinking agent. *In situ* crosslinking is induced by acid, added to the continuous phase, and takes place directly after drop generation[204]. However, dissolution of solid calcium salt particles leads to a heterogeneous calcium ion distribution in the droplets, causing a non-uniform gel formation. Alternatively, ion chelating agents like ethylenediaminetetraacetic acid (EDTA), enable direct mixing of Ca^{2+} in soluble form to the dispersed phase by preventing gelation and allowing for homogenous and controlled crosslinking[205]. In this case, $CaCl_2$ is equimolar mixed with EDTA where the free Ca^{2+} is completely complexed at pH of 8. Alginate solidification in the emulsified droplets can be performed at a desired time point (after incubation etc.) by addition of small volume (0.05 % v/v) acetic acid. This induces Ca^{2+} release and rapid gelation of the alginate, resulting in monodispersed, spherical and uniform alginate beads. High cell viability and cell proliferation in the generated microbeads were demonstrated, proving the compatibility of this method for encapsulation of mammalian cells[205].

1.8.2. Matrigel

Matrigel® (or EHS matrix) is a basement membrane matrix extracted from Englebreth-Holm-Swarm (EHS) tumours, with a complex composition consisting mainly of the glycoproteins laminin and entactin, collagen type IV, a heparan sulfate proteoglycan (perlecan), as well as proteases, growth factors and other proteins like transferrin and clusterin[206]. Matrigel matrixes show remarkable biological activity by promoting differentiation of various cell types, as well as cell growth stimulation in tissue explants[206]. Furthermore, Matrigel is used to mimic extracellular matrix (ECM) for culturing of cancer and stem cells and maintain self-renewal and

pluripotency of stem cells[207]. For this reasons, Matrigel has been widely exploited for 3D cell culturing in microtiter plate formats[208] or in gel microbeads[209, 210]. Microfluidic encapsulation of cells in Matrigel occurs similarly to standard droplet generation, with the difference that the microfluidic device needs to be permanently cooled at 4 °C, since the matrix solidifies at ambient temperatures above 20 °C. Hence, gelation is achieved by incubation at 37 °C for 15-30 min, depending on the size of the droplets and the volume of the emulsion. The advantages of Matrigel regarding the enhanced cell viability and non-complicated solidification process has not been exploited yet for functional screening on single-cell level, nor for FACS-based selection.

1.8.3. Agarose

Agarose is a linear, non-charged polysaccharide built up of disaccharide units of D-galactose and 3,6-anhydro-L-galactopuranose (Fig. 7). It is extracted from red algae (Rhodophyta) and represents the major fraction in agar, besides agaropectin[192]. Similarly to agar, agarose is a thermal-responsive polymer which undergoes sol-gel transition upon cooling (thermal crosslinking)[211] by aggregation of double helical structures formed by the physical entanglement of anhydro bridges on the individual molecules[212] (Fig. 7).

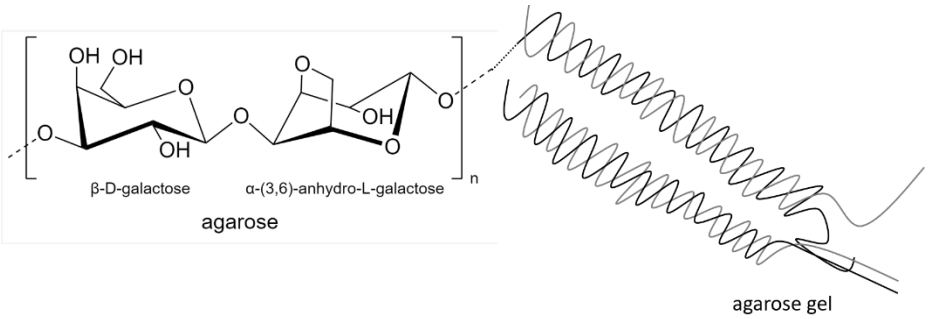

Figure 7. Chemical structure of agarose and agarose hydrogel. Image was modified from Zhang *et al.* (2015)[211].

Agarose hydrogels are widely used in biological, biochemical and medical fields, including cell culture, DNA analytical techniques (agarose gel electrophoresis), chromatography (gel filtration, affinity, and ion exchange chromatography), drug delivery, wound dressing, tissue engineering or cell encapsulation[213]. Advantageous physical properties of agarose, like physiological gelation temperature in the range of 31-36 °C which is reversible only after reaching the melting point (65-85 °C) and the uncomplicated handling of agarose hydrogels, make it attractive for encapsulation of live cells in agarose microbeads. Furthermore, it was demonstrated that agarose matrices allow for effective diffusion of big molecules such as antibodies, which is essential for many bioassays and screening procedures[214]. Chemical modifications of agarose, like hydroxyethylation[215], reduces the number of intrastrand hydrogen bonds, decreasing the melting and gelling temperatures of standard agarose. Such low or ultra-low gelling temperature agaroses (below 20 °C) are suitable for microfluidic encapsulation of living cells since they allow for working at physiological temperatures, while reducing the risk of solidification and chip clogging during the droplet formation process[216].

2. Objective

The objective of this work in the frame of the doctoral research was the establishment and validation of a generic ultra-high-throughput screening platform for selection of novel biomolecules based on their desired functionality. The bioactive molecules should be produced by a secretor cell and sensed with respect to their biologic activity by a report cell line. To allow for high-throughput library screening, secretor cells should be yeast cells, while reporter cells should be mammalian cell lines. Functional screening procedures should be established for three different applications: 1) Identification of antibodies that are able to reach the cytoplasm of mammalian cells; 2) identification of small signalling proteins (IL-3, TNFα) to induce a reporter cell response; and 3) identification of agonistic antibodies that trigger prescribed cellular signalling pathways.

In the context of screening of cytoplasm-penetrating antibodies, a robust secretor-reporter system needed to be generated and a technique for phenotype-genotype coupling needed to be established. To this end, microfluidic-assisted droplet generation was envisaged, since it facilitates generation of huge amount distinct microreactors. Different microfluidic systems (custom-made and commercially available), protocols and oil-surfactant mixtures should be tested to achieve an efficient high-throughput droplet production. Furthermore, in order to enable FACS-based selection of desired candidates, generation procedure for hydrogel microbeads had to be developed. Three hydrogel-forming agents (alginate, agarose and Matrigel®) with different crosslinking mechanisms were chosen on the basis of their applicability for encapsulation of live cells. Hydrogel microbeads generation should be optimized and properties of the hydrogels regarding their stability, microfluidic compatibility and retaining of cell viability should be characterized and evaluated.

A standard fluorescence activated cell sorting device should be adopted for analysis and sorting of cell-containing hydrogel microdroplets (GMD-FACS). For this purpose, sorting parameters should be optimized in order to ensure integrity of the hydrogel microbeads during the FACS processing and accurate sorting process, at the same time. Technical optimizations and sorting parameters needed to be validated by sorting of hydrogel beads, containing different yeast populations, and sorting efficiency and yeast cell viability and growth should be investigated.

Additionally, a functional read-out based on mammalian reporter cells was desired. Therefore, the encapsulation procedure needed to be adjusted for mammalian cells and appropriate co-cultivation conditions for yeast and mammalian cells should be identified. To this end, yeast growth and heterologous expression and secretion of candidate molecules from yeast cells should be assessed and optimized under conditions compatible with mammalian cell culture (temperature, media, etc.) in order to identify optimal conditions for both cell types.

For validation of the functional screening and selection concept, proof-of-concept screens needed to be established and performed. Two different mammalian cell lines with fluorescent reporter systems were available: Ba/F3-CIS-d2EGFP (murine reporter cells), which respond to stimulation with murine interleukin 3 (mIL-3) by expression of green fluorescent protein (GFP) and NF-κB/Jurkat/GFP (human immortalized T lymphocytes), which can be stimulated by human tumour necrosis factor alpha (hTNFα) or by T cell activation (anti-CD3 + anti-CD28) and express GFP as well. Yeast-based expression and secretion system needed to be

established and sufficient secretion of mIL-3 and hTNFα for induction of reporter cell response should be realised.

In case of Ba/F3-CIS-d2EGFP, a non-functional mIL-3 mutant should be generated with minimal sequence alterations. Reporter cell fluorescence levels after co-encapsulation with either activating mIL-3 wt-, or non-activating mIL-3-secreting yeast cells should be measured and co-culturing conditions should be optimized for effective FACS-selection of active mIL-3 variants. Mixing experiments and functional selection using different ratios of yeast cells secreting the active mIL-3 wt variant with an excess of non-activating mIL-3 mutant-secreting yeast cells should be conducted in order to demonstrate the feasibility of the concept for function-based screening. Furthermore, a small randomized mIL-3 library should be generated and secreted from yeast cells. Functional selection for regain of cytokine function should be performed by co-encapsulation in hydrogel microbeads with Ba/F3 reporter cells and FACS-based selection.

In case of NF-κB/Jurkat/GFP reporter cell line, co-encapsulation with hTNFα-secreting yeast cells should be performed and sufficient reporter cell activation should be achieved. In order to assess the applicability of the system for yeast-based screening of functional antibodies, anti-CD3 antibody (muromonab or OKT3) should be secreted from yeast cells and T cell activation of the reporter cell line should be tested by cocultivation of yeast and reporter cells in microdroplets.

In summary, the presented work aimed at development and validation of a novel functional screening platform in an ultra-high-throughput manner. Such technology is high-in-demand in the biotechnological field and we believe it could contribute for the accelerated discovery of new functional biologics, including cytokines, agonistic or internalizing antibodies.

3. Materials

3.1. Bacterial Strains

The following *Escherichia coli* strains with corresponding genotypes were used:

- **DH5α** - F⁻ Φ80*lac*ZΔM15 Δ(*lac*ZYA-*arg*F) U169 *rec*A1 *end*A1 *hsd*R17 (rK–, mK+) *pho*A *sup*E44 λ– *thi*-1 *gyr*A96 *rel*A1
- **Top10** - F⁻ mcrA (mrr-hsdRMS-mcrBC) 80lacZ M15 lacX74 recA1 ara139 (ara-leu)7697 galU galK rpsL (StrR) endA1 nupG

3.2. Yeast Strains

S. cerevisiae EBY100 - MATa URA3-52 trp1 leu2Δ1 his3Δ200 pep4:HIS3 prb1Δ1.6R can1 GAL (pIU211:URA3)

3.3. Mammalian Cell Lines

	Cell line	***Cultivation medium***
Reporter cell lines	**Ba/F3-CIS-d2EGFP** murine pro B cell line	RPMI-1640 + 10 % (v/v) FBS + 1 % (v/v) Pen/Strep mix + 10 ng/ml murine interleukin 3 (mIL-3)
	NF-κB/Jurkat/GFP human T cell acute lymphoblastic leukemia	RPMI-1640 + 10 % (v/v) FBS + 1 % (v/v) Pen/Strep mix
Cancer cell lines	**HeLa** human adenocarcinoma epithelial cells	DMEM + 10 % (v/v) FBS + 1 % (v/v) Pen/Strep mix
	SK-BR-3 human epithelial breast cancer cells	DMEM + 10 % (v/v) FBS + 1 % (v/v) Pen/Strep mix
	MDA-MB 468 human mammary gland adenocarcinoma cancer cells	DMEM + 10 % (v/v) FBS + 1 % (v/v) Pen/Strep mix
	CHO-KI Chinese hamster ovary	DMEM/F12 Ham + 10 % (v/v) FBS + 1 % (v/v) Pen/Strep mix
Protein expression	**CHO-FlipIn-hTNFα** Chinese hamster ovary cell, stably expressing and secreting human TNFα	DMEM/F12 Ham + 10 % (v/v) FBS + 1 % (v/v) Pen/Strep mix + 0.8 mg/ml hygromycin
	Expi293F human embryonic kidney cells optimized for antibody production	Expi293™ Expression Medium with 4 mM L-glutamine, cultivation as suspension cultures with 110 rpm orbital shaking
	Expi293F-C225 human embryonic kidney cells, stably expressing and secreting cetuximab (C225)	Expi293™ Expression Medium with 4 mM L-glutamine + 1 µg/ml puromycin
	Expi293F-SP34 human embryonic kidney cells, stably expressing and secreting anti-CD3 antibody (clone SP34)	Expi293™ Expression Medium with 4 mM L-glutamine + 1 µg/ml puromycin

3.4. Plasmids

3.4.1. Plasmids for secretion from yeast *S. cerevisiae*

(1) pYD-app8-mIL-3wt-T2A-mCherry

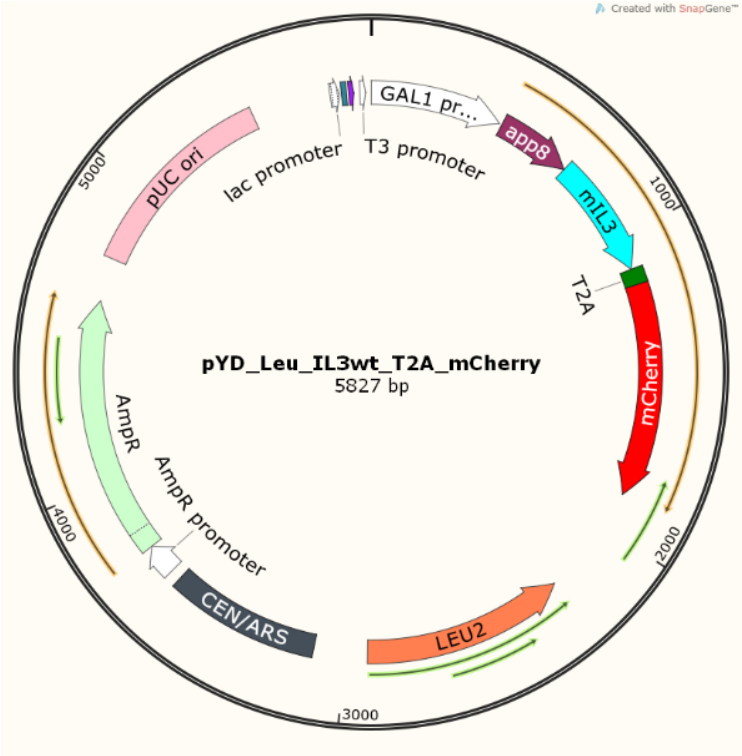

Figure 8. Vector map of pYD-app8-mIL-3-T2A-mCherry. Important components are annotated. **AmpR:** beta-lactamase-mediated ampicillin resistance, **pUC ori:** origin of replication for *E. coli*, **CEN/ARS:** origin of replication for yeast (*S. cerevisiae* CEN6 centromere fused to an autonomously replicating site), **LEU2:** beta-isopropylmalate dehydrogenase (IMDH) for leucine biosynthesis, **GAL1 promoter**: yeast promoter with upstream activating sequence mediating Gal4-dependent induction[217], **app8:** leader sequence for secretion from *S. cerevisiae*[218], **mIL3:** gene for mature murine interleukin 3 (D_{33}-C_{166}), **T2A:** ribosome skipping peptide[219], **mCherry:** red fluorescent protein, constitutively fluorescent.

(2) pYD-app8-mIL-3_ E49G-T2A-mCherry

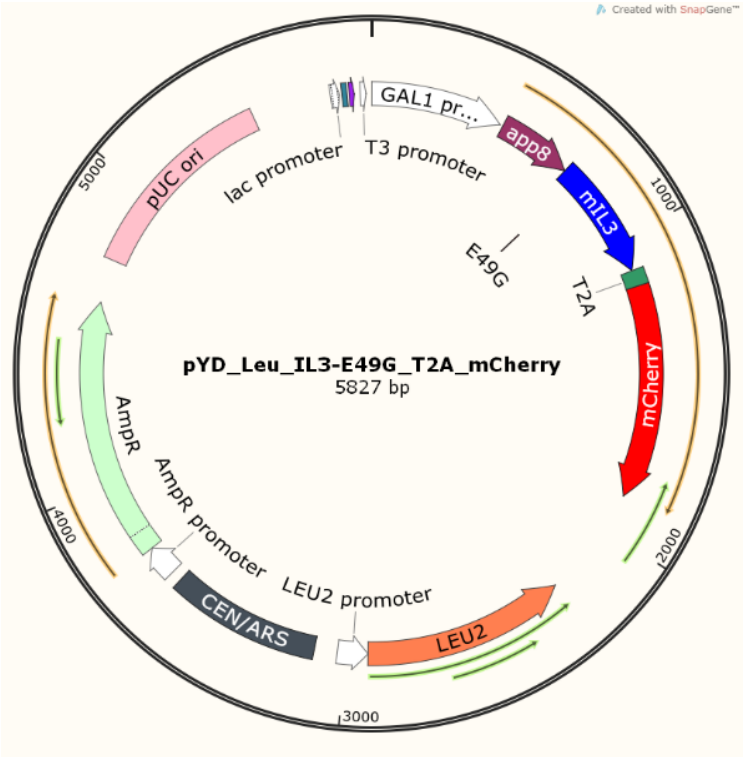

Figure 9. Vector map of pYD-app8-mIL-3_E49G-T2A-mCherry. Important components are annotated. **AmpR:** beta-lactamase-mediated ampicillin resistance, **pUC ori:** origin of replication for *E. coli*, **CEN/ARS:** origin of replication for yeast (*S. cerevisiae* CEN6 centromere fused to an autonomously replicating site), **LEU2:** beta-isopropylmalate dehydrogenase (IMDH) for leucine biosynthesis, **GAL1 promoter**: yeast promoter with upstream activating sequence mediating Gal4-dependent induction[217], **app8:** leader sequence for secretion from *S. cerevisiae*[218], **mIL3 E49G:** gene for mature murine interleukin 3 (D_{33}-C_{166}) with a single amino acid substitution E49G, **T2A:** ribosome skipping peptide[219], **mCherry:** red fluorescent protein, constitutively fluorescent.

(3) pYD-app8-hTNFα-T2A-mCherry

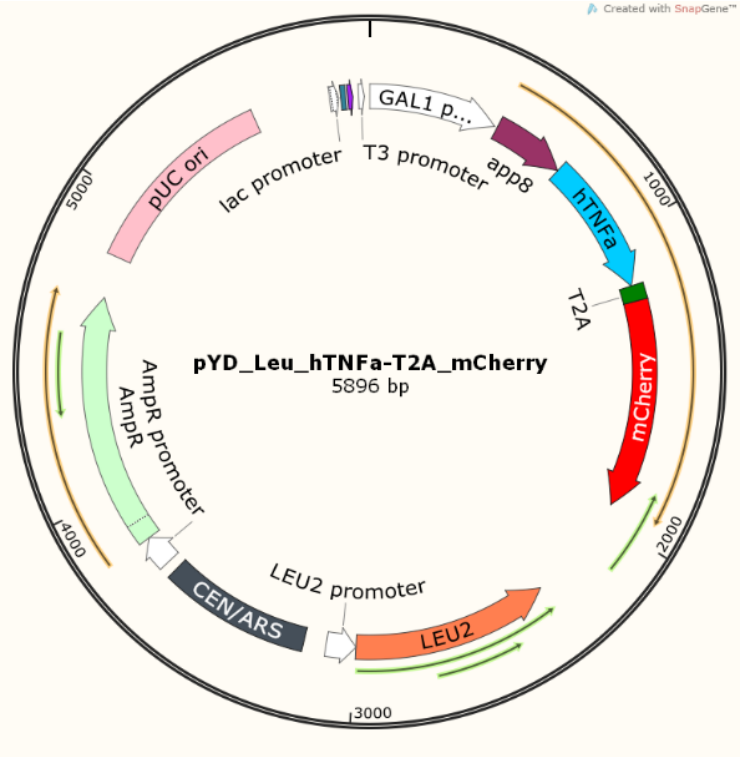

Figure 10. Vector map of pYD-app8- hTNFα-T2A-mCherry. Important components are annotated. **AmpR:** beta-lactamase-mediated ampicillin resistance, **pUC ori:** origin of replication for *E. coli*, **CEN/ARS:** origin of replication for yeast (*S. cerevisiae* CEN6 centromere fused to an autonomously replicating site), **LEU2:** beta-isopropylmalate dehydrogenase (IMDH) for leucine biosynthesis, **GAL1 promoter**: yeast promoter with upstream activating sequence mediating Gal4-dependent induction[217], **app8:** leader sequence for secretion from *S. cerevisiae*[218], **hTNFα:** gene for human tumor necrosis factor alpha, **T2A:** ribosome skipping peptide[219], **mCherry:** red fluorescent protein, constitutively fluorescent.

(4) pYD-app8-OKT3-HC-T2A-mCherry

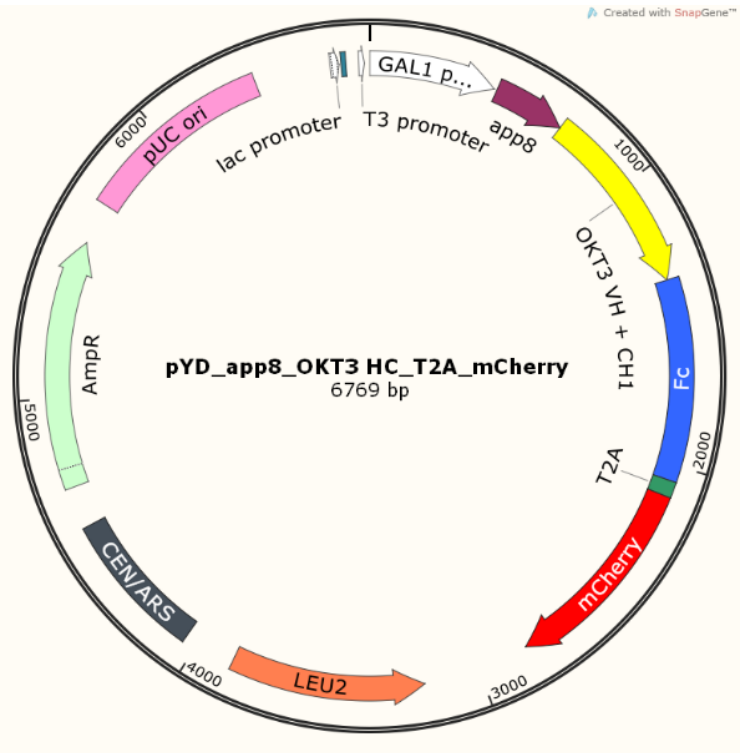

Figure 11. Vector map of pYD-app8-OKT3-HC-T2A-mCherry. Important components are annotated. **AmpR:** beta-lactamase-mediated ampicillin resistance, **pUC ori:** origin of replication for *E. coli*, **CEN/ARS:** origin of replication for yeast (*S. cerevisiae* CEN6 centromere fused to an autonomously replicating site), **LEU2:** beta-isopropylmalate dehydrogenase (IMDH) for leucine biosynthesis, **GAL1 promoter**: yeast promoter with upstream activating sequence mediating Gal4-dependent induction[217], **app8:** leader sequence for secretion from *S. cerevisiae*[218], **OKT3 VH:** gene for the humanized heavy chain of murine anti-CD3 antibody (muromomab), **CH1:** gene for human IgG1 CH1 domain, **Fc:** gene for human IgG1 Fc fragment , **T2A:** ribosome skipping peptide[219], **mCherry:** red fluorescent protein, constitutively fluorescent.

(5) pCT-app8-OKT3-LC

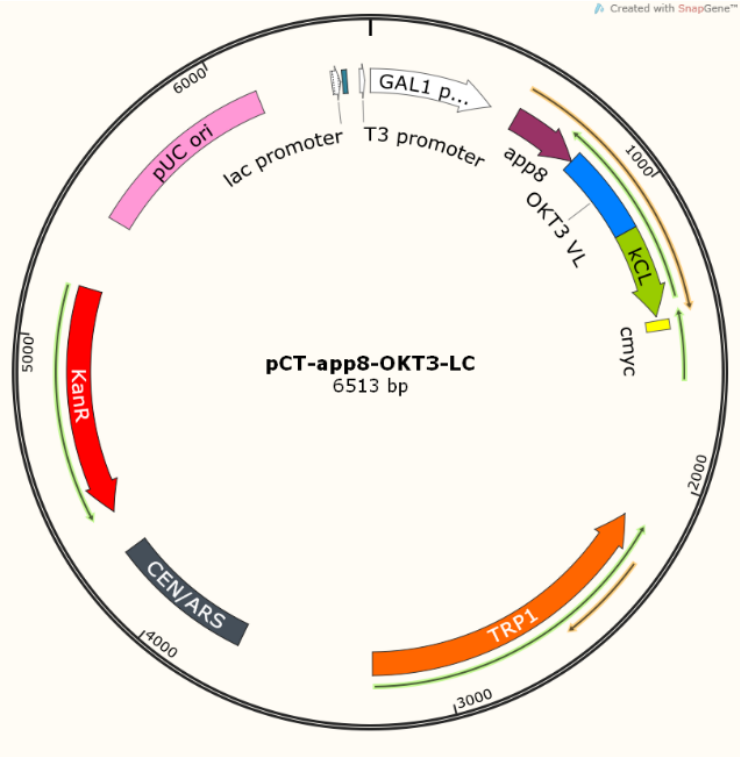

Figure 12. Vector map of pCT-app8-OKT3-LC. Important components are annotated. **KanR:** aminoglycosidase kinase (APH(3'))-mediated kanamycin resistance, **pUC ori:** origin of replication for *E. coli*, **CEN/ARS:** origin of replication for yeast (*S. cerevisiae* CEN6 centromere fused to an autonomously replicating site), **TRP1:** phosphoribosylanthranilate isomerase for tryptophan biosynthesis, **GAL1 promoter**: yeast promoter with upstream activating sequence mediating Gal4-dependent induction[217], **app8:** leader sequence for secretion from *S. cerevisiae*[218], **OKT3 VL:** gene for the humanized light chain of murine anti-CD3 antibody (muromomab), **κCL:** gene for human kappa constant region, **cmyc:** gene for c-Myc tag peptide.

3.4.2. Plasmids for antibody expression in mammalian cells

(6) pTT5-Trastuzumab-HC-wt

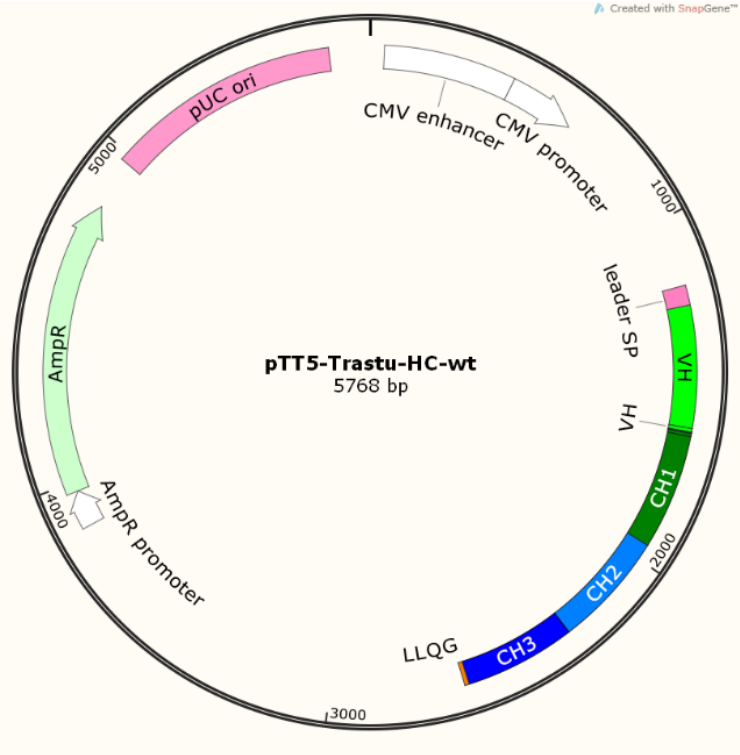

Figure 13. Vector map of pTT5-Trastuzumab-HC-wt. Important components are annotated. **AmpR:** beta-lactamase-mediated ampicillin resistance, **pUC ori:** origin of replication for *E. coli*, **CMV promoter:** cytomegalovirus promoter for high level expression in eukaryotes, **leader SP:** leader sequence for secretion into the culture medium from mammalian cells, **VH, CH1, CH2, CH3:** domains of the heavy chain of the humanized anti-HER2 antibody trastuzumab, **LLQG:** recognition tag for site specific conjugation using microbial transglutaminase.

(7) pTT5-hT4-LC

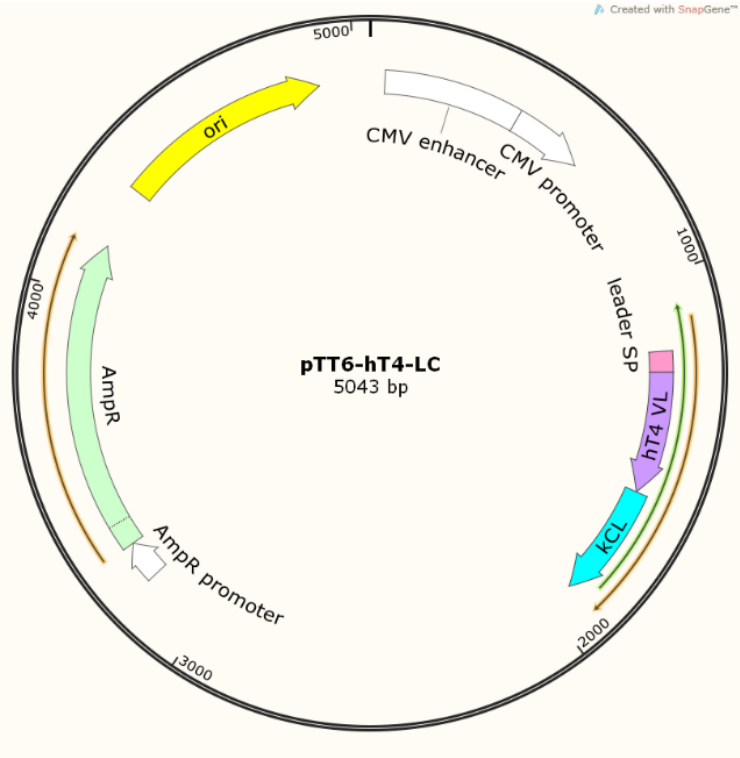

Figure 14. Vector map of pTT5-hT4-LC. Important components are annotated. **AmpR:** beta-lactamase-mediated ampicillin resistance, **pUC ori:** origin of replication for *E. coli*, **CMV promoter:** cytomegalovirus promoter for high level expression in eukaryotes, **leader SP:** leader sequence for secretion into the culture medium from mammalian cells, **hT4 VL:** gene sequence for the variable domain of the light chain of the engineered murine autoantibody hT4, **κCL**: gene for human kappa constant region.

(8) pTT5-Trastuzumab-LC

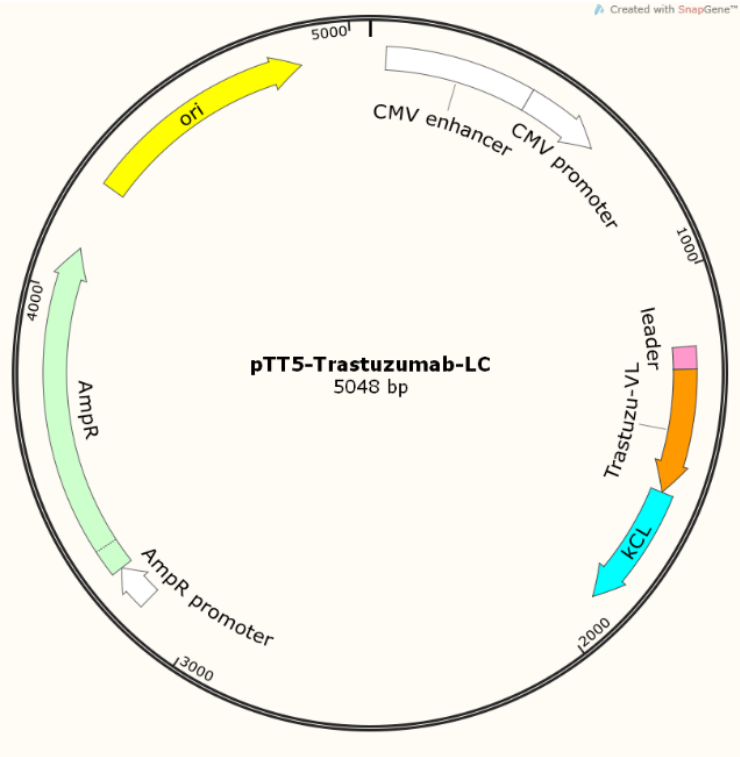

Figure 15. Vector map of pTT5-hT4-LC. Important components are annotated. **AmpR:** beta-lactamase-mediated ampicillin resistance, **pUC ori:** origin of replication for *E. coli*, **CMV promoter:** cytomegalovirus promoter for high level expression in eukaryotes, **leader SP:** leader sequence for secretion into the culture medium from mammalian cells, **Trastuzu-VL:** gene sequence for the variable domain of the humanized anti-HER2 antibody trastuzumab, **κCL**: gene for human kappa constant region.

(9) pTT5-Trastuzumab-HC-3×(GFP_{11})

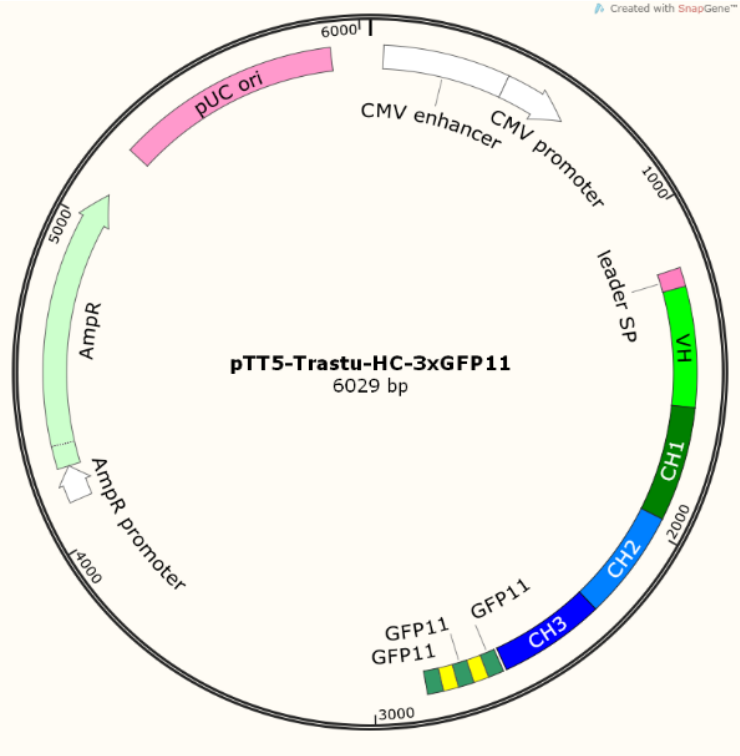

Figure 16. Vector map of pTT5-Trastuzumab-HC-3×(GFP_{11}). Important components are annotated. **AmpR:** beta-lactamase-mediated ampicillin resistance, **pUC ori:** origin of replication for *E. coli*, **CMV promoter:** cytomegalovirus promoter for high level expression in eukaryotes, **leader SP:** leader sequence for secretion into the culture medium from mammalian cells, **VH, CH1, CH2, CH3:** domains of the heavy chain of the humanized anti-HER2 antibody trastuzumab, **GFP11**: gene for 11th β-sheet of GFP (a 16 aa long split GFP tag), **yellow:** 15 aa long glycine-serine linker

(10) pQCXIP-spGFP$_{1-10}$

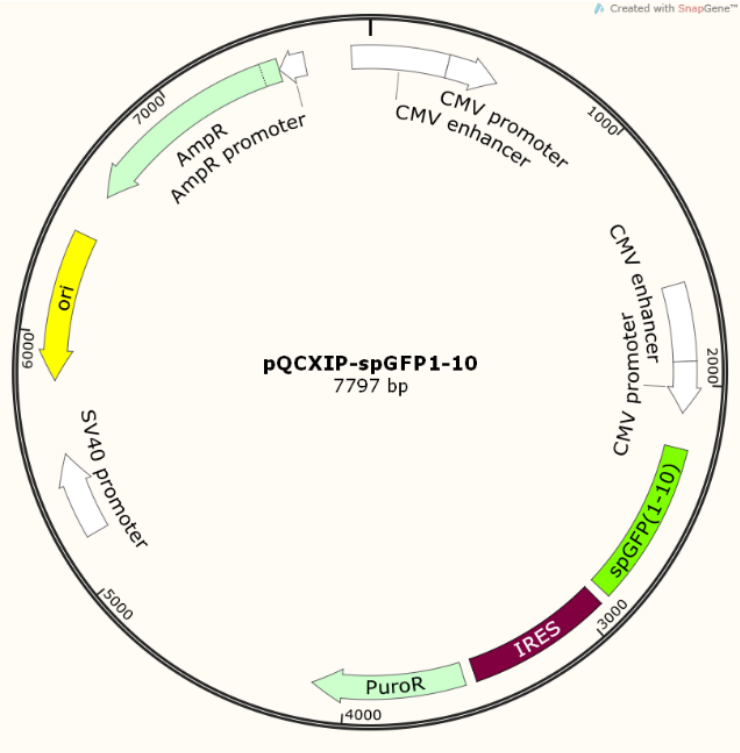

Figure 17. Vector map of pQCIP-spGFP$_{1-10}$. Important components are annotated. **AmpR:** beta-lactamase-mediated ampicillin resistance, **pUC ori:** origin of replication for *E. coli*, **CMV promoter:** cytomegalovirus promoter for high level expression in eukaryotes, **spGFP(1-10):** gene for superfolder green fluorescent protein β-sheets 1 to 10. **IRES:** viral internal ribosome entry site for translation of polycistronic constructs. **PuroR:** puromycin N-acetyl-transferase (PAC)-mediated puromycin resistance.

3.5. Oligonucleotides

3.5.1. Sequencing primers

Name	*Sequence (5' – 3')*
pTT5 seq up	CTGCGCTAAGATTGTCAGT
pTT5 seq lo	CCATATGTCCTTCCGAGTG
app8 seq up	GCCATTGTCCAACAGCACAAATAAC
pYD seq lo	TACGAGCTAAAAGTACAGTGGGAAC
mCherry seq lo	CTCCTTGATGATGGCCATG

3.5.2. Cloning primers

Name	*Sequence (5' – 3')*
app8-mIL3wt up	GAAGAAGGGGTACAACTCGATAAAAGAGATACCCACCGTTTAAC
mIL3wt-T2A lo	CAGCAGGCTGCCGCGGCCCTCACATTCCACGGTTCCACGGTTAGGAG
mIL3wt-T2A up	TCTCCTAACCGTGGAACCGTGGAATGTGAGGGCCGCGGCAGCCTGCTG
mCherry-pYD lo	CACTGTTGTTATCAGATCAGCGGGTTTAAACTCACTATTACTTGTACAGCTCGTCCATG
app8-mIL3-E49G up	GAAGAAGGGGTACAACTCGATAAAAGAGATACCCACCGTTTAACCAGAACGTTGAATT GCAGCTCTATTGTCAAGGGTATTATAGG
mIL-3 degenerative up	GTTGAATTGCAGCTCTATTGTCNNRNNHHNNATAGGGAAGCTCCCAGAAC
app8-hTNFα1 up	CAGATCATCTTCTCGAACCCCGAGTGACAAGCCTGTGGCCCACGTGGTGGC
app8-hTNFα2 up	AAGAAGGGGTACAACTCGATAAAAGAGTCAGATCATCTTCTCGAACCCCG

3.5.3. Next generation sequencing and single clone screening primers

	Primer	*Sequence*
mIL-3 initial library	NGS IL3 Bib fwd	ACACTCTTTCCCTACACGACGCTCTTCCGATCT**ACATCAC GTCTACACCACGAC**tgctgctaaagaagaagggg
	NGS IL3 Bib rev	GACTGGAGTTCAGACGTGTGCTCTTCCGATCT**GTCGTGG TGTAGACGTGATGT**gataacgtatctgtcctcaggatc
mIL-3 library R1	NGS IL3 Bib R1 fwd	ACACTCTTTCCCTACACGACGCTCTTCCGATCT**CATCTGCA TCACTCT**tgctgctaaagaagaagggg
	NGS IL3 Bib R1 rev	GACTGGAGTTCAGACGTGTGCTCTTCCGATCT**AGAGTGA TGCAGATG**gataacgtatctgtcctcaggatc
mIL-3 library R2	NGS IL3 Bib R2 fwd	ACACTCTTTCCCTACACGACGCTCTTCCGATCT**CATCTGCA TCACGCG**tgctgctaaagaagaagggg
	NGS IL3 Bib R2 rev	GACTGGAGTTCAGACGTGTGCTCTTCCGATCT**CGCGTGA TGCAGATG**gataacgtatctgtcctcaggatc
mIL-3 library R3	NGS IL3 Bib R3 fwd	ACACTCTTTCCCTACACGACGCTCTTCCGATCT**CATCTGCA TCACGTG**tgctgctaaagaagaagggg
	NGS IL3 Bib R3 rev	GACTGGAGTTCAGACGTGTGCTCTTCCGATCT**CACGTGA TGCAGATG**gataacgtatctgtcctcaggatc
1:10,000 mix	NGS IL3 Mix fwd	ACACTCTTTCCCTACACGACGCTCTTCCGATCT**TCTATATCGACA CTGAGT**tgctgctaaagaagaagggg
	NGS IL3 Mix rev	GACTGGAGTTCAGACGTGTGCTCTTCCGATCT**ACTCAGTGTCG ATATAGA**gataacgtatctgtcctcaggatc
	NGS IL3 MixR1 fwd	ACACTCTTTCCCTACACGACGCTCTTCCGATCT**TCTATATCGCAC TCT**tgctgctaaagaagaagggg

1:10,000 mix R1	NGS IL3 MixR1 rev	GACTGGAGTTCAGACGTGTGCTCTTCCGATCT**AGAGTGCGATA TAGA**gataacgtatctgtcctcaggatc
1:10,000 mix R2	NGS IL3 MixR2 fwd	ACACTCTTTCCCTACACGACGCTCTTCCGATCT**TCTATATCGCAC GCG**tgctgctaaagaagaagggg
	NGS IL3 MixR2 rev	GACTGGAGTTCAGACGTGTGCTCTTCCGATCT**CGCGTGCGATA TAGA**gataacgtatctgtcctcaggatc
mIL-3 wt specific	IL3 wt E23 fwd	CAGCTCTATTGTCAAGGAG
	IL3 rev	ACATTCCACGGTTCCACG

3.6. Chemicals

Compound	***Supplier***
1H,1H,2H,2H-Perfluorooctanol (PFO)	Sigma-Aldrich, St. Louis, USA
2-Mercaptoethanol	Carl Roth GmbH, Karlsruhe, Germany
Acetic acid	Carl Roth GmbH, Karlsruhe, Germany
Acrylamide/Bisacrylamide (37.5:1)	Carl Roth GmbH, Karlsruhe, Germany
Agar-agar	Carl Roth GmbH, Karlsruhe, Germany
Agarose	Carl Roth GmbH und Co KG, Karlsruhe
Agarose (ultra-low gelling temperature)	Sigma-Aldrich, St. Louis, USA
Ammonium acetate	Carl Roth GmbH, Karlsruhe, Germany
Ammonium persulfate (APS)	Carl Roth GmbH, Karlsruhe, Germany
Ammonium sulfate	Carl Roth GmbH, Karlsruhe, Germany
Ampicillin, sodium salt	Carl Roth GmbH, Karlsruhe, Germany
Bromophenol blue	Carl Roth GmbH, Karlsruhe, Germany
Citric acid	Carl Roth GmbH, Karlsruhe, Germany
Coomassie Brilliant Blue-G250	Carl Roth GmbH und Co KG, Karlsruhe
Coomassie Brilliant Blue-R250	Carl Roth GmbH, Karlsruhe, Germany
D-Galactose	Carl Roth GmbH, Karlsruhe, Germany
D-Glucose	Carl Roth GmbH, Karlsruhe, Germany
Dimethyl sulfoxide (DMSO)	Thermo Fisher Scientific, Waltham, USA
EDTA (disodium salt)	Carl Roth GmbH und Co KG, Karlsruhe
Ethanol	Carl Roth GmbH, Karlsruhe, Germany
Glycerol	Carl Roth GmbH, Karlsruhe, Germany
Glycine	Carl Roth GmbH und Co KG, Karlsruhe
HCl	Carl Roth GmbH, Karlsruhe, Germany
HDGreen™ DNA/RNA staining reagent	Intas Science Imaging, Göttingen, Germany
HFE-7500 3M™ Novec™ engineered fluid	Fluorochem, Hadfield, Derbyshire, UK
Imidazole	Carl Roth GmbH, Karlsruhe, Germany
Isopropanol	Carl Roth GmbH und Co KG, Karlsruhe
Isopropyl β-D-1 thiogalactopyranoside(IPTG)	Carl Roth GmbH und Co KG, Karlsruhe
Light Mineral Oil	Sigma-Aldrich, St. Louis, USA
Magnesium chloride	Carl Roth GmbH, Karlsruhe, Germany
Meliseptol	B. Braun Melsungen AG, Melsungen
Nickel chloride	Merck KGaA, Darmstadt, Germany
PicoSurf™ fluorosurfactant	Sphere Fluidics, Cambridge, UK
Polyethylenimine, 25 kDa, linear (PEI)	Polysciences, Eppelheim, Germany
Potassium chloride	Carl Roth GmbH, Karlsruhe, Germany
Potassium dihydrogen phosphate	Carl Roth GmbH, Karlsruhe, Germany

Potassium hydrogen phosphate	Carl Roth GmbH, Karlsruhe, Germany
Potassium hydroxide	Carl Roth GmbH, Karlsruhe, Germany
Sodium azide	Sigma-Aldrich, St. Louis, USA
Sodium chloride	Carl Roth GmbH, Karlsruhe, Germany
Sodium dihydrogen phosphate dihydrate	Carl Roth GmbH, Karlsruhe, Germany
Sodium dodecyl sulfate (SDS)	Carl Roth GmbH, Karlsruhe, Germany
Sodium hydroxide	Carl Roth GmbH, Karlsruhe, Germany
Sorbitan oleate (Span 80)	Sigma-Aldrich, St. Louis, USA
TEMED	Merck KGaA, Darmstadt, Germany
Tris(hydroxymethyl)aminomethan (Tris)	Carl Roth GmbH und Co KG, Karlsruhe
Trisodium citrate	Carl Roth GmbH, Karlsruhe, Germany
Triton X-100	Carl Roth GmbH, Karlsruhe, Germany
Tryptone/Peptone	Carl Roth GmbH, Karlsruhe, Germany
TWEEN-20	Carl Roth GmbH, Karlsruhe, Germany
Yeast extract	Carl Roth GmbH und Co KG, Karlsruhe
Yeast nitrogen base w/o amino acids and ammonium sulfate (BD Difco™)	Fischer Scientific, Waltham, Massachusetts, USA

3.7. Mammalian Cell Culture Media and Reagents

Component	***Supplier***
Dulbecco's Modified Eagle's Medium high glucose (DMEM, D6429)	Sigma-Aldrich, St. Louis, USA
Dulbecco's Modified Eagle's Medium/Nutrient Mixture F-12 Ham (DMEM/F12 Ham, D6421)	Sigma-Aldrich, St. Louis, USA
Expi293™ Expression Medium	Thermo Fisher Scientific Inc., Waltham, USA
Fetal bovine serum superior (FBS)	Biochrom GmbH, Berlin, Germany
Hygromycin B (50 mg/mL)	Thermo Fisher Scientific Inc., Waltham, USA
L-Glutamine 200 mM	Sigma-Aldrich, St. Louis, USA
Opti-Prep™ density medium	Sigma-Aldrich, St. Louis, USA
Penicillin-Streptomycin (100x) (P4333)	Sigma-Aldrich, St. Louis, USA
Puromycin Dihydrochloride (10 mg/ml)	Thermo Fisher Scientific Inc., Waltham, USA
RPMI-1640 (R8758)	Sigma-Aldrich, St. Louis, USA
Trypan Blue Solution, 0.4 %	Thermo Fisher Scientific Inc., Waltham, USA
Trypsin-EDTA solution	Sigma-Aldrich, St. Louis, USA

3.8. Solutions and Buffers

Solution/buffer	***Composition***
Agarose solution for encapsulation	3 % (w/v) ultra-low gelling temp. agarose 50 % RPMI-1640 50 % DMEM-F12 Ham

Alginate solution for encapsulation	2 % (w/v) sodium alginate 300 mM D-mannitol 50 mM CaCl2 50 mM EDTA pH 8
Ampicillin stock solution	100 mg/mL ampicillin
APS stock solution	10 % APS
Coomassie de-staining solution 1	10 % (v/v) acetic acid 25 % (v/v) isopropanol
Coomassie de-staining solution 2	10 % (v/v) acetic acid
Coomassie staining solution	0.2 % (w/v) Coomassie Brilliant Blue R-250 0.2 % (w/v) Coomassie Brilliant Blue G-250 30 % (v/v) isopropanol 7.5 % (v/v) acetic acid
dNTP mixture	5 mM dATP 5 mM dCTP 5 mM dGTP 5 mM dTTP
dYT medium	1 % (w/v) yeast extract, 1.6 % (w/v) tryptone 0.5 % (w/v) NaCl 1.5 % (w/v) agar-agar (for agar plates)
SD medium	5.4 g/L Na_2HPO_4 8.6 g/L $NaH_2PO_4xH_2O$ 20 g/L glucose 5 g/L ammonium sulfate 1.6 g/L yeast nitrogen base (w/o amino acids) 5 g/L Bacto casamino acids
SG medium	5.4 g/L Na_2HPO_4 8.6 g/L $NaH_2PO_4xH_2O$ 20 g/L galactose 5 g/L ammonium sulfate 1.6 g/L yeast nitrogen base (w/o amino acids) 5 g/L Bacto casamino acids
Kanamycin stock solution	50 mg/mL kanamycin
Phosphate buffered saline (PBS)	137 mM NaCl 2.7 mM KCl 10 mM Na_2HPO_4 1.8 mM KH_2PO_4 pH 7.4
Protein A elution buffer	100 mM citric acid 20 mM trisodium citrate pH 3.0

Protein A neutralizing buffer	50 mM M Tris-HCl (pH 9) 150 Mm NaCl
Protein A binding buffer	4 mM NaH_2PO_4 6 mM Na_2HPO_4 pH 7
Protein denaturing loading buffer	0.25 M Tris-HCl pH 8 7.5 % (w/v) SDS 25 % (v/v) glycerin 0.25 mg/mL bromphenol blue 12.5 % (v/v) 2-mercaptoethanol
TAE buffer (50×)	2 M Tris 1 M acetic acid 0.1 M EDTA
YPD medium	20 g/L dextrose 20 g/L tryptone 10 g/L yeast extract

3.9. Consumables and Kits

Consumable	***Supplier***
Amicon® Ultra Centrifugal Filters (3000 NMWL)	Merck Millipore, Darmstadt, Germany
Cell culture 96 well plates	Carl Roth GmbH, Karlsruhe, Germany
Centrifuge Tubes, 15/50 ml	Sarstedt AG, Nümbrecht, Germany
Centrifuge tubes, 50 ml (up to 15.500 g)	Carl Roth GmbH, Karlsruhe, Germany
Corning cell culture flasks (25 or 75 cm2)	Sigma-Aldrich, St. Louis, USA
Corning Erlenmeyer cell culture flasks	Sigma-Aldrich, St. Louis, USA
Elektroporation cuvettes	BioRad, Munich, Germany
Nunc MaxiSorp ELISA plates	eBioscience, San Diego, USA
Petri dishes, 92x16 mm und 150x20 mm	Sarstedt AG, Nümbrecht, Germany
Reaction vessels, 1,5/2 ml	Sarstedt AG, Nümbrecht, Germany
ZelluTrans® dialysis membran T3	Carl Roth GmbH, Karlsruhe, Germany
HiTrap Protein A HP, 1 ml column	GE Healthcare, Little Chalfont, UK
PD-10 Desalting Columns	GE Healthcare, Little Chalfont, UK
PureYield™ Plasmid Midiprep System	Promega, Fitchburg, USA
Wizard Plus® SV Minipreps DNA Purification System	Promega, Fitchburg, USA
Wizard® SV Gel and PCR Clean-Up System	Promega, Fitchburg, USA
Zymoprep™ Yeast Plasmid Miniprep II	Zymo Research Europe, Freiburg, Germany
PDMS microfluidic devices	Wunderlichips GmBH, Zurich, Switzerland

3.10. Instruments

Device	*Manufacturer*
Accuri C6 flow cytometer	Becton Dickinson, New Jersey, USA
Äkta Purifier UPC-900 P900 Frac-920, Unicorn 5 software	GE Healthcare, Little Chalfont, UK
Äkta Start, Unicorn start software	GE Healthcare, Little Chalfont, UK
Arpege 110, TP100 liquid nitrogen storage system	Air Liquide, Paris, France
BioSpec-nano Micro-volume UV-Vis Spectrophotometer	Shimadzu, Kyoto, Japan
Influx™ Fluorescence-Activated Cell Sorter (FACS)	Becton Dickinson, New Jersey, USA
GelDoc-It 2 Imaging System	UVP, LLC, Upland, USA
Gene Pulser und pulse controller	Bio-Rad Laboratories, Hercules, USA
Infinite M1000	Tecan, Männedorf, Switzerland
Leica TCS SP8 with LAS AF software	Leica Microsystems, Wetzlar, Germany
MCO-19AICUV CO2 incubator	Panasonic, Kadoma, Japan
Mr. Frosty™ isopropanol freezing container	Thermo Fisher Scientific Inc., Waltham, USA
New BrunsWick S41i	Eppendorf, Hamburg, Germany
PCR Cycler Eppendorf Mastercycler	Eppendorf, Hamburg, Germany
TC20™ Automated Cell Counter	Bio-Rad Laboratories, Hercules, USA
µEncapsulator microfluidic system	Dolomite Bio, Royston, UK
Ultra-Turrax® dispersing device	IKA, Staufen im Breisgau, Germany

4. Methods

4.1. Microbiological Methods

4.1.1. Transformation and culturing of bacteria

Escherichia coli strains were cultivated in dYT medium, or grown on dYT agar plates. Liquid cultures were incubated at 37 °C and 180 rpm orbital shaking. Agar plates were incubated overnight in static incubator at 37 °C.

For transformation with plasmid, electrocompetent *E. coli* were generated. To this end, cells were inoculated in 50 mL dYT medium at an OD_{600} of 0.1. Cells were expanded until OD_{600} of 0.5-0.8 was reached (exponential growth phase). Cells were pelleted at 4 °C, 4000 × g, for 10 min and washed three times with 50 mL ice-cold dH_20. Bacterial cells were subsequently separated in 5 × 100 µL aliquots and transferred to electroporation cuvettes where 100 ng plasmid were mixed. Electroporation was performed at 200 Ω, 2.5 kV, 25 µF on *Gene Pulser II* device. Following electroporation, cells were resuspended in 1 mL fresh dYT medium and recovered for 1 h at 37 °C. Finally, the cells were plated on dYT agar plates containing selective antibiotics and incubated overnight at 37 °C.

Plasmid extraction from *E. coli* was performed using *PureYield™ Plasmid Miniprep* or *Midiprep System* according to manufacturer's protocol. Plasmid concentration was determined on *BioSpec-nano Micro-volume UV-Vis Spectrophotometer*.

4.1.2. Transformation and culturing of yeast

Saccharomyces cerevisiae was transformed according to the protocol of Benatuil *et. al* (2010)[40]. Briefly, 1 µg purified plasmid backbone was mixed with 300 ng DNA insert (for gap repair cloning) and added to 100 µL electrocompetent *S. cerevisiae* cells. Yeast cells were electroporated as described in 4.1.1 and recovered for 2 h in 2 mL YPD medium at 30 °C, 180 rpm. Subsequently, the cells were pelleted by centrifugation at 4000 × g for 3 min and washed once with sterile PBS. Finally, the yeast was plated on minimal SD agar and incubated for 48-72 h at 30 °C in a static incubator.

Transformed yeast cells were propagated in liquid medium (SD) at 30 °C, 180 rpm. Expression induction was performed by cell harvesting and transfer in minimal SG medium and incubation overnight at 30 °C, 180 rpm. Alternatively, single yeast clones were inoculated in a mixture of 75 % SD + 25 % SG for simultaneous propagation and induction overnight.

4.2. Mammalian Cell Culture

4.2.1. Culturing adherent cell lines

Adherent cell lines were cultured under standard sterile conditions in a humidified atmosphere with 5 % CO_2 in T75 culture flasks. Cells were passaged twice a week after reaching over 90 % confluency. For this purpose, culture medium was aspirated and cells were washed with 10 ml sterile PBS. Next, 1 mL Trypsin-EDTA solution was added and the cells were incubated for 5-10 min at 37 °C until complete detachment of the cells could be optically observed (light microscopy). Trypsin reaction was stopped by adding 4-6 mL serum-containing culture

medium and the cells were diluted according to the grow rates of the corresponding cell line (in the range of 1:2 to 1:10). The flask was finally filled up to 10 mL with fresh pre-warmed medium and the cells were further incubated.

4.2.2. Culturing suspension cell lines

Reporter cell lines (Ba/F3-CIS-d2EGFP and NF-κB/Jurkat/GFP) were cultured in T75 culture flasks at 37 °C in a humidified atmosphere with 5 % CO_2. Cells were passaged three times a week after reaching a maximal cell density of 3 × 10^6 cells/mL. To this end, the cell density was determined using dead cell stain (Trypan Blue) and *TC20™ Automated Cell Counter.* Next, cells were diluted with fresh pre-warmed medium to reach a final cell density of 0.2 × 10^6 cells/mL for Ba/F3-CIS-d2EGFP and 0.3 × 10^6 cells/mL for NF-κB/Jurkat/GFP using 10-15 ml end volume medium.

Expi293F™ cells were used for recombinant antibody expression. Those cells were cultured in 30 mL serum-free medium in 125 mL shaker flasks on an orbital shaker at 110 rpm, 37 °C, 8 % CO_2. Cells were passaged every 3-4 days after reaching a cell density of 4-7 × 10^6 cells/mL. Cell density was determined as described above and cells were seeded at a density of 0.5 × 10^6 cells/mL in fresh pre-warmed medium.

4.2.3. Antibody expression in mammalian cells

Expi293F™ cells were transiently co-transfected with the corresponding vectors coding for the trastuzumab heavy and light chains using polyethylenimine (PEI). To this end, the cells were diluted in 30 ml serum-free expression medium to a cell density of 2.5 × 10^6 viable cells/mL. Plasmid DNA (30 µg in total) were mixed with 90 µg of PEI (dissolved in dH_2O) in 3 mL expression serum-free medium and were incubated for 15 min at room temperature. Subsequently, the pre-complexed DNA-PEI mixture was added dropwise to the cell suspension. After 24 h incubation at standard conditions, 0.5 % (w/v) tryptone was added to the cell suspension and antibody expression was performed for 3-4 days at standard culturing conditions. Finally, culture supernatant was harvested by centrifugation, filtered using 0.45 µm sterile filter, and subjected to protein A chromatography.

4.2.4. Cryopreservation of mammalian cell lines

For cryopreservation in the vapor phase of liquid nitrogen, cells were harvested and at least 5 × 10^6 viable cells were resuspended in 1 mL growth medium supplemented with 10 % (v/v) DMSO and 20 % (v/v) FBS. Resuspended cells were transferred into cryogenic storage vials and placed into a *Mr. Frosty™* isopropanol freezing container for slow temperature decrease at - 80 °C. The following day, the vials were transferred to the liquid nitrogen tank.

4.3. Molecular Biology Methods

4.3.1. Polymerase chain reaction (PCR)

PCR was used for amplification and generation of DNA fragments for gap repair cloning and plasmid ligation. Furthermore, colony PCR screening of transformed bacterial and yeast cells, harbouring desired plasmids was performed. For PCR amplification different polymerases were utilized: Q5 DNA polymerase (NEB) was used for amplification of longer DNA fragments and for generation of gene fragments for cloning, OneTaq DNA polymerase (NEB) and Taq DNA Polymerase (Qiagen) were utilized for colony PCR screening. All PCR samples were performed according to supplier's standard protocol and primer annealing temperatures were calculated using NEB Tm calculator tool (https://tmcalculator.neb.com/#!/main).

Overlap extension (OE)-PCR was performed for introduction of extended desired sequence by multiple oligonucleotides. To this end, PCR containing the first primer pair (with partially complementary region to the template) was performed for 10 cycles, and subsequently the second primer pair (with complementary region only to the first oligonucleotides) was added and PCR was performed for further 30 cycles.

Colony PCR screen was performed after lysis of the cells of interest (bacteria or yeast) in 50 µL H_2O or 10 mM NaOH, respectively, by heating at 98 °C for 10-15 min. After centrifugation of the cell debris, 1 µL cell lysate was used as template for the PCR.

4.3.2. Restriction digest

Restriction digest of plasmids and DNA fragments prior to cloning was performed using specific high-fidelity restriction enzymes (NEB). Digest reactions were performed according to NEB's standard protocols and sample volumes were scaled up accordingly, if necessary.

4.3.3. DNA ligation

For generation of a Trastuzumab heavy chain plasmid, harboring a triple GFP_{11} sequence at the C-terminus, DNA ligation was performed. Therefore, 100 ng digested plasmid backbone were mixed with 20 ng DNA fragment containing the triple GFP_{11} sequence. T4 DNA ligase (NEB) and the corresponding reaction buffer were added according to the standard protocol. Ligation was performed for 30 min at room temperature or overnight at 16 °C and was directly used (5 µL) for transformation of *E. coli*.

4.3.4. Agarose gel electrophoresis

Analysis of DNA amplification, restriction digest, and plasmid preparation was performed *via* agarose gel electrophoresis. To this end, 1 % (w/v) agarose solution in TAE buffer was mixed with HDGreen™ DNA staining reagent and was poured into an agarose gel chamber. DNA samples were mixed with 6 × loading dye (NEB) and applied in the agarose gel pockets, as a standard 1 kb plus (NEB) DNA ladder was used. Electrophoresis was performed at 110 V for 20 – 30 min in TAE buffer. Finally, agarose gel was irradiated with UV light and analysed on a GelDoc-It2 device with a 535 nm emission filter.

4.3.5. DNA purification

DNA fragments (PCR amplification products or restriction digest products) were purified using *Wizard® SV Gel and PCR Clean-up System* either directly from the reaction mix, or after separation by agarose gel electrophoresis and excision of the desired band from the gel. The purification was performed according to manufacturer's protocol.

4.3.6. Antibody purification and characterization

Antibodies were purified by protein A chromatography using a *HiTrap Protein A HP* column. To this end, mammalian culture supernatants (after heterologous expression in Expi293F™ cells) were mixed with 50 % (v/v) protein A binding buffer and loaded on the pre-equilibrated column. Following a wash step with 10 mL binding buffer, antibodies were eluted isocratic with protein A elution buffer and collected in 1 mL fractions with 200 µL protein A neutralizing buffer.

Collected fractions were analysed by sodium dodecyl sulfate polyacrylamide gel electrophoresis (SDS-PAGE) under reducing conditions, using 10 % polyacrylamide gels. Therefore, 10 µL of each fraction were mixed with 5 µL protein denaturing loading buffer and heated up to 98 °C for 10 min. Protein samples were loaded onto the gel and protein marker was used as a size standard. Electrophoretic protein separation was performed for 40 min at 40 mA and maximum voltage. Protein bands were stained with Coomassie staining solution and background staining was removed by incubation in de-staining solutions 1 and 2, until distinct protein bands were observable.

Fractions, containing the desired protein were pooled and dialyzed overnight in 5 L PBS at 4°C. On the following day, protein concentration was determined by absorption measurement at 280 nm and calculation with the corresponding extinction coefficient (ε) of each antibody, according to the Lambert-Beer law (Equation 3). If necessary, antibody solutions were concentrated using *Amicon® Ultra Centrifugal Filters* with a molecular cut-off of 3000 Da.

Equation 3. Lambert-Beer Law

$$A = \varepsilon \times c \times d$$

A = absorption at 280 nm
ε = molar extinction coefficient ($M^{-1}cm^{-1}$) at 280 nm
c = concentration (M)
d = path length (cm)

4.4. Generation of Hydrogel Microbeads

4.4.1. Microfluidic cell encapsulation

Microfluidic cell encapsulation was performed on µEncapsulator System, consisting of three pressure pumps, three respective flow rate sensors, a temperature control unit (TCU), microfluidic sample chip, and a two-reagent flurophilic droplet-generation chip with an etch depth of 50 µm at the junction. Fluorinated oil (Novac 7500) with 2 % PicoSurf™ surfactant was used as a continuous phase, plain Novac 7500 was used as a running fluid for the pressure pumps. Samples to be co-encapsulated were pipetted on the sample chip (100 µL each) and the microfluidic device was closed. Encapsulation process was started by turning-on the pressure pumps for the two aqueous channels, followed by the pump for the continuous phase. Flow rates between 3-5 µL/min for

the dispersed phases and 30-50 µl/min for the continuous phase were used. Target flow rates were set using the software and were adjusted until stable droplet formation was observable. Depending on the samples, the TCU was set either to 37.5 °C or to 4 °C, 15 min prior encapsulation start. Droplet-containing emulsion was collected in sterile 1.5 mL reaction vessels, placed in the tempered collection container holder of the device. Following complete encapsulation of the samples on the sample-chip, the microfluidic device was paused, running fluid was removed from the sample chip, new samples were applied, and encapsulation process was restarted.

4.4.2. Alginate microbeads

For encapsulation of cells in calcium alginate hydrogel microbeads, alginate solution was prepared as described in 3.8 and was filtered using a 0.45 µm sterile filter. Cell encapsulation medium was prepared as listed in Table **2** and was pre-warmed at 37 °C. Mammalian reporter cells and secretor yeast cells were centrifuged, washed twice with sterile PBS, and were separately resuspended in the alginate-containing cell encapsulation medium. Cells were co-encapsulated as described above (4.4.1) and w/o emulsion was incubated at 37 °C, 8 % CO_2 at 110 rpm orbital shaking. Alginate was solidified by addition of 0.05 % (v/v) acetic acid to the emulsion for 2 min. After vortexing, the emulsion was centrifuged shortly (100 × g, 10 s) and the excess fluorinated oil under the emulsion was removed. Emulsion was broken by addition of approx. 1 volume of PFO and inverting carefully. After phase separation (centrifugation for 10 s at 100 × g), the lower phase containing PFO and remaining fluorinated oil was removed, and alginate microdroplets were resuspended in alginate curing Tris buffer. Following a centrifugation step (10,000 × g, 5 min), alginate microbeads were filtered using a 70 µm cell strainer and were further processed by FACS.

4.4.3. Matrigel microbeads

Matrigel was stored as 1 mL aliquots at -20 °C. Prior usage (10 – 24 h) Matrigel was placed in a refrigerator at 4 °C where it liquefied. Cell encapsulation solution was prepared as described in Table 2, and all components were cooled on ice the entire time in order to prevent hydrogel solidification. Microfluidic system was tempered at 4 °C during the whole encapsulation process (4.4.1). After incubation overnight at 37 °C, 8 % CO2, 110 rpm, the emulsion was broken as described above and the Matrigel microbeads were recovered in PBS.

4.4.4. Agarose microbeads

Ultra-low gelling temperature agarose (3 % w/v) was dissolved in 50 % DMEM-F12 Ham and 50 % RPMI-1640 medium mix using a microwave. The agarose solution was then placed in a water bath at 37 °C. Cell encapsulation medium consisted of the components listed in Table 2 and all components were pre-warmed at 37 °C in order to avoid agarose solidification. Prior to cell resuspension, the cell encapsulation medium was sterile filtered using a 0.2 µm sterile filter. The TCU of the µEncapsulator was set to 37.5 °C and 15 min later cells were co-encapsulated as described in 4.4.1. Following incubation step overnight at 37 °C, 8 % CO_2, 110 rpm, the emulsion was placed on ice for 15 min or at 4 °C for 30 min in order to let the agarose solidify. Next, the emulsion was broken as described in 4.4.2 and agarose microbeads were resuspended in cold sterile PBS. Prior FACS, agarose microbeads were filtered using a 70 µm cell strainer to prevent clogging of the sample line and nozzle of the device.

Table 2. Composition of cell encapsulation media, containing different hydrogel-building molecules.

Components	*Alginate (2 % w/v)*		*Matrigel®*		*Agarose (3 % w/v)*	
	End concentration	Volume for 4 mL	End concentration	Volume for 4 mL	End concentration	Volume for 4 mL
Hydrogel solution	0.5 %	1 mL	40 %	1.6 mL	0.75 %	1 mL
FBS	20 %	800 µL	×	×	20 %	800 µL
Opti-Prep™ density gradient medium	20 %	800 µL	16 %	640 µL	20 %	800 µL
Galactose (20 % in medium mix)	2 %	400 µL	2 %	400 µL	2 %	400 µL
Penicillin-Streptomycin solution	1 %	40 µL	1 %	40 µL	1 %	40 µL
Medium Mix (50 % RPMI-1640 + 50 % DMEM-F12 Ham)		1 mL		1.3 mL		1 mL

4.5. Cell-Based Experiments

4.5.1. Cell internalization assay with cytotransmab HerT4

For investigation of cellular internalization and distribution of HerT4 cytotransmab, three different cell lines with different Her2 expression level were chosen: SK-Br-3 ($Her2^{high}$), CHO-KI ($Her2^{int}$) and MDA-MB 468 ($Her2^{low}$). Cells were seeded on glass cover slides in 6-well culturing plates at a cell density of 3×10^5 cells/well for SK-BR-3 and MDA-MB 468, and 2×10^5 cells/well for CHO-KI. Cells were propagated for 36 h at 37 °C, 5 % CO_2 for reaching a sufficient confluency (70-80 %). Cells were treated with 1 µM antibodies (trastuzumab wt or HerT4) diluted in culture medium without serum for 8 h at 37 °C, 5 % CO_2. Subsequently, cells were washed with PBS and fixed with 4 % PFA in PBS for 15 min at room temperature. Next, cells were permeabilized using 0.3 % Triton X-100 in PBS for 10 min and blocked overnight with 2 % BSA in PBS at 4 °C. Cells were stained with anti-human IgG-Alexa 488 conjugate, diluted 1:500 in 1 % BSA + 0.3 % Triton X-100 in PBS for 1 h at room temperature. Detection antibodies were washed 3 times with PBS and cells were mounted on microscopic slides. Cellular internalization was analysed on Leica confocal microscope.

4.5.2. GFP complementation assay with cytotransmab HerT4

Cytoplasm-penetration properties of HerT4 were investigated using split GFP complementation assay as described by Kamiyama *et al.* (2016)[220]. For this purpose, CHO-KI cells were seeded in an 8-well chamber slide at a cell density of 8000 cells/well. Cells were propagated for 36 h at standard culturing conditions and were transfected with 300 ng/well pQCIX-spGFP_{1-10} plasmid (Fig. 17), complexed with 900 ng PEI. Treatment with antibodies was performed 24 h post-transfection. To this end, Trastuzumab-3×(GFP_{11}) and HerT4-3×(GFP_{11}) were diluted at a concentration of 2 µM in fresh culture medium without FBS and GFP complementation was analysed 6, 8, and 10 h after treatment on Leica confocal microscopy.

4.5.3. Optimization mammalian medium for growth and induction of yeast

Yeast cells were inoculated at a cell density of 5×10^6 cells/mL in 3 mL of different standard mammalian media (DMEM high glucose, RPMI-1640, DMEM-F12 Ham, or mix of 50 % RPMI-1640 + 50 % DMEM-F12 Ham). Cells were cultivated at 30 °C or 37 °C, 180 rpm and OD_{600} was measured every 60 min for a time span of 10 h. Yeast induction was determined by measuring the fluorescence intensity of the intracellular expression marker (mCherry) by flow cytometry after 24 h of cultivation in the corresponding mammalian medium, supplemented with 2 % galactose. The percentage of mCherry-fluorescent cells was used as a measure of yeast induction.

4.5.4. Co-cultivation of yeast and mammalian cells

Yeast cells were expanded and induced overnight at 30 °C, 180 rpm. 1×10^7 yeast cells were mixed with 1×10^6 reporter cells in 1 mL mammalian medium mix (50 % RPMI-1640 + 50 % DMEM-F12 Ham), supplemented with 10 % FBS, 2 % galactose, and 1 % Pen/Strep. Cells were transferred to a 50 mL centrifugation tubes, which were sealed with a gas-permeable membrane in order to prevent evaporation of the medium. Cells were cocultured overnight at 37 °C, 110 rpm in a humidified atmosphere with 8 % CO_2 or at 30 °C, 180 rpm. Activation of the reporter cells was estimated based on the GFP fluorescence, measured on BD Influx™ cell sorter.

4.5.5. Co-encapsulation of yeast and reporter mammalian cells in microdroplets

Yeast cells were expanded and induced overnight at 30 °C, 180 rpm. 4×10^7 yeast cells were pelleted by centrifugation at 500 × g for 3 min and were washed with sterile PBS. Cells were resuspended in 1 mL encapsulation medium and tempered according to the used hydrogel-forming polymer (37 °C for agarose and alginate and 4°C for Matrigel). 2×10^7 viable reporter cells were harvested by centrifugation at 800 × g for 5 min at room temperature and were washed twice with sterile PBS. Cells were resuspended in 1 mL encapsulation medium and were tempered as well.

Co-encapsulation was performed as described in 4.4.1 and resulting emulsions were placed into a rotating incubator and incubated for 17-18 h at 37 °C, 110 rpm, in a humidified atmosphere and 8 % CO_2.

4.5.6. FACS of gel microdroplets

Prior to analysis and sorting, the emulsion with the co-encapsulated cells was treated accordingly to the type of hydrogel (sections 4.4.2, 4.4.3 and 4.4.4) and recovered hydrogel microbeads were transferred to aqueous buffer (Tris buffer with 1 mM $CaCl_2$ for alginate and PBS for agarose and Matrigel microbeads).

Sorting of hydrogel beads was performed on BD Influx™ Cell Sorter, equipped with a 200-micron nozzle tip (BD Biosciences 645895), with a 6 kHz drop frequency. BD FACSFlow™ sheath fluid (Fisher Scientific 10638814) was used in case of agarose and Matrigel and Tris buffer with 1 mM $CaCl_2$ was used for alginate, with 3.0 psi sheath pressure.

After each sorting round, the sorted yeast-containing agarose beads were plated on selective SD agar plates and incubated for 3 days at 30 °C in a static incubator. The colonies were harvested from the plates using sterile SD and stored at 4 °C until further usage.

4.5.7. Analysis of yeast cell enrichment

Monitoring of sorting efficiency was performed using bulk populations after each sorting round. To this end, yeast cells of the non-sorted mix and of the corresponding sorting rounds were inoculated at a cell density of 1×10^7 cells/ml in test tubes containing 2 mL of DMEM-F12 Ham medium, supplemented with 2 % galactose and 1 % Pen/Strep. Cells were cultivated for 24 – 48 h at 30 °C, 180 rpm and after cell density measurement, the yeast cultures were centrifuged for 15 min, 17 000 × rcf in 1.5 mL reaction tubes. The supernatant (1 mL) was transferred to a new tube and pH was neutralized with 100 µL 1M HEPES buffer. 1 x 10^5 reporter cells/sample were harvested and washed twice with sterile PBS. Reporter cells were resuspended in 100 µL RPMI medium, supplemented with 20 % FBS and 1 % Pen/Strep. The volume of yeast supernatant (max. 100 µL), added to the reporter cells, was normalized to the final cell density of the yeast culture. Reporter cells were subsequently incubated overnight (15-18 h) at 37 °C, 5 % CO_2 in a 96 well plate. Enrichment of functional wt mIL-3-secreting yeast cells was verified by the measurement of elevated GFP-fluorescence signal, normalized to background fluorescence of non-activated Ba/F3 reporter cells. GFP fluorescence signal (10,000 viable cells/sample) was determined using BD Accuri™ C6 flow cytometer.

Efficiency of the functional screening approach was analysed using NGS of the non-sorted population, as well as of the bulk populations after each selection round. To this end, yeast cell populations were propagated for 24 h at 37 °C in SD medium. 1×10^8 cells were centrifuged and plasmid preparation was performed using *Zymoprep™ Yeast Plasmid Miniprep Kit* according to the manufacturer's protocol. Specific oligonucleotides, comprising partial Illumina adapters and a DNA barcode were designed (3.5.3). PCR was performed using 0.5 µL plasmid preparation from each population as a template utilizing Q5 Polymerase (NEB) according to the standard protocol (NEB). PCR amplicons were purified using *Wizard® SV Gel and PCR Clean-Up System* following the manufacturer's protocol. Samples were sent for NGS to GENEWIZ (Leipzig, Germany) and sequencing data analysis was performed using Geneiuos 2020.1.

Colony PCR with single clones after the second sorting round was performed using a specific primer pair (3.5.3), where a 400 bp PCR product indicated the presence of wt mIL-3 coding DNA sequence. For the colony PCR, each colony was resuspended in 50 µL 20 mM NaOH and was heated at 98 °C for 15 min in 200 µL PCR tubes. After cooling down, the samples were centrifuged to pellet the cell debris and 1 µL supernatant per clone was used as a template. PCR was performed utilizing Taq DNA Polymerase (Qiagen) according to the standard manufacturer's protocol. PCR consisted of initial denaturation step (94 °C - 3 min); 30 cycles of denaturation (94 °C – 30 s), annealing (60 °C – 30 s), and elongation (72 °C – 30 s); final elongation (72 °C – 5 min). Colony PCR was analysed using agarose gel electrophoresis.

5. Results and Discussion

5.1. Generation and Cell Internalization of Cytotransmab HerT4

A long-term goal of this thesis was the identification and functional characterization of antibodies that are able to reach the cell cytoplasm, aimed at addressing intracellular targets. The cytotransmab-technology promises versatile generation of cytosol-penetrating full-length antibodies using antibodies with any desired specificity, simply by substitution of the original VL domain by the VL domain of a hT4 auto-antibody derived from a lupus mouse model[91]. In order to validate this claim, we generated HerT4 (Fig. 18A): anti-Her2 IgG1 antibody trastuzumab (Herceptin®), combined with the hT4 VL domain from Choi *et al.* (2014) (Figure S1A) and tested its cellular internalization and cytoplasmic penetration in comparison to the wildtype trastuzumab antibody.

5.1.1. Cellular internalization test in Her2 expressing cell lines

Cellular internalization was assessed in three cell lines with different antigen (Her2) expression levels. In case of trastuzumab wt, internalisation is mediated by receptor endocytosis combined with recycling of a significant part of the antibodies together with the receptor back to the cell surface[221]. This process was observable in form of gradual decrease in fluorescence intensity in accordance to the lower antigen expression levels of the CHO-KI and MDA-MB 468 cells, combined with punctual distribution of the fluorescence signals throughout the cellular interior, except in the cell nucleus (Fig. 18B), suggesting entrapment in intracellular vesicles.

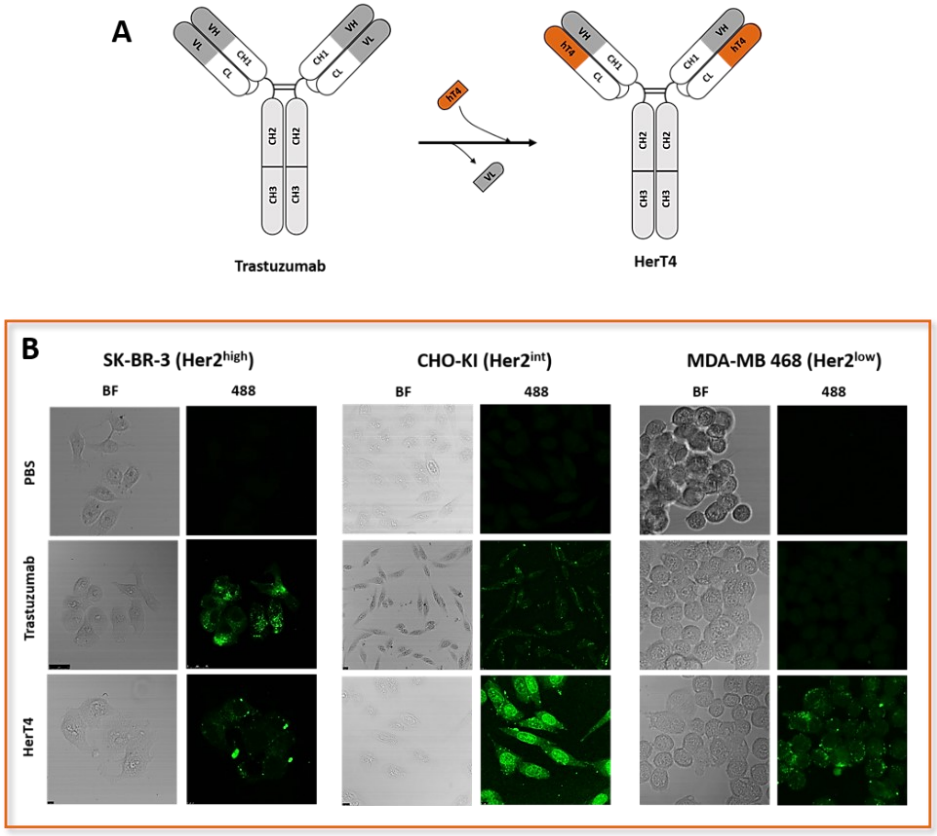

Figure 18. HerT4 cytotransmab and its cellular internalization and distribution. (A) Generation of trastuzumab-based cytotransmab. The trastuzumab VL domain is exchanged for the humanized hT4 VL domain, which facilitates cytoplasm penetration. Image is modified from Choi *et al.* (2014)[91]. **(B)** Cellular internalization test with trastuzumab wt and HerT4. Three cell lines with different Her2 expression levels (high, intermediate, and low) were treated with 1 µM trastuzumab wt or HerT4 antibodies for 8 h. Cells were stained with anti-human IgG-Alexa 488 conjugate and analysed using confocal microscopy.

In contrast, cellular internalization of the HerT4 antibody did not correlate with the Her2 display levels on the different cell lines. Strongest fluorescence intensity was detected in case of CHO-KI cells, where accumulation in the nucleus could be assumed (Fig. 18B). Fluorescence distribution in this case seems more homogenous, indicating possible release of the cytotransmab in the cytoplasm in accordance to the proposed endosomal escape mechanism of hT4-VL-baring antibodies[92]. Enhanced cellular internalization in CHO-KI cells could be explained by higher density of heparan sulfate proteoglycans (HSPG) on the cellular surface[222] in comparison to the other two cell lines, confirming loss of antigen specificity of the parental antibody through the substitution of the VL, as declared by Kim *et al.* (2018)[93].

5.1.2. Cytoplasmic penetration of HerT4

In order to examine in detail the capacity of endosomal escape and cytoplasmic release of the trastuzumab-based cytotransmab, a GFP fragment complementation assay[223] was performed. Spontaneous reassembly of two non-fluorescent fragments (GFP_{1-10} and GFP_{11}) of green fluorescent protein results in formation of matured fluorophore, with fluorescence properties identical to the native GFP protein[224]. Cytoplasmic expression of the bigger GFP fragment, consisting of β-sheets 1 to 10 of the β-barrel structure of the protein, is achieved by transient transfection of mammalian cells. After treatment with a cytotransmab, carrying the 11^{th} GFP β-sheet in form of a 16 amino-acid-long protein tag, GFP reassembly occurs only after release of the cytotransmab in the cytoplasm, excluding any fluorescence signals from antibodies entrapped in vesicles. This method allows for live cell imaging and enables direct verification of cytoplasmic penetration without risk of false-positive signals derived from cell permeabilization and antibody staining procedures.

In order to enhance the GFP complementation signal induced by one antibody molecule and enable time-resolved analysis of GFP signal increase, a tandem GFP_{11}-tag consisting of three GFP_{11}-sequences in a row, each separated by a triple G_4S-linker sequence, was genetically fused on the C-terminus of trastuzumab heavy chain resulting in six GFP_{11} peptides per antibody molecule (Fig. 19A). Tandem GFP tags facilitate linear increase of the GFP signal intensity depending on the number of the GFP_{11} moieties by simultaneous reassembly of multiple GFP molecules[220].

Incubation of GFP_{1-10}-expressing CHO-KI cells with the HerT4-GFP_{11} cytotransmab (Figure S1B), resulted in GFP fluorescence detectable 6 h after treatment with increased intensity 8 h post-treatment (Fig. 19B). At the same time, trastuzumab-GFP_{11} construct did not show any GFP complementation signal even after 8 h of treatment with the same concentration of the construct. This indicates successful cytoplasmic penetration only in case of the cytotransmab and demonstrates the suitability of the assay for distinguishing between endosomal entrapment and cytosolic localization of the tested constructs.

Nonetheless, this approach demonstrated a significant shortcoming in the face of limited transfection efficiency of the mammalian cells with the split-GFP_{1-10}-carrying plasmid, resulting in a very low number of cytotransmab-treated cells with detectable GFP complementation. Only 10-15 % of all cells exhibited detectable GFP signal after co-transfection with a plasmid coding for actin-fused GFP_{11} and comparable number of cells were fluorescent after transfection with vector coding for EGFP-actin fusion protein (Fig. 19C).

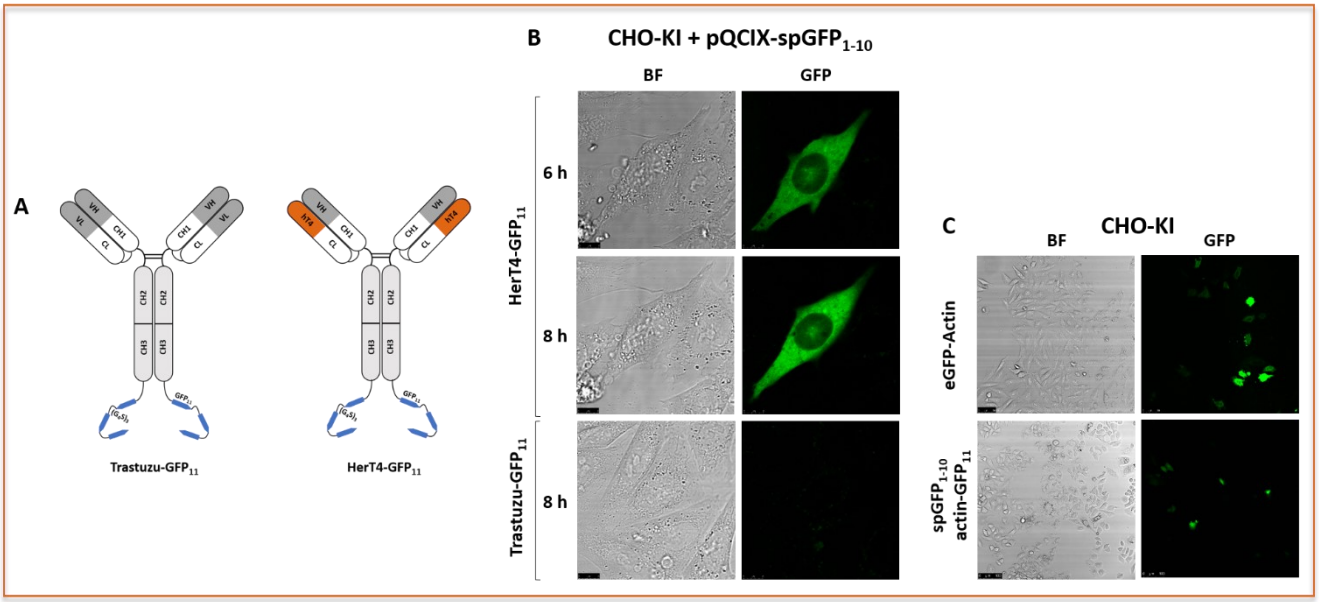

Figure 19. GFP complementation assay for proof of cytoplasmic delivery of HerT4. (A) Antibody constructs with C-terminal GFP_{11} complementation tags. Three consecutive GFP_{11} sequences were fused genetically on the C-terminus of the trastuzumab heavy chain. GFP_{11}-tags were separated by 15 amino acids long glycine-serine linker in order to ensure flexibility. **(B)** GFP complementation assay with CHO-KI cells transiently transfected with expression vector for GFP_{1-10}. Cells were treated with 2 µM of each antibody construct and were analysed *via* live cell confocal imaging 6 h and 8 h after treatment. **(C)** Complementation assay positive control with $spGFP_{1-10}$-expressing CHO-KI cells which were co-transfected with actin-GFP_{11}, and a transfection control with CHO-KI wt cells transfected with EGFP-Actin plasmid.

The presented experiments demonstrate that implementation of the split GFP complementation system would be a feasible and elegant strategy for screening and selection of antibodies or other molecules based on their cytosol-penetrating properties. However, significant improvements are required in order to enable efficient FACS-based detection and sorting of cells by means of GFP complementation.

Firstly, reliable and consistent expression levels of the GFP_{1-10} fragment within the whole mammalian cell population should be achieved. In order to avoid variations between the transfection experiments, a stably transfected cell line expressing sufficient amount of the GFP_{1-10} protein should be established. Furthermore, since the GFP complementation signal is homogeneously distributed within the cytoplasm of the mammalian cells, overall fluorescence intensity of the cells is rather low, representing a limitation for FACS-mediated screening. Further enhancement of the GFP signal intensity could be achieved by genetic fusion of the GFP_{1-10} fragment to streptavidin leading to tetramerization of the fusion protein. By introducing a peptidic streptavidin tag along the GFP_{11} sequence on the cytotransmab, a spatially proximity of the reassembled GFP molecules is accomplished leading to enhanced GFP intensity as demonstrated by Kim *et al.* (2018)[93].

Secondly, the development of a screening setup for cytosol-penetrating molecules represents further challenges regarding the library format and the phenotype-genotype coupling. Since only soluble molecules are able to penetrate cellular membranes and undergo GFP complementation, the screened candidates should be secreted by the library host (yeast). Microfluidic co-encapsulation of the library-secreting yeast cells together with the stably expressing split-GFP_{1-10} reporter cell line would ensure desired phenotype-genotype linkage and enable sorting on basis of cell penetration properties of the library variants (Fig. 20). Establishment of FACS-based

selection of desired candidates by generation of hydrogel microbeads and GMD-FACS would enable ultra-high-throughput screening of a high number of variants, making the approach suitable for yeast-based libraries.

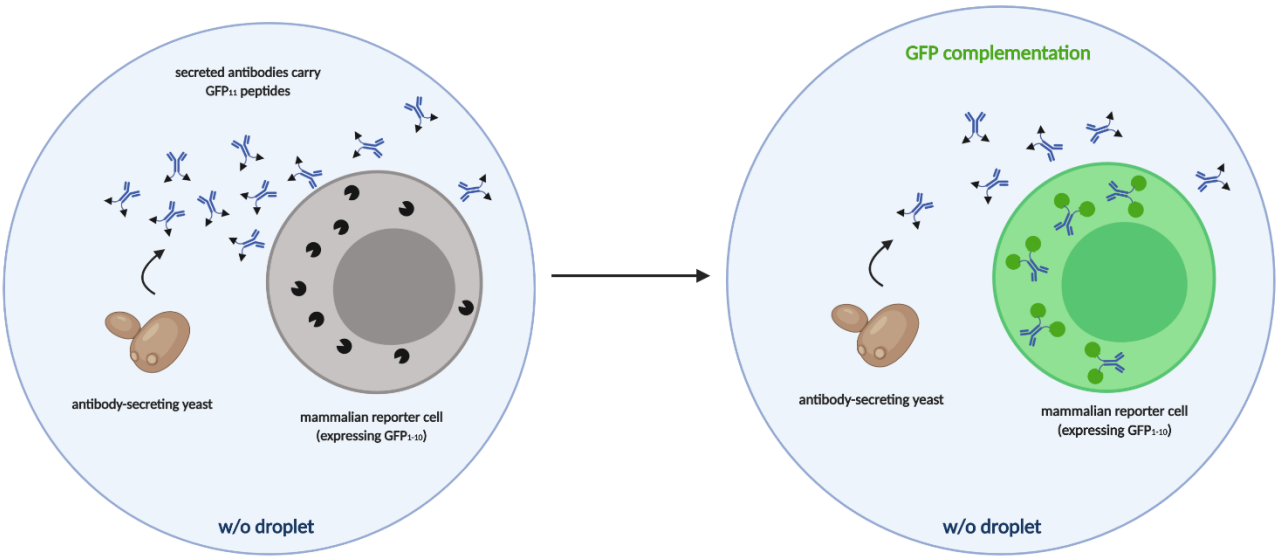

Figure 20. Concept for selection of cytoplasm-penetrating antibodies. Antibody-secreting yeast cells are encapsulated together with mammalian reporter cells in microdroplets in w/o emulsion. Secreted antibodies carry GFP_{11} peptides on the C-terminus and accumulate in the microdroplet. Antibody-variants with cytosol penetrating properties localize in the cytoplasm of the mammalian reporter cell, where GFP complementation with the cytosolic expressed GFP_{1-10} takes place leading to enhanced GFP fluorescence signal of the mammalian cell. By sorting of the droplets containing GFP-positive mammalian cell, yeast cells secreting the desired cytosol-penetrating antibody variants are enriched (phenotype-genotype coupling). Scheme was generated with Biorender.

Since the establishment of a functional screening procedure of this kind represents a versatile tool for selection of molecules with desired biological functions not only limited to cytosolic-penetration, this work was focused on the development of a novel technical procedure for efficient compartmentalization of living yeast and mammalian cells in picolitre-sized droplets and a FACS-compatible selection procedure in form of hydrogel microbeads.

Development of a stable GFP_{1-10}-expressing cell line and an enhanced split GFP complementation system was meanwhile object of the master's thesis work of Janna Sturm and Carolin Dombrowsky.

5.2. Generation of Hydrogel Microbeads

5.2.1. High-throughput generation of hydrogel-containing microdroplets

Different procedures were tested for the generation of hydrogel-forming microdroplets:

Bulk emulsification is the simplest method, based on the generation of aqueous droplets dispersed in an oil phase by applying shear stress (Fig. 21A). Following the procedure of Fang *et al.* (2017) for co-encapsulation of antibody-secreting *Pichia pastoris* and fixed mammalian target cells by bulk emulsification of agarose-containing medium[225], 1.5 % low-melting agarose was emulsified in light mineral oil supplemented with 1.5 % (v/v) Span 80 surfactant by stirring with an *Ultra-Turrax®* dispersing device. After cooling at 4 °C by gentle stirring and breaking the emulsion by multiple washing steps with light mineral oil and with PBS, the agarose beads were filtered through a 70 µm cell strainer and were analysed on a light microscope.

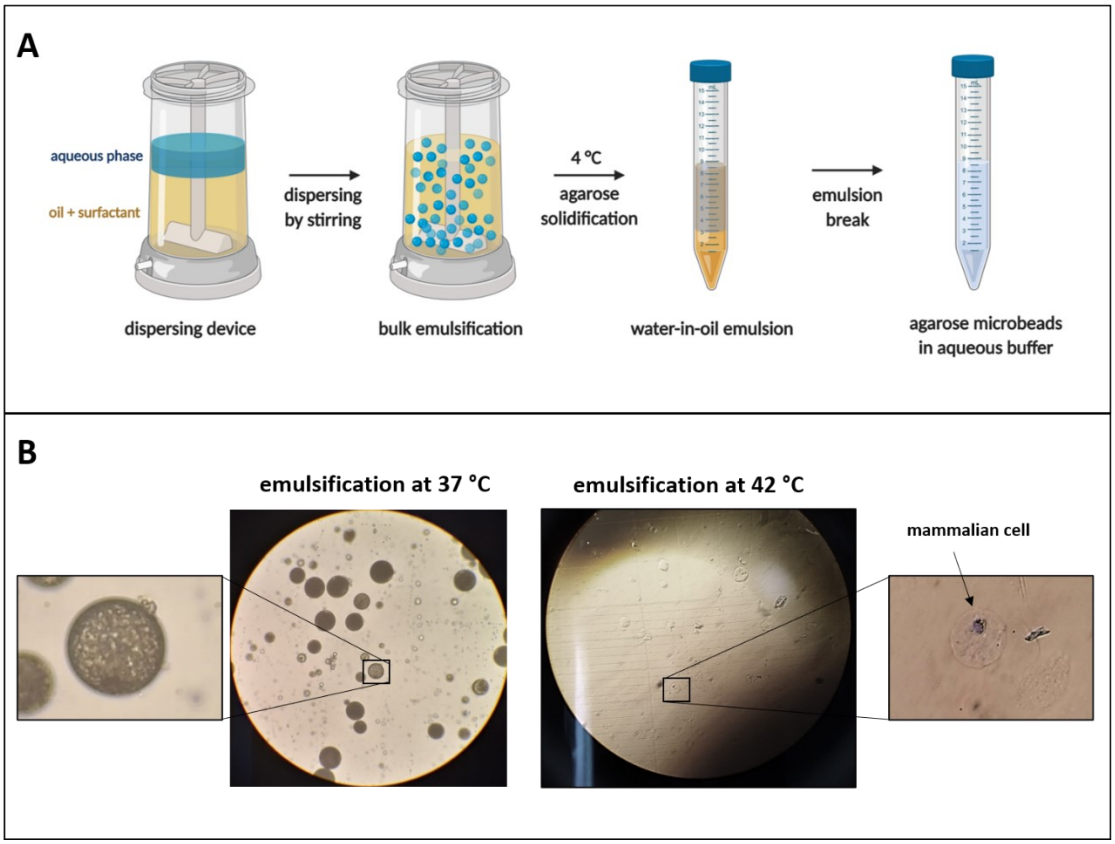

Figure 21. Formation of agarose microbeads by bulk emulsification of agarose-containing medium. (A) Scheme of the bulk emulsification procedure in light mineral oil with 1.5 % Span 80 surfactant. Image was generated with Biorender. **(B)** Microscopical analysis of agarose microbeads generated by bulk emulsification at 37 °C and 42 °C.

Bulk emulsification at 37 °C resulted in spherical agarose beads with dense texture (Fig. 21B, on the left), most likely due to partially solidification during the dispersing process. Increasing the emulsification temperature to 42 °C led to highly transparent microbeads, yet the form of the particles was non-uniform (Fig. 21B, on the right). In both cases, bead recovery process by washing and filtering resulted in very low yield of agarose microbeads containing cells. Additionally, emulsification process at 42 °C is not compatible with living mammalian cells and would cause drastic reduction in the cell viability.

In order to increase the amount of microbeads with desired size and morphology, microfluidic droplet generation was envisaged. Custom-made microfluidic devices consist most commonly of single-use poly-di-methyl-siloxane (PDMS) microfluidic chips with desired architecture and channel sizes (Fig. 22A) which are bonded onto microscopic glass slides. Microfluidic channels are connected through steel fluidic couplers with the tubing (Fig. 22B). In the simplest configuration, the fluids are injected with the help of syringes operated by peristaltic syringe pumps, enabling control of the flow rates. Adjusting of the flow rates occurs mostly empirically until stable droplet formation is observed, where exclusively monodispersed droplets are produced (Fig. 22C).

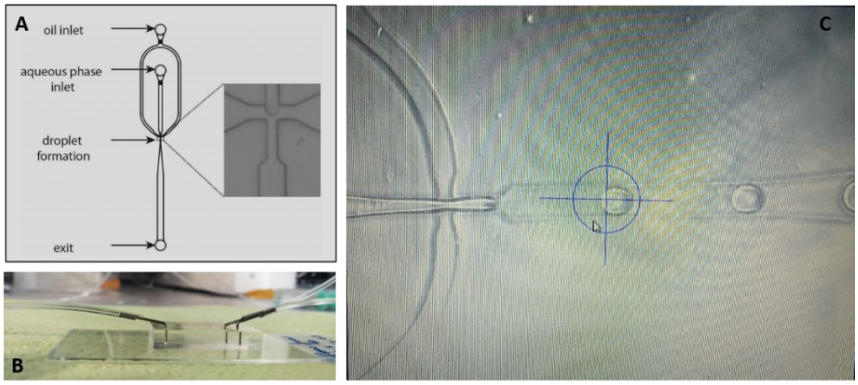

Figure 22. Custom-made microfluidic system. (A) Schematic of the geometry of a flow focusing PDMS microfluidic chip. Image was modified from Duarte *et al.* (2017)[226]. **(B)** Image of an PDMS microfluidic chip assembled with channel connectors and tubing. **(C)** Image of droplet generation using a flow-focusing PDMS microfluidic chip.

PDMS microfluidic devices are designed for combination with a microscope (and optionally a high-speed camera) for control and observation of the droplet formation. Since reliable tempering of the complete microfluidic equipment at 42 °C including the syringe pumps and the microscope was not possible, encapsulation of agarose-containing medium was not pursued. As an alternative, sodium alginate was chosen since it has found broad application in cell encapsulation experiments (see chapter 1.8.1). Two different gelation strategies for generation of calcium alginate beads were tested, both leading to generation of a high quantity of alginate microbeads. External gelation of a 1 % sodium alginate solution emulsified using the PDMS chip was achieved by dripping the emulsified droplets from the outlet tubing directly into Ca^{2+}-containing Tris buffer (100 mg/mL $CaCl_2$) combined with gentle shaking of the collection vessel. However, hydrogel microbeads generated in this way did not exhibit spherical form and were prone to clumping (Fig. 23A), resulting in dramatic loss of the microbeads during the filtering step with a 70 µm cell strainer. Internal gelation method as developed by Utech *et al.* (2015)[205] resulted in more homogeneous alginate microbeads with spherical shape, nicely dispersed in the aqueous solution after recovery (Fig. 23B).

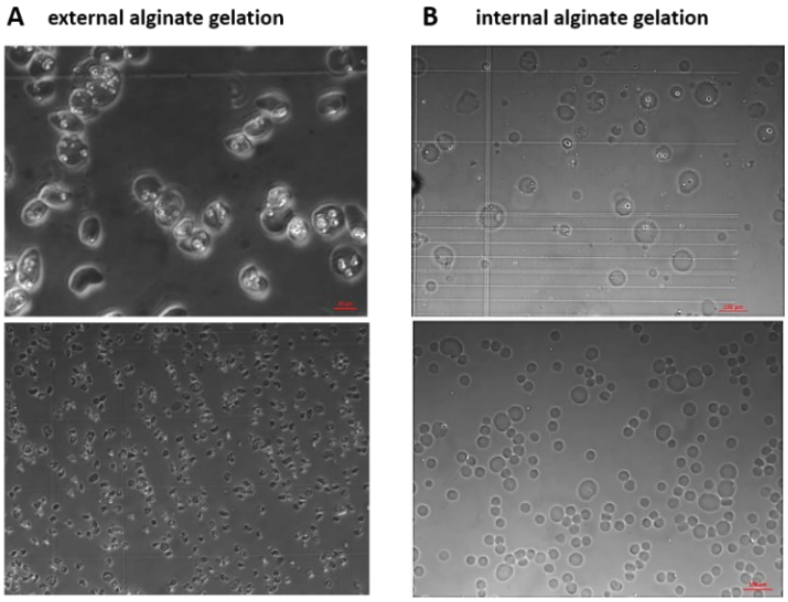

Figure 23. Formation of calcium alginate microbeads with the help of PDMS microfluidic chip and peristaltic syringe pumps. (A) External alginate gelation by dripping of the emulsified droplets into calcium-containing solution. **(B)** Internal alginate gelation by addition of Ca-EDTA complex to the encapsulation medium.

Although droplet generation using custom-made PDMS microfluidic chips allowed for production of a sufficient quantity monodispersed calcium alginate microbeads, encapsulation flow rates were limited to 1-2 µL/min due to the high viscosity of the alginate solution. Furthermore, pressure fluctuations from the peristaltic pumps led frequently to disturbances in the droplet generation resulting in droplets with varying sizes (Fig. 23B lower image). In order to achieve faster and more consistent droplet generation and to enable encapsulation of other hydrogels with thermal crosslinking mechanisms (agarose and Matrigel), a commercially available microfluidic system (µEncapsulator) was obtained. The µEncapsulator system consists of pressure pumps and flow rate sensors for precise control of the flow rates (Fig. 24). It comprises also a temperature controlling unit (TCU), a microscope with integrated high-speed camera and is compatible with a variety of reusable microfluidic chips made of glass, which makes them long-living and stable to high pressures.

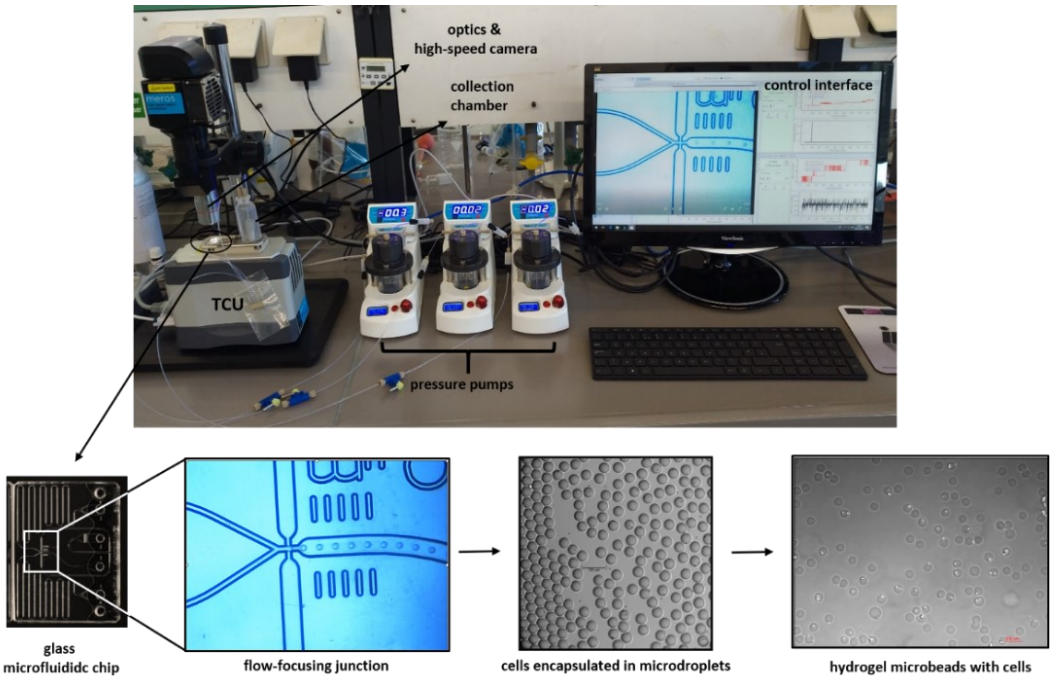

Figure 24. Composition of the µEncapsulator system and images of droplets and hydrogel microbeads generated with the device.

Cell encapsulation using the µEncapsulator system and a microfluidic chip with 50 µm junction in combination with fluorinated oil with 2 % PicoSurf surfactant as continuous phase resulted in highly homogeneous and stable droplets (Fig. 24). The size of the monodispersed droplets was estimated using area calculation of 100 droplets (ImageJ). Droplet formation at flow rates of 4 µL/min and 35 µL/min for the aqueous and oil phases, respectively, generated microdroplets with 44 µm diameter and 45 pL volume on average. Generation of hydrogel microbeads was successful using internal gelation of alginate, as well as thermal crosslinking of ultra-low gelling temperature agarose and Matrigel.

5.2.2. GMD-FACS of agarose and alginate microbeads

Sorting of hydrogel microbeads using a standard FACS device (BD Influx™) required some technical changes and settings optimization. Particle size plays a decisive role in the sorting process, thus standard settings for sorting of yeast and mammalian cells needed to be adopted to the significantly bigger hydrogel microbeads. To this end, a 200-micron outer nozzle was installed, which enabled sufficient sheathing of the microbeads with sheath buffer, required for generation of a stable stream, as well as for effective charging and deflection of the FACS drops. Furthermore, in case of alginate hydrogel, the sheath fluid for the FACS device needed to be exchanged and optimized, since PBS-based sheath buffer dissolved the microbeads by precipitation of non-soluble calcium phosphates. Therefore, Tris buffer with 1 mM $CaCl_2$ was used as sheath fluid for the FACS processing of alginate microbeads.

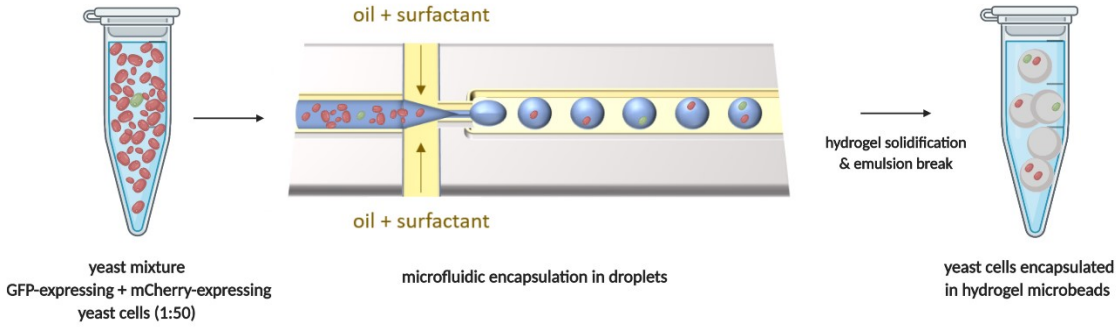

Figure 25. Generation of hydrogel microbeads containing yeast cells. Green fluorescent yeast cells (EBY100-tGFP) were mixed with red fluorescent yeast cells (EBY100-mCherry) at a 1:50 ratio. Encapsulation was performed using the µEncapsulator system with cells resuspended in medium containing either ultra-low gelling temperature agarose or alginate, dissolved in Ca-EDTA solution. Directly after encapsulation the hydrogel was solidified and following emulsion break, the yeast-loaded hydrogel microbeads were sorted by FACS.

The sorting process of hydrogel microbeads was validated using GFP-producing yeast cells mixed with an excess of red fluorescent protein (mCherry)-expressing yeast cells, which were together encapsulated in alginate or agarose microbeads (Fig. 25). FACS selection of GFP-expressing yeast cells was successful both for agarose and alginate, resulting in predominantly green fluorescent yeast populations after a single sorting round (Fig. 26 A and B, sort outcome). Moreover, fluorescence microscopy of sorted populations revealed reliable selection of desired populations and specific discrimination between beads containing cells with one fluorescent marker or both (Fig. 26 on the left).

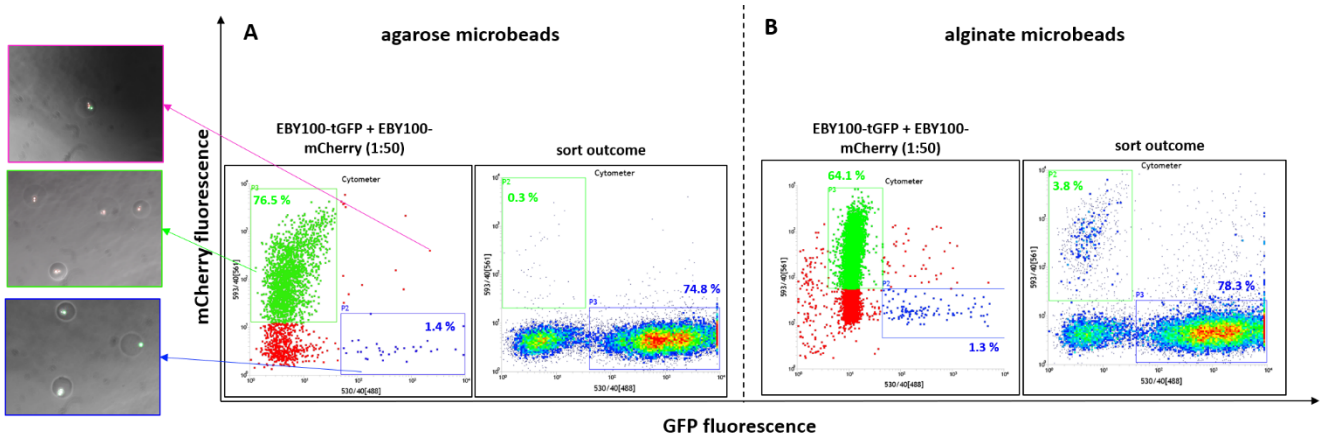

Figure 26. Test of GMD-FACS efficiency using yeast cells encapsulated in (A) agarose and (B) alginate microbeads. Yeast-loaded hydrogel microbeads were sorted by FACS. Sorting efficiency was analysed by sorting mCherry-positive (green), GFP-positive (blue), and double-fluorescent (magenta) events, followed by fluorescence microscopy (on the left). Analysis of sort outcome was performed after propagation of the sorted GFP-positive yeast on agar medium.

5.2.3. Mammalian cell viability and reporter cell activation using different hydrogels

Since a reporter cell line stably expressing split-GFP$_{1-10}$ for detection of cytoplasm-penetrating antibodies was not available, two other reporter cell lines were utilized for verification of the functional selection concept. Ba/F3-CIS-d2EGFP cells were used to demonstrate the suitability of the system for isolation of biologically active cytokines (interleukin-3) (chapter 5.3), while NF-κB/Jurkat/GFP reporter cells served as a model for establishing a functional screening procedure for selection of agonistic antibodies (chapter 5.4). In order to evaluate possible negative effects of the encapsulation procedure and droplet microenvironment upon the viability and functionality of the mammalian reporter cells, reporter cells were encapsulated in droplets, containing different hydrogel-forming agents (agarose, alginate, Matrigel). Hydrogel microbeads were recovered after incubation overnight in the w/o emulsion and dead cells were stained with propidium iodide, followed by flow cytometrical analysis (Fig. 27A).

Cell viability measurement revealed minimal negative effects of the encapsulation procedure and incubation conditions in emulsion when no hydrogel-forming polymer was added to the encapsulation mix, with over 75 % viable cells of both reporter cell lines (Fig. 27B, medium only). By adding alginate, drastic reduction of the cell viability could be observed, especially in case of the NF-κB/Jurkat/GFP cells. This effect is most likely caused by limited nutritional supply inside the microdroplets, where a big portion of the droplet volume is occupied by the polymer. Furthermore, in case of alginate, the hydrogel crosslinking procedure involves a short incubation step under acidic conditions, which seemed to induce additional negative effects and can be observed as a small cell population with high GFP fluorescence, but elevated PI-signal (Fig. 27A, black arrow). In case of Matrigel, Ba/F3-CIS-d2EGFP cells demonstrated higher cell viability of about 60 %. However, no hydrogel microbeads could be recovered from cell-containing droplets incubated overnight, whereas Matrigel-formation was possible by solidification and beads recovery directly after encapsulation. This indicated digestion of Matrigel overnight by secreted cell proteases, a phenomenon which has been previously reported[227]. For this reason, Matrigel was not further used for encapsulation experiments despite higher viability of the cells in the presence of this matrix. At

the same time, encapsulation in agarose microbeads resulted in similar viability of both reporter cell lines, with variations in the range of 30-70 %, between different samples.

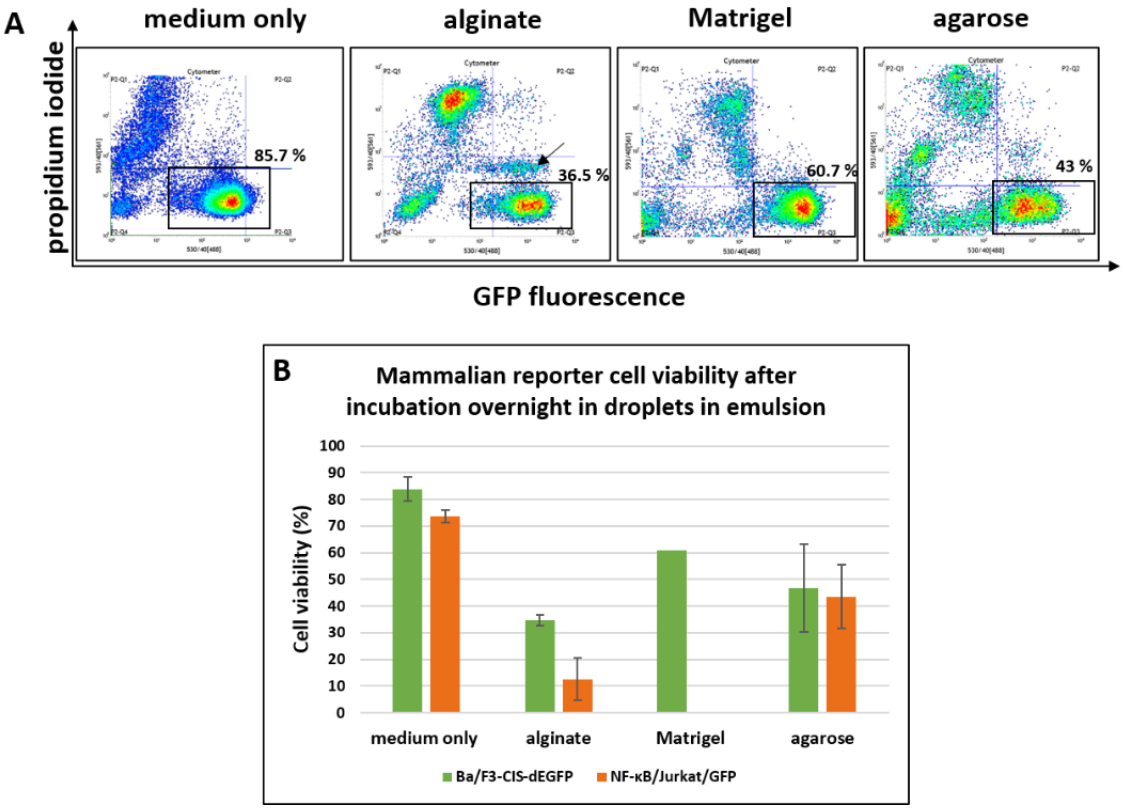

Figure 27. Mammalian cell viability in different hydrogel microbeads. (A) Two-dimensional FACS plots of Ba/F3-CIS-d2EGFP reporter cells encapsulated in droplets and incubated overnight in emulsion. Cells were encapsulated in medium with or without addition of hydrogel-forming polymers (alginate, Matrigel, and agarose). Water-in-oil emulsion was incubated overnight at 37 °C, 8 % CO_2, 110 rpm. On the following day, hydrogels were solidified and the emulsion was broken. Dead cells were stained with propidium iodide (PI) and microbeads (or free cells in case of medium only) were analysed using flow cytometry. Fraction of living cells was defined as the population with strong GFP signal and low PI-fluorescence (black box). **(B)** Cell viability of Ba/F3-CIS-d2EGFP and NF-κB/Jurkat/GFP reporter cells in droplets containing different hydrogel-forming polymers determined by flow cytometry. Error bars are the result of three independent encapsulation experiments.

Next, the expression of the reporter protein (GFP) upon activation of the reporter system in droplets was investigated. To this end, the reporter cells were encapsulated in medium containing different hydrogel forming polymers with or without addition of reporter activators (murine interleukin-3 (mIL-3) for Ba/F3-CIS-d2EGFP (Fig. 30) and human tumour necrosis factor alpha (hTNFα) in case of NF-κB/Jurkat/GFP (Fig. 47)). Following incubation overnight in emulsion at 37 °C, hydrogel microbeads were gelled and GFP fluorescence was analysed by flow cytometry (Fig. 28).

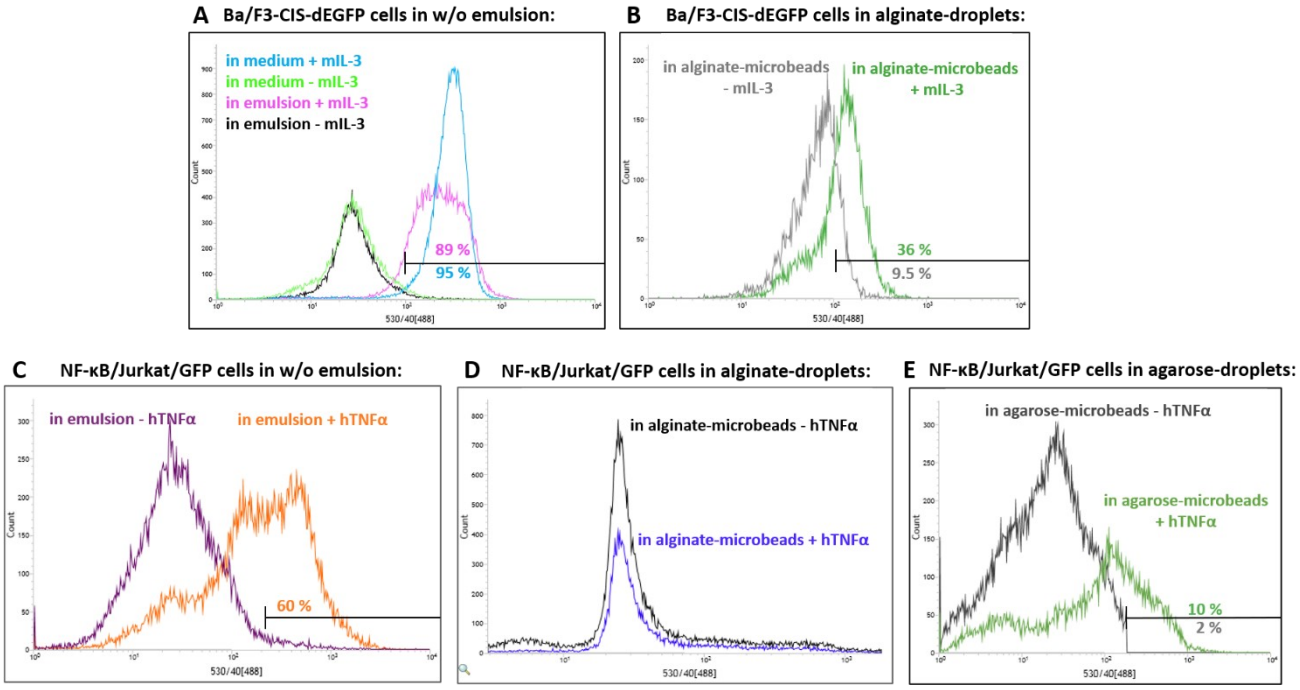

Figure 28. Activation of reporter cells encapsulated in droplets containing different polymers. (A) GFP fluorescence signal of Ba/F3-CIS-d2EGFP cells encapsulated in droplets consisting only of medium with or without addition of murine interleukin-3 (20 ng/mL) and incubated in emulsion (black and magenta). For comparison activation of reporter cell in a 96-well plate in the same medium composition (blue and green). **(B)** GFP fluorescence of Ba/F3-CIS-d2EGFP cells encapsulated in alginate-containing (1 % (w/v)) medium, incubated overnight in emulsion and crosslinked prior to flow cytometry analysis. **(C)** Activation of NF-κB/Jurkat/GFP cells encapsulated in droplets consisting only of medium with or without addition of human tumour necrosis factor alpha (20 ng/mL) and incubated in emulsion. **(D)** GFP fluorescence of NF-κB/Jurkat/GFP cells encapsulated in medium, containing 1 % (w/v) alginate, incubated overnight in emulsion and crosslinked on the next day prior analysis. **(E)** Activation of NF-κB/Jurkat/GFP cells encapsulated in agarose-containing (0.75 % w/v)) medium, incubated overnight in emulsion and solidified prior analysis.

Reporter protein expression was sufficient for both cell lines if encapsulated in droplets without addition of hydrogel-forming agent (Fig. 28A and C). In case of Ba/F3-CIS-d2EGFP, 89 % of all analysed cells exhibited elevated GFP fluorescence intensity in comparison with cells encapsulated without addition of mIL-3 (black and magenta histograms). At the same time incubation in a 96-well plate in the same medium composition resulted in slightly higher number of GFP-positive cells (95 %) and increased mean fluorescence intensity ((Fig. 28A blue histogram), indicating a weak negative effect of the encapsulation procedure and incubation in the w/o emulsion on the mammalian cells. The assessment of reporter cell activation indicates that GFP expression correlates tightly with the viability of the reporter cells under the tested conditions. In case of NF-κB/Jurkat/GFP, no GFP positive cells could be observed after encapsulation in alginate microbeads (Fig. 28D), whereas 60 % of the Jurkat cells demonstrated strong GFP expression in medium-only droplets and 10 % in agarose-containing droplets. These results are again in accordance with the cell viability measured under the indicated conditions (Fig. 27B). Generally, NF-κB/Jurkat/GFP demonstrated significantly lower cell viability and activation levels in comparison to Ba/F3-CIS-d2EGFP, which seemed more robust and resistant to the process.

5.3. Functional Selection of Active Interleukin-3 Variants

For proof-of-concept verification of the functional selection approach, a cytokine-responsive murine reporter cell line was utilized (Fig. 30) in combination with cytokine-secreting *S. cerevisiae* cells. Cytokines are small signalling proteins secreted by immune cells with growth-promoting, pro- or anti-inflammatory effects[228]. Implementation of interleukin-3 for induction of reporter cell activation, was chosen due to the small size, monomeric protein structure and high potency of this cytokine. Furthermore, the murine Ba/F3-CIS-d2EGFP reporter cells demonstrated higher cell viability and reporter cell activation under the tested conditions in hydrogel microdroplets, compared to the second available reporter cell line (NF-κB/Jurkat/GFP). Since implementation of agarose as hydrogel-forming polymer sustained higher cell viability for both reporter cell lines, it was preferred for the further encapsulation experiments and screens over alginate.

Based on the murine Ba/F3 reporter cell line, a workflow for isolation of biologically active mIL-3 variants was designed. The functional screening procedure is illustrated in Figure 29.

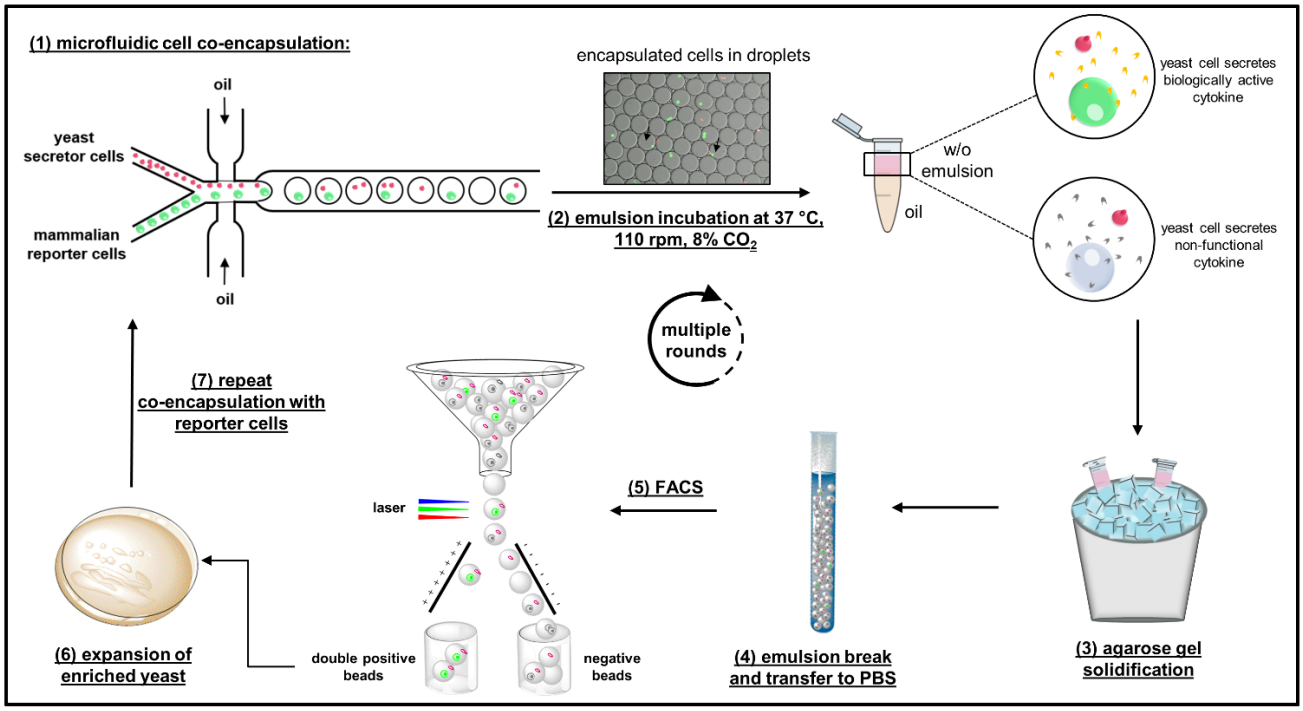

Figure 29. Workflow scheme of a functional screening procedure for selection of active mIL-3 cytokine variants.

The mIL-3-responsive mammalian reporter cells are co-encapsulated with cytokine-secreting *S. cerevisiae* in agarose-containing microdroplets (Fig. 29) and are incubated overnight at 37 °C, 110 rpm, 8 % CO_2 in the w/o emulsion. Actively secreting yeast cells express an intracellular red fluorescence protein (mCherry). Since the reporter cells are mIL-3-dependent for cell growth and are propagated in the presence of the cytokine, they are fluorescent at beginning of the encapsulation process. However, if a reporter cell is co-encapsulated in a droplet with a yeast cell which secretes a non-functional cytokine, the GFP intensity of the reporter cell reduces over time. In contrary, in the presence of a yeast cell secreting a biologically active mIL-3 variant, the GFP fluorescence intensity remains high. Following the incubation step, the agarose in the droplets is solidified by incubation on

ice and agarose microbeads are recovered in PBS. Selection by FACS is conducted by sorting of double-fluorescent agarose microbeads, containing mCherry-positive yeast and GFP-positive mammalian cells. Sorted hydrogel microbeads are plated on selective agar for expansion of yeast cells and the encapsulation and sorting process is repeated in multiple rounds until sufficient enrichment of biologically active cytokines is achieved.

5.3.1. Murine interleukin-3-dependent activation of a reporter cell line

For the purpose of a proof-of-concept functional screen, a murine Ba/F3 reporter cell line, expressing GFP upon stimulation with mIL-3 was used (Fig. 30). Interleukin-3 is an important regulator of hematopoiesis and growth factor inducing proliferation of pluripotent stem cells, as well as supports the functional activity of some fully differentiated cells[229].

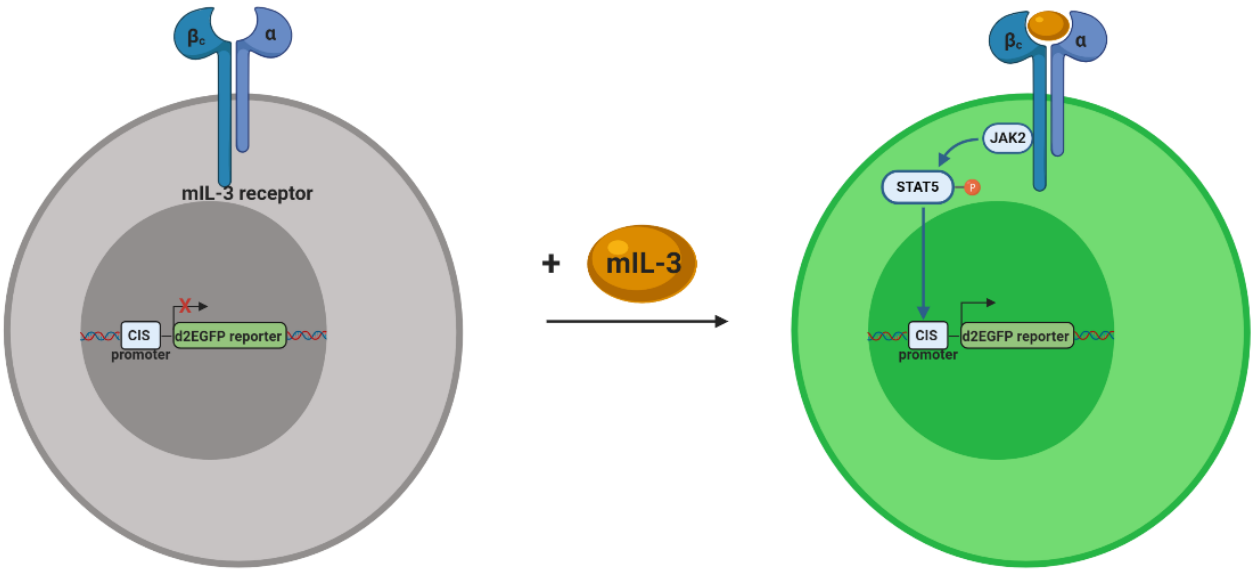

Figure 30. Activation of GFP expression in Ba/F3-CIS-d2EGFP reporter cells. Gene for destabilized green fluorescent protein (d2EGFP) is placed under the control of the STAT5-inducible CIS promoter. Upon binding of murine interleukin-3 to its receptor, the JAK2/STAT5 pathway is activated leading to expression of the reporter protein and strong GFP fluorescence of the reporter cells. Scheme was generated with Biorender according to Reddy *et al.* (2000)[230] and Robin *et al.* (2010)[231].

Expression of destabilized green fluorescent protein (d2EGFP) is induced upon binding of mIL-3 to its receptor on the reporter cell surface and activation of the JAK2/STAT5 pathway (Fig. 30). Short-lived GFP reporter was used in order to enable faster GFP degradation upon mIL-3 deprivation, since mIL-3 is required for propagation and cultivation of the reporter cells. D2EGFP is generated by fusion of enhanced GFP to mouse ornithine decarboxylase (MODC), which is one of the mammalian proteins with most rapid turnover (most short lived)[232]. This fusion strategy reduces the half-live of the GFP reporter from approx. 15 hours[233] to 2 hours[232].

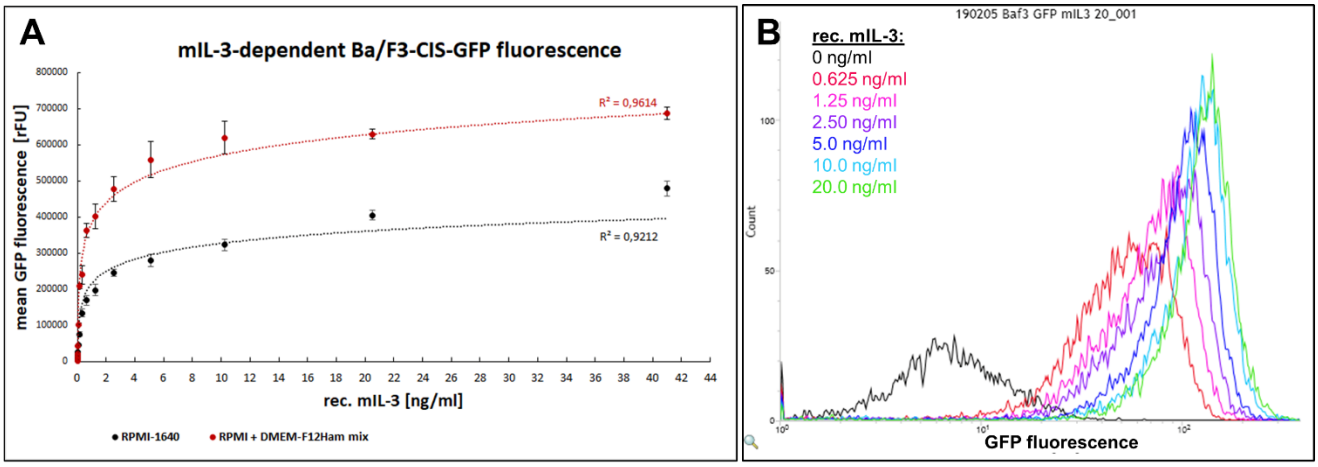

Figure 31. Reporter activation in Ba/F3-CIS-d2EGFP cell line in dependency to the mIL-3 concentration. (A) Mean GFP fluorescence intensity determined by flow cytometry after incubation overnight of reporter cells in a 96-well plate with a dilution row (2.5 pg/mL – 41 ng/mL) of recombinant mIL-3 in standard cultivation medium (RPMI-1640) or a medium mix (50 % RPMI-1640 + 50 % DMEM-F12 Ham + 2 % w/v galactose). GFP signal was normalized to the negative control (reporter cells incubated without mIL-3). Dashed lines represent logarithmic trendlines. Error bars are result of measurement of three biological replicates. **(B)** Flow cytometry histograms of reporter cells activated with different concentrations of rec. mIL-3 obtained on BD Influx™ Cell Sorter.

First, the response of the mIL-3 inducible reporter cell line in relation to the mIL-3 concentration was examined and revealed a dose-dependent increase in the GFP fluorescence intensity upon stimulation with recombinant mIL-3 with concentrations in the range of 0.01 – 40 ng/ml (Fig. 31A). Additionally, flow cytometry analysis confirmed sufficient population separation of the non-activated (0 ng/mL rec. mIL-3) and weakly-activated (0.625 ng/mL rec. mIL-3) reporter cells (Fig. 31B), which proves the compatibility of the reporter system with a FACS-based positive selection.

5.3.2. Generation of a non-functional mIL-3 mutant

A non-activating mIL-3 variant with minimal sequence alterations (single amino acid substitution) was desired for verification of the functional screening approach. Based on the study of Klein *et. al* (1997) regarding the receptor-binding site of human IL-3, one amino acid substitution (E22G) in human IL-3 was determined as suitable for our purposes, since it resulted in >300 fold reduction in growth-promoting activity, while retained the relative binding to the α receptor subunit of human IL-3 receptor[234]. In order to identify the corresponding position in the murine mIL-3 ortholog, a structural alignment with human mIL-3 was performed, revealing a conserved glutamate at position 49 in the murine IL-3 sequence (Fig. 32B) with a similar spatial orientation to E22 in hIL-3 (Fig. 32A).

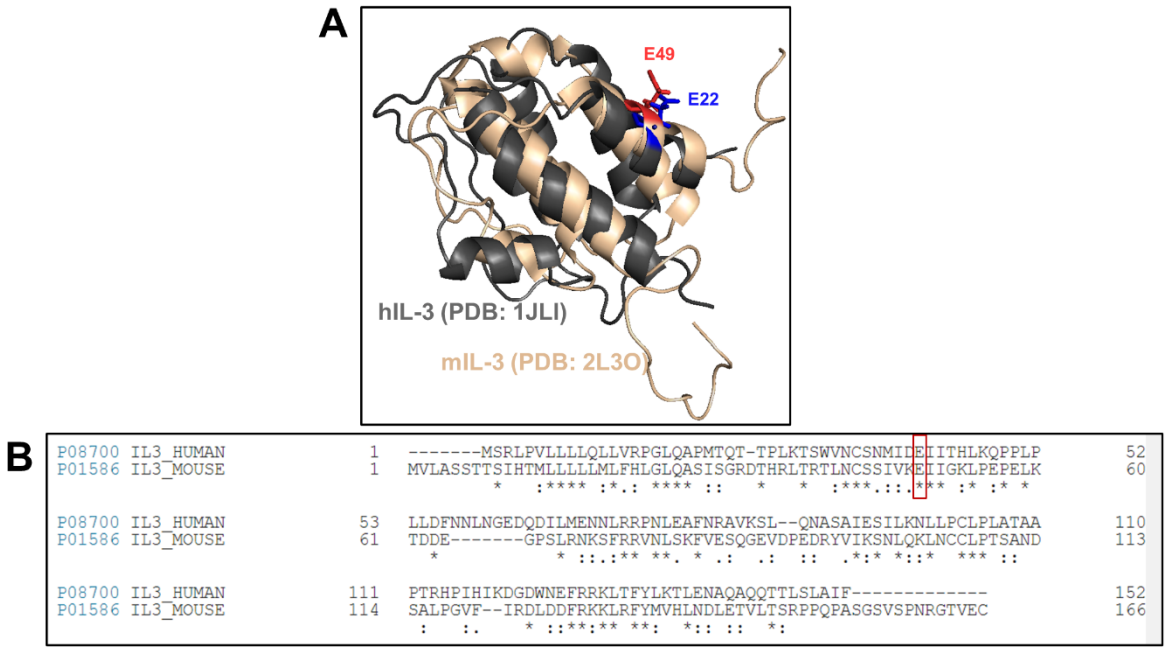

Figure 32. Structural and sequential comparison of human and murine IL-3. (A) Protein structures were obtained from PDB and aligned using PyMol. **(B)** Amino acid sequences were obtained and aligned using UniProt data base.

Sequences of wildtype mIL-3 and the mutant E49G were constructed for secretion by *S. cerevisiae* as illustrated in Figure 33. Galactose-induced transcription (GAL1 promoter) leads to generation of a single mRNA transcript, comprised of the transcripts of mIL-3 and red fluorescent protein (mCherry). Ribosomal skipping peptide (T2A) between the two genes facilitates the translation of two separate proteins: mIL-3 with N-terminal secretion signal (app8[218]) is secreted in the culture medium, while mCherry remains trapped intracellularly and accumulates in a correlation to the expression rate of the cytokine[219], serving as an expression control. This construct enabled the detection of agarose microbeads containing an actively secreting yeast cells during the selection process by FACS.

Figure 33. Gene construct for the expression and secretion of mIL-3 in *S. cerevisiae*.

5.3.3. Reporter cell activation by mIL-3 in yeast culture supernatant

A reporter cell activation assay using yeast supernatant was performed in order to verify successful secretion of mIL-3 wt and E49G mutant from *S. cerevisiae* and to prove the functionality of the cytokine with respect to the reporter system. To this end, yeast cells were cultured under expression conditions (2 % w/v galactose in medium) until sufficient cell density and mCherry-fluorescence were reached (Fig. 34C). Cytokine-containing yeast supernatant was then harvested and added to the reporter cells (Fig. 34A). In case of sufficient secretion of the wt mIL-3, GFP expression in the mammalian cells is induced and the cells remain fluorescent, while in case of the non-functional E49G mutant a decrease in the fluorescence intensity over time is expected.

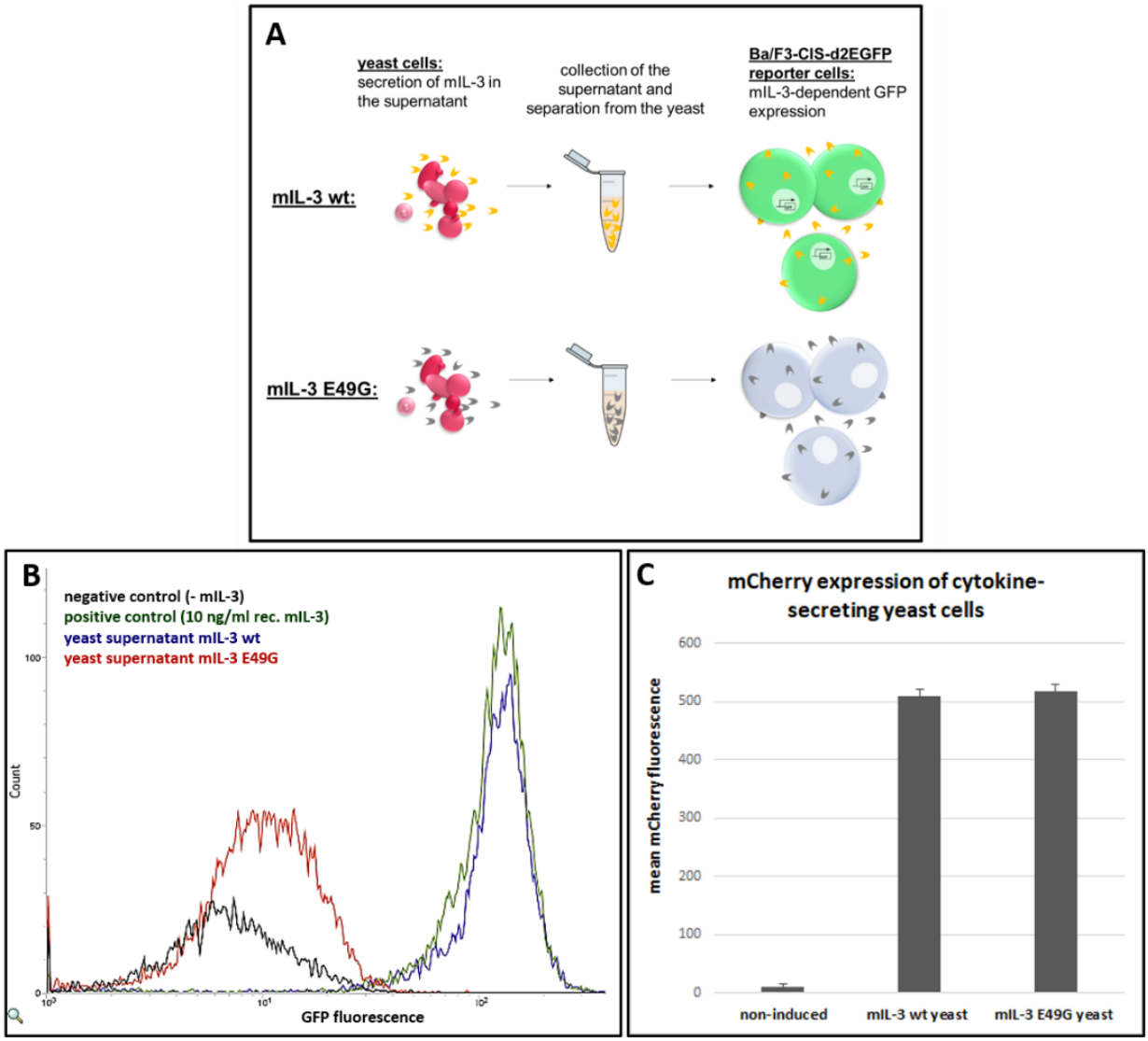

Figure 34. Reporter cell activation assay using yeast supernatant. (A) Scheme of the assay components. **(B)** Flow cytometry histograms of Ba/F3-CIS-d2EGFP reporter cells incubated with yeast supernatant after expression and secretion of mIL-2 wt or mIL-3 E49G from *S. cerevisiae*. **(C)** Mean mCherry fluorescence in rFU of yeast cells before and after induction with galactose. Error bars are result of two flow cytometry measurements of the corresponding samples.

Reporter cell activation assay was analysed by flow cytometry after 16-18 h of treatment of the reporter cells with the yeast supernatant (Fig. 34B). Ba/F3-CIS-d2EGFP cells incubated with the culture supernatant of the mIL-3 wt- secreting yeast exhibited strong GFP fluorescence (blue histogram), while yeast supernatant containing the mutated mIL-3 variant induced GFP expression levels comparable to the negative control (red and black histograms). Simultaneously, mCherry fluorescence intensity was identical for both mIL-3 variants (Fig. 34C) and the discrepancy in the yeast culture densities was negligible, indicating similar expression rates of both proteins. This result confirms successful cytokine secretion and accumulation in the yeast supernatant and at the same time verifies our assumption, that the single amino acid substitution E49G leads to strongly diminished reporter cell activation.

5.3.4. Growth of *S. cerevisiae* in different mammalian culture media

Investigation of reporter cell viability and activation levels revealed a thight correlation between cell viability and GFP expression rates (chapter 5.2.3). For a functional read-out by combination of yeast secretor and mammalian reporter cells, culturing conditions (O_2, CO_2, humidity, medium, temperature, etc.) suitable for both species should be identified. Generally, *S. cerevisiae* prefers 30 °C and slightly acidic cell extract-based media[235], while mammalian cells need to be cultured by strict conditions – 37 °C, 5 % CO_2, in defined synthetic media with complex composition. In order to address this problem, yeast cell growth in three standard mammalian culture media (DMEM, RPMI-1640, and DMEM-F12 Ham) was compared at two different temperatures (Fig. 35).

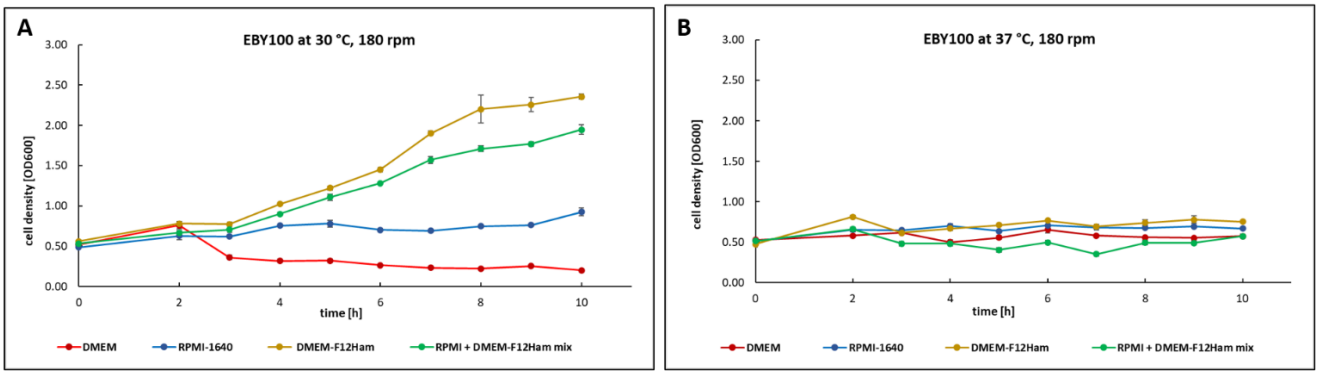

Figure 35. Growth curve of *S. cerevisiae* EBY100 in different mammalian culture media. (A) Culturing at 30 °C with 180 rpm orbital shaking. **(B)** Culturing at 37 °C with 180 rpm orbital shaking. Cell density was measured photometrically every hour for 10 h. Error bars are result of three photometrical measurements of the corresponding sample.

Cell proliferation was observed only at 30 °C (Fig. 35A), while at 37 °C no increase in the optical density even after 10 h could be measured for all samples (Fig. 35B). Moreover, sufficient cell growth was detected only in case of DMEM-F12 Ham medium (Fig. 35A, yellow curve), most likely due to the inorganic microelements contained in the F12 nutrition mix (e.g. cupric sulfate, ferric sulfate, zinc sulfate). Since the Ba/F3 reporter cells are commonly cultured in RPMI-1640 medium, but no significant yeast growth was observed in this medium (Fig. 35A, blue curve), a 1:1 mixture of RPMI-1640 + DMEM-F12 Ham was tested, resulting in slightly reduced, but sufficient yeast cell growth and viability (Fig. 35A, green curve). Furthermore, the activation of the reporter cells by rec. mIL-3 was not impaired in this medium mix, but stronger GFP fluorescence was measured (Fig. 31A, red curve) and reporter cell viability remained over 90 % in the 50 % RPMI-1640 + 50 % DMEM-F12 Ham medium mix (Fig. 36, red curve). Nevertheless, induction of yeast cells and protein expression seemed to correlate to the growth rates of the *S. cerevisiae*, which reduced drastically by lowering the proportion of the DMEM-F12 Ham in the medium mix (Fig. 36). Thus, in order to achieve a sufficient induction level, yeast cells were induced in minimal SG medium prior to co-encapsulation and coculturing experiments with mammalian reporter cells.

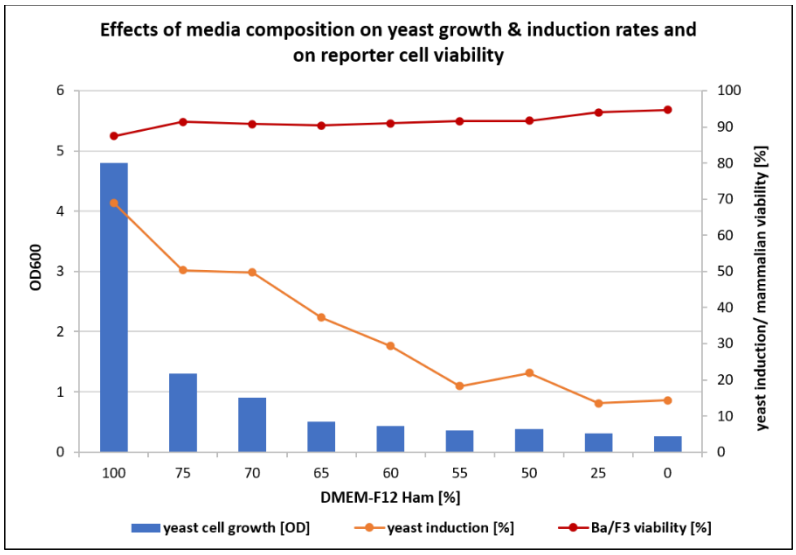

Figure 36. Medium-dependent yeast cell growth and induction rates, as well as mammalian reporter cell viability. DMEM-F12 Ham medium was mixed with RPMI-1640 in different ratios (0 % – 100 %) and supplemented with 2 % galactose and 1 % Pen/Strep. Yeast cell density (OD_{600}) was determined photometrically after 24 h of incubation at 30 °C, 180 rpm and induction levels were determined as fraction mCherry positive cells (%) by flow cytometry. Reporter cell viability was measured after staining with propidium iodide (PI) by flow cytometry and percent viable cells was plotted on the graph for each medium composition.

5.3.5. Cocultivation of mIL-3-secreting yeast cells and reporter cells in test tubes

Next, the activation of the reporter cells in the presence of live cytokine-secreting yeast cells was tested. Since no yeast cell growth could be observed at 37 °C (Fig. 35B), a concern regarding the cytokine secretion rates at 37 °C arose. In order to estimate which temperature is suitable for the purposes of coculturing in microdroplets, mammalian reporter cells were mixed with pre-induced cytokine-secreting yeast cells in medium and incubated at 37 °C and at 30 °C overnight, respectively (Fig. 37). Activation of the reporter cells was measured by means of flow cytometry (GFP fluorescence) and was used as a factor to determine the conditions supporting sufficient cytokine secretion from the yeast and high cell viability of the mammalian cells.

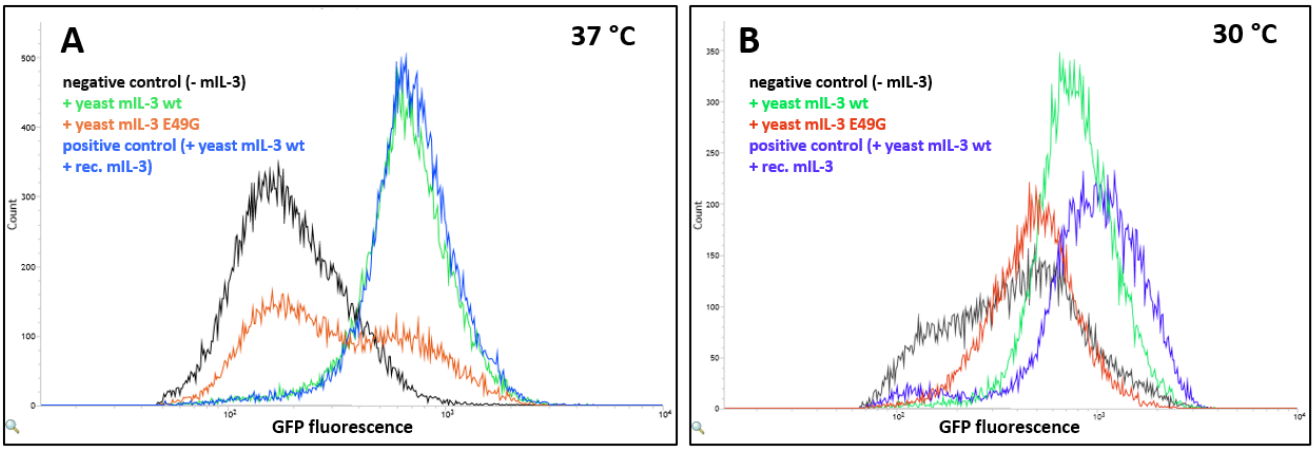

Figure 37. Cocultivation of live mammalian reporter (Ba/F3-CIS-d2EGFP) and yeast (*S. cerevisiae* EBY100) cells. Both cell types were suspended in 1 mL medium mix (50 % RPMI-1640 + 50 % DMEM-F12 Ham), supplemented with 2 % w/v galactose and 1 % Pen/Strep and were cocultured in 50 mL reaction tubes. Negative and positive controls represent reporter cells alone, without addition of cytokine, or reporter cells mixed with yeast cells and 20 ng/mL rec. mIL-3, respectively. **(A)** Incubation at 37 °C. **(B)** Incubation at 30 °C. Flow cytometry analysis was performed after 18 h of cocultivation. Histograms depict the GFP fluorescence signal of the mammalian reporter cells only.

Significant GFP fluorescence signal separation between the Ba/F3 reporter cells cocultured with the non-activating E49G mutant and the wildtype mIL-3 could be observed at 37 °C (Fig. 37A). Furthermore, the mIL-3 wt secretion level from the yeast cells was sufficient to induce maximal reporter cell activation, which could not be enhanced further by the addition of recombinant mIL-3 (Fig. 37A, positive control). In contrast, coculturing at 30 °C resulted in high reporter cell mortality, leading to insufficient activation of the mammalian cells, even after stimulation with rec. mIL-3 (Fig. 37A, positive control). With the aid of this experiments, coculturing at 37 °C, 8 % CO_2 in humidified atmosphere in a medium consisting of 50 % RPMI-1640 + 50 % DMEM-F12 Ham + 2 % galactose w/v + 1 % Pen/Strep, was determined as optimal for the means of functional screening procedure in microdroplets.

5.3.6. Activation of reporter cells by co-encapsulation with cytokine-secreting yeast

Activation of the mammalian reporter cells by secreted cytokines from yeast cells in agarose microdroplets was tested by co-encapsulation of the Ba/F3-CIS-d2EGFP cells together with yeast cells secreting either mIL-3 wt or the non-functional E49G mIL-3 mutant. Both samples were handled identically (as illustrated in Fig. 29) and were incubated as emulsion for 18 h at 37 °C. Microscopical analysis of the droplets in emulsion was performed directly after encapsulation and after the incubation period (Fig. 38). Directly after co-encapsulation with mIL-3 wt-, or mIL-3 E49G-secreting yeast cells, the mammalian cells in both samples showed strong GFP fluorescence (due to cultivation in presence of rec. mIL-3 for cell expansion), while no fluorescence background in the droplets could be observed (Fig. 38, 0 h). After incubation of the droplet- w/o-emulsion overnight, the droplets containing the non-functional mIL-3 variant exhibited diffuse fluorescence, spread throughout the whole droplet, implying cell lysis and release of the remaining GFP in the droplet (Fig. 38A, 18 h). In case of the activating mIL-3 wt-secreting yeast, significantly more mammalian cells appear intact, leading to mainly cell-concentrated GFP fluorescence with higher intensity when yeast cells are colocalised in the droplet. (Fig. 38B, 18 h).

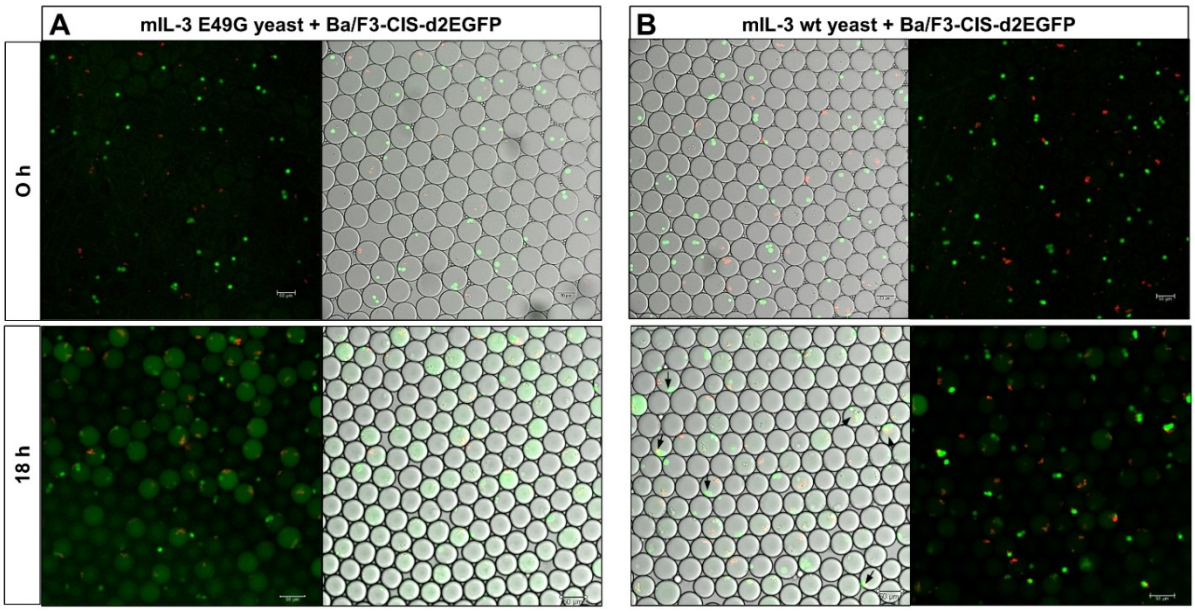

Figure 38. Microscopical analysis of co-encapsulated reporter and yeast cells. (A) Ba/F3-CIS-d2EGFP cells were co-encapsulated with mIL-3 E49G- secreting yeast. **(B)** Ba/F3-CIS-d2EGFP cells were co-encapsulated with mIL-3 wt- secreting yeast. Cells were co-encapsulated in agarose-containing droplets in w/o emulsion and were analysed on a confocal fluorescence microscope without solidification directly after emulsification (0 h) and after 18 h incubation at 37 °C, 8 % CO_2. Black arrows indicate droplets with yeast and mammalian cells in the same droplet.

These observations were confirmed by flow cytometry analysis of the solidified agarose microbeads (Fig. 39). While the mCherry fluorescence intensity of both samples remains identical, indicating the same cytokine expression levels (Fig. 39B), the GFP fluorescence in case of co-encapsulation with wt mIL-3 is significantly stronger (Fig. 39C). By comparison of the GFP intensity of the double-fluorescent agarose microdroplets, the mIL-3 wt-containing microbeads exhibited noticeably stronger GFP fluorescence (Fig. 39D) with 1 % lying in the high-stringency sorting gate (Fig. 39A P2-Q2).

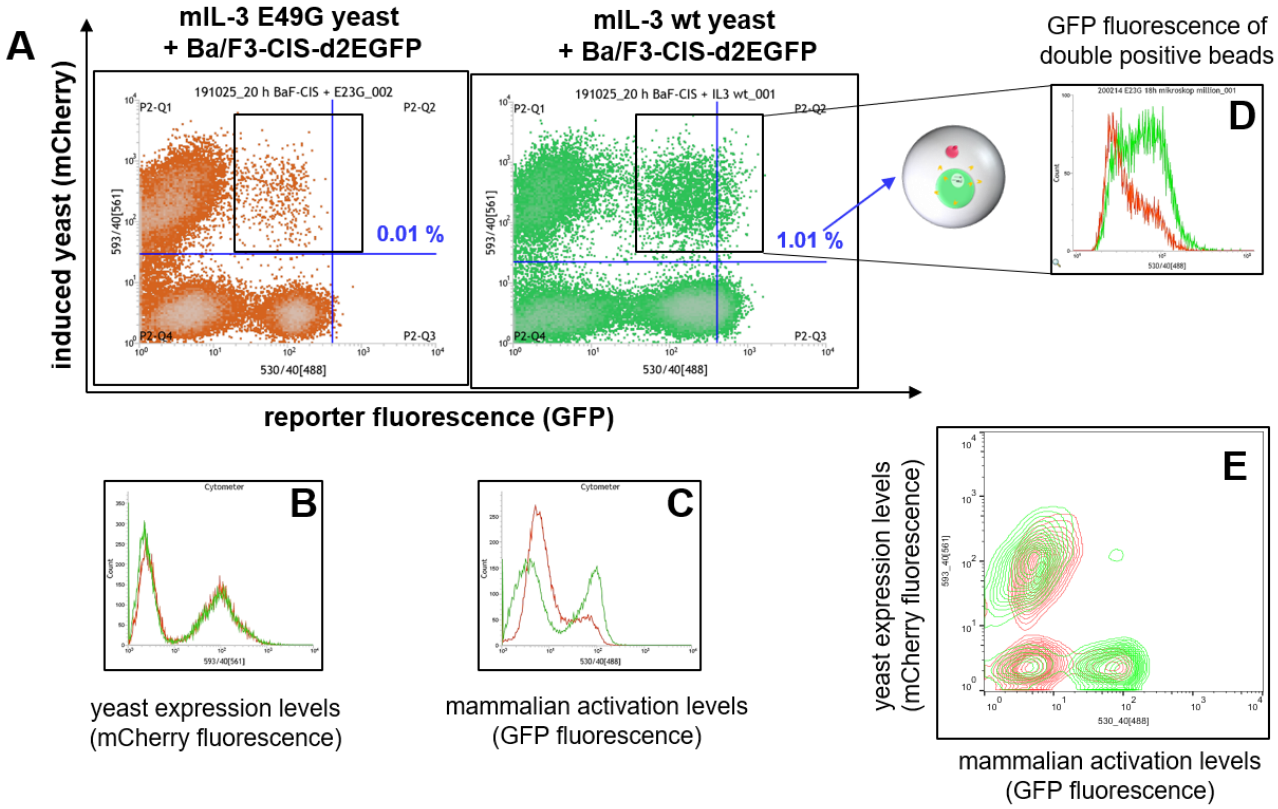

Figure 39. Flow cytometry of agarose microbeads containing mammalian reporter cells and cytokine- secreting yeast cells (mIL-3 E49G and mIL-3 wt) after 18 h incubation in emulsion at 37 °C. (A) Two-dimensional FACS plot: x-axis represents GFP fluorescence of reporter cells and y- axis depicts the mCherry fluorescence of yeast cells. Gating strategy (blue) represents the double-fluorescent hydrogel microbeads identified as positive events during sorting (P2-Q2). **(B)** Overlay of the mCherry fluorescence signals of both samples. **(C)** Overlay of the GFP fluorescence signals of both samples. **(D)** Overlay of the GFP fluorescence intensity of the agarose microbeads containing mammalian and yeast cells (black box) from both samples. **(E)** Two-dimensional overlay of both samples (generated with FlowJo).

The number of agarose microbeads with significantly enhanced GFP signal (1 %) is limited by multiple factors including mammalian and yeast cell viability, cell distribution in the droplets, and co-encapsulation efficiency. Cell distribution in the droplets is dependent on the cell density of the encapsulated suspension and on the droplet size and can be predicted by Poisson's equation (Equation 2). Thus, optimal occupancy (one yeast and one mammalian cell) occurs only in a fraction of all droplets, affecting directly the FACS selection. In case low cell density of both cell types is used for co-encapsulation, the co-encapsulation efficiency drops drastically, resulting in a very high number of useless droplets. On the other side, high cell density leads to encapsulation of multiple yeast/mammalian cells in one droplet, and sorting of multiple yeast clones based on mammalian response induced by a single yeast cell (false positive). However, during subsequent co-encapsulation and

selection cycles, the enriched false-positive yeast cells are eliminated to a large extend. Since our functional screen approach enables multiple screening rounds for specific enrichment of activating variants, more than one yeast cell per droplet is tolerated. Cell densities of 4×10^7 yeast cells/mL ($\lambda = 0.9$) and 2×10^7 mammalian cells/mL ($\lambda = 0.45$) were used for co-encapsulation. In order to determine the actual distribution of cells in the droplets, co-encapsulated cells in w/o emulsion were analysed microscopically (Fig. 38, 0 h). While about 55 % of all droplets were empty, approx. 23 % of the occupied droplets contained one yeast and 50 % one mammalian cell (Fig. 40B). Generally, yeast cells are prone to flocculation[236], which reflects the higher number of droplets with more than one yeast cell (38 %) in comparison to the fraction of droplets with more than one mammalian cell (19 %). Based on the microscopical analysis of 226 droplets, an average of 0.6 yeast and 0.41 mammalian cells per droplet were estimated, resulting in a theoretical co-encapsulation probability of about 15 % (Equation 4). On account that only about 70 % of the yeast cells exhibited sufficient mCherry fluorescence, the fraction of droplets containing an actively secreting yeast cell and a viable mammalian cell was determined by flow cytometry to be in the range between 8 % and 10 % of all droplets (Fig. 40A). Furthermore, since nutrition and space are limited inside the picolitre-volume droplets, co-encapsulation of a yeast cell with multiple mammalian cells could lead to false negative signals, due to reduced viability of the mammalian cells during the incubation step. To avoid losing desired variants due to false negative events, oversampling the yeast diversity during the co-encapsulation step at least 100 times is necessary. Nevertheless, with a generation speed of about 8×10^6 droplets/h using the µEncapsulator system, at least 8×10^5 yeast cells could be successfully co-encapsulated with a mammalian reporter cell in just one hour, making this system feasible for the screening of yeast-based libraries.

Equation 4. Calculation of co-encapsulation probability using Poisson's law.

$$P(x_1; x_2) = \frac{e^{-\lambda_1} \times {\lambda_1}^{x_1}}{x_1!} \times \frac{e^{-\lambda_2} \times {\lambda_2}^{x_2}}{x_2!}$$

$$P(x_1 \geq 1; x_2 \geq 1) = (1 - e^{-\lambda_1}) \times (1 - e^{-\lambda_2})$$

P = co-encapsulation probability
x_1 = number of mammalian cells in a droplet
λ_1 = average number of mammalian cells per droplet
x_2 = number of yeast cells in a droplet
λ_2 = average number of yeast cells per droplet

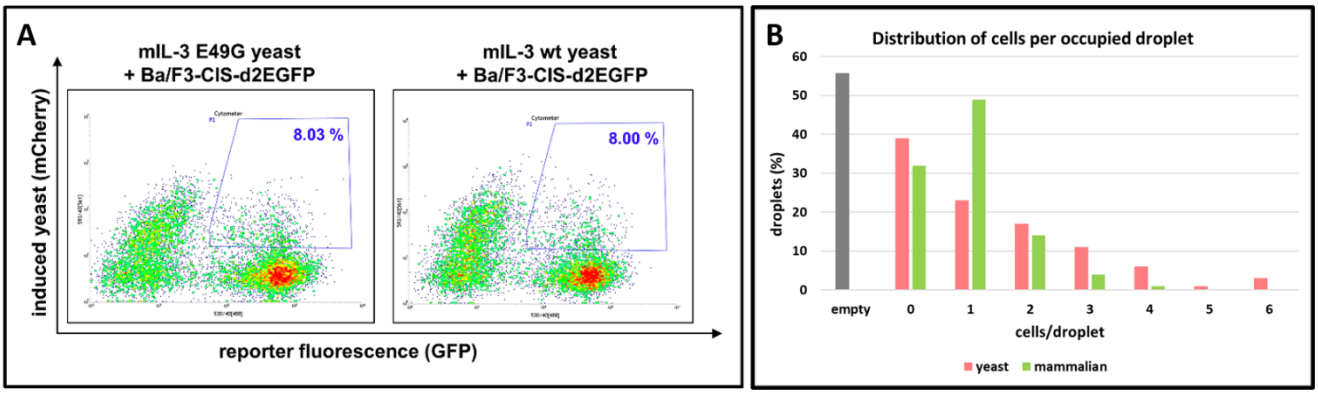

Figure 40. Analysis of cell distribution in the microdroplets and co-encapsulation efficiency of reporter and yeast cells. (A) Flow cytometrical analysis of co-encapsulation efficiency directly after co-encapsulation (0 h). Agarose containing droplets were generated by co-encapsulation of mammalian reporter cells with either mIL-3 wt- or mIL-3 E49G-secreting yeast cells, which were priorly induced overnight in autoinduction medium. Directly after encapsulation the w/o emulsion was cooled for 15 min on ice for agarose microbeads formation. Agarose microbeads were subsequently analysed on BD Influx™ FACS. Population in the blue gate represents double positive agarose microbeads, containing at least one mCherry-positive yeast and one GFP-positive reporter cell. **(B)** Distribution of yeast and mammalian cells inside the droplets. 226 droplets were analysed based on fluorescence microscopy images, 100 of the droplets contained cells and 126 were empty. Number of yeast and mammalian cells per corresponding droplet were estimated optically with help of the fluorescence signal of the cells (mCherry for yeast and GFP for mammalian reporter cells). Percentage of droplets with defined number of cells of a given cell type (0 to 6) per droplet was plotted.

5.3.7. Mixing experiments with an excess of the non-functional mutant and FACS-selection

In order to demonstrate the applicability of our system for a mammalian-based functional screen, the mIL-3 wt-secreting yeast cells were mixed with the yeast cells secreting the non-functional E49G mutant at different ratios (1:10, 1:100, 1:1,000, and 1:10,000). The mixed yeast cells were then co-encapsulated with the Ba/F3-CIS-d2EGFP reporter cells as illustrated in Figure 29 and only double-fluorescent agarose microbeads with strong GFP fluorescence were sorted (Figure S2). Enrichment of yeast cells secreting the functional mIL-3 wt cytokine was monitored by reporter cell activation assay using supernatants of the sorted populations, as well as by single yeast clone analysis by PCR with mIL-3 wt- specific primer (Figure S3), followed by verification of positive clones *via* reporter cell activation assay with supernatants from the corresponding single clone.

In case of the 1:10 and 1:100 mixing experiments, enrichment of mIL-3 wt-secreting yeast cells was detected after a single selection round (Fig. 41). Supernatant from bulk populations, after the selection procedure and yeast expansion, induced enhanced activation of the reporter cells (Fig. 41A and B), with a significant increase in the mean GFP fluorescence signal in case of the 1:100 mix. PCR screen of random single clones indicated 3 and 2 single clones with wildtype mIL-3 sequence from 13 tested clones after the first-round of the selection of the 1:10 and 1:100 mix, respectively (Figure S3A and B). Reporter cell activation assay with supernatants from the corresponding single clones confirmed biological activity of the secreted cytokines for all PCR-positive clones, except one (Fig. 41C). Nonetheless, the low reporter cell activation in case of clone 13 from the 1:10 mix lies with high probability on the very low cell density of the yeast culture, from which the supernatant was harvested.

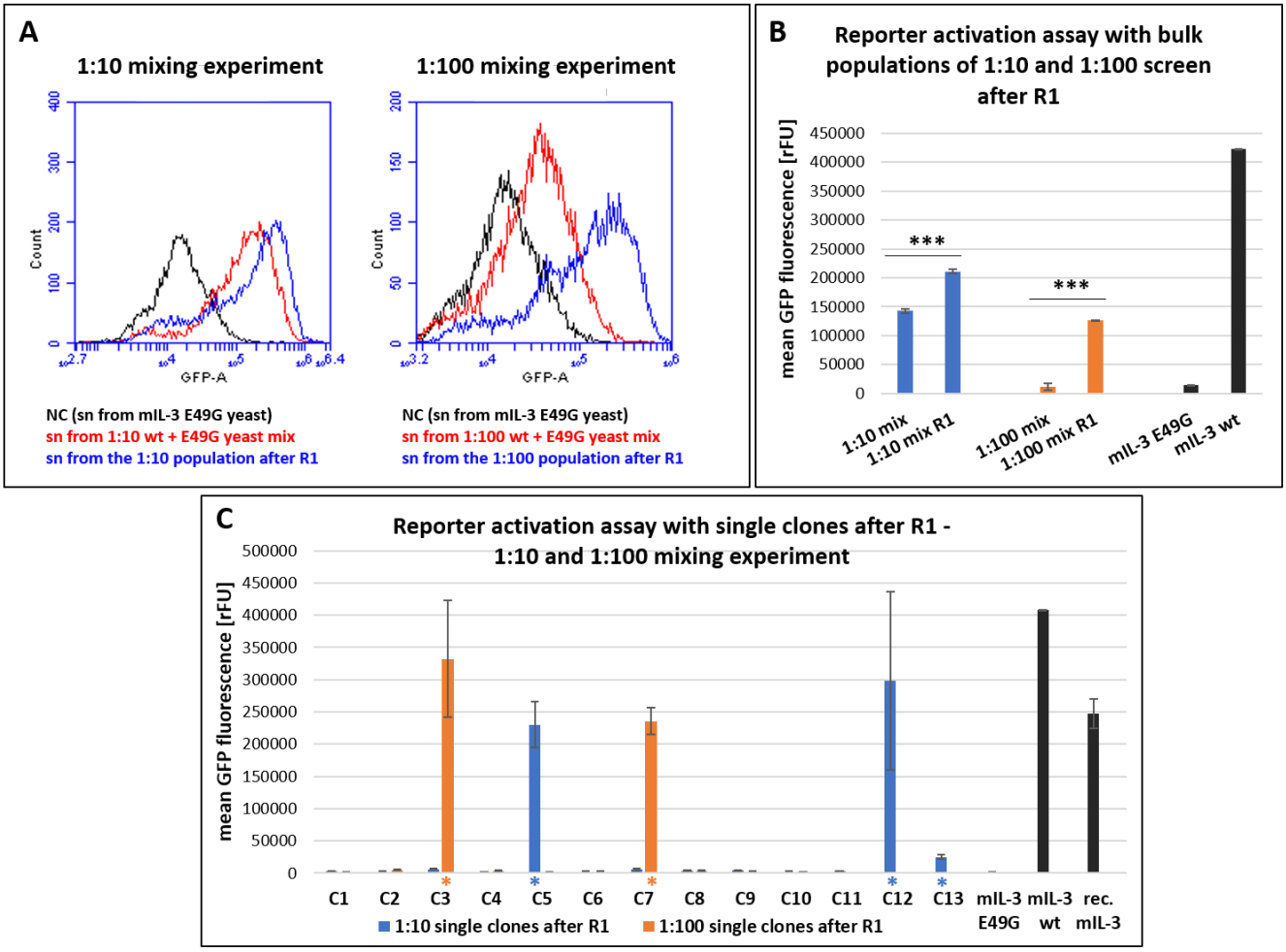

Figure 41. Analysis of enrichment of reporter cell-activating yeast (mIL-3 wt) after a single functional screening round of a 1:10 and 1:100 dilution with a non-functional mutant (mIL-3 E49G). (A) Flow cytometry histograms of reporter cell activation assay with supernatants (sn) of the populations before and after functional screening. **(B)** Mean GFP fluorescence of mammalian reporter cells after treatment with sn from the populations before and after functional screening in agarose microbeads. Statistical significance was analysed by One-way ANOVA, followed by Tukey HSD post-hoc test and was depicted with asterisks (*** P<0.001). **(C)** Reporter cell activation assay (mean GFP fluorescence) with sn from single clones after R1 of functional screening of the 1:10 and 1:100 mix. Single clones identified as mIL-3 wt by PCR screen are marked with an asterisk.

In case of 1:1,000 and 1:10,000 mixing experiments, two consecutive functional screening rounds were performed leading to gradual enrichment of reporter cell-activating yeast in the sorted populations from both samples (Fig. 42A and B). PCR screening after the second selection round revealed about 26 % mIL-3 wildtype clones for the 1:1,000 mixing experiment (Figure S3C) and about 17 % in case of the 1:10,000 sample (Figure S4). All of those clones demonstrated secretion of biologically active cytokine, confirmed by a reporter cell activation assay with supernatants from the respective positive clones (Fig. 42A and C). This corresponds to a 259- and 1666-times enrichment of mIL-3 wt-secreting yeast in the sorted populations, respectively (Table 3).

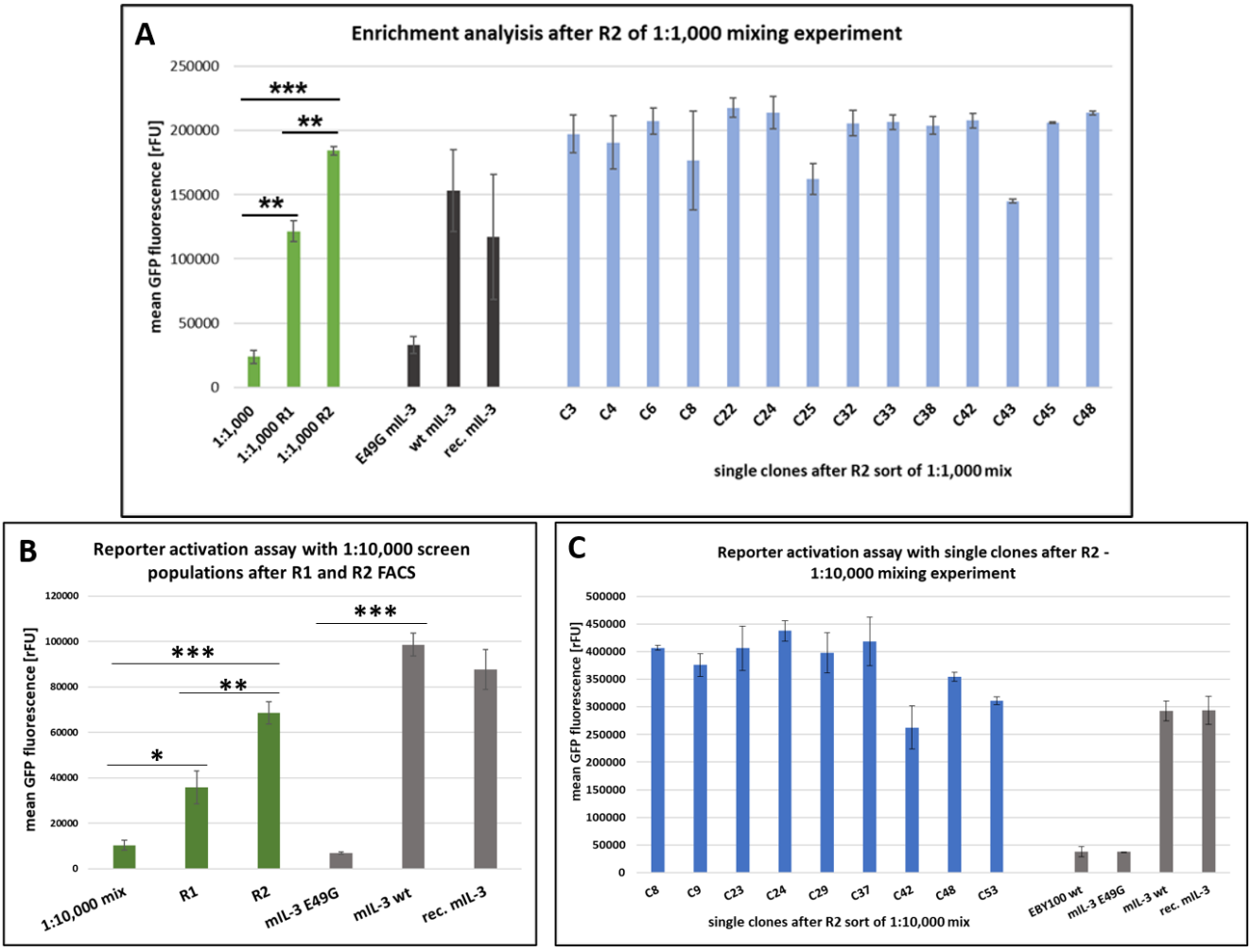

Figure 42. Analysis of enrichment of reporter cell-activating yeast (mIL-3 wt) after two consecutive functional screening rounds of a 1:1,000 and 1:10,000 dilution with a non-functional mutant (mIL-3 E49G). (A) Reporter cell activation assay with supernatants from bulk populations after the first and second sorting round of the 1:1,000 mixing experiment, as well as sn from single clones after the R2 functional selection, which were identified as mIL-3 wt in a PCR screen. **(B)** Reporter activation with supernatants from the bulk populations from the 1:10,000 mixing experiments after the R1 and R2 of functional screening. **(C)** Reporter activation using supernatants from single clones after second functional selection round of 1:10,000 mixed yeast (mIL-3 wt : mIL-3 E49G). Tested single clones were identified as positive in a PCR screen using mIL-3 wt- specific primer. Statistical significance was analysed by One-way ANOVA, followed by Tukey HSD post-hoc test. GFP signals from relevant samples were statistically compared and the statistical significance was marked with asterisks (* P<0.05; ** P<0.01; *** P<0.001).

All mixing experiments using an excess of yeast cell secreting the non-functional mIL-3 mutant, resulted in enrichment of yeast cells secreting the wildtype mIL-3 cytokine with biological activity. This proves the feasibility of the demonstrated selection approach based on functionality of secreted molecules from yeast cells, paired with mammalian reporter cell-based fluorescent readout through compartmentalisation in droplets with picolitre volume and FACS of hydrogel microbeads. The mixing experiments demonstrated one limitation of the process, regarding the enrichment degree to a maximum of 15-26 % (Table 3) of activating clones. However, this is compatible with most screening campaigns, since sufficient number of functionally active single clones could easily be identified by single clone analysis. If necessary, further increase in the enrichment degree could be achieved by decreasing the yeast cell density used for the co-encapsulation process. This would minimize

encapsulation of multiple yeast cells in the same droplet and thus, sorting of false positive yeast cells would be avoided.

Table 3. Overview of the results of the mixing experiments with the non-functional mIL-3 E49G mutant.

Ratio	*Round 1*		*Round 2*	
(wt : mutant)	Wildtype Clones	Wildtype Enrichment	Wildtype Clones	Wildtype Enrichment
1:10	3 of 13 (23.1 %)	2.3 times	not performed	
1:100	2 of 13 (15.4 %)	15.4 times	not performed	
1:1,000	2 of 52 (3.85 %)	38.5 times	14 of 54 (25.9 %)	259.3 times
1:10,000	not analysed		9 of 54 (16.7 %)	1666.6 times

5.3.8. Generation of a mIL-3 randomized library and screening for active variants

Functional screening procedure using mIL-3 + Ba/F3-CIS-d2EGFP activator-reporter system was verified using different ratios of yeast secretor cells producing the biologically active wildtype cytokine mixed with an excess of the non-functional mutant (E49G). Next, in order to test the functional screening approach in the context of yeast-based library comprising different cytokine variants, a small library was constructed by randomization of the knockout position (E49G) and the two surrounding amino acids (K48 and I50) (Fig. 43). Using a degenerative primer with NNR NNH HNN sequence (Fig. 43), a library with a theoretical diversity of 74,000 DNA sequences and 4,000 proteins was generated. Statistically, formation of only one mIL-3 wildtype molecule (1:4,000) was allowed and only generation of sequences with a codon distinct from the original glutamate codon (GAA instead of GAG)) at the position 49 was possible.

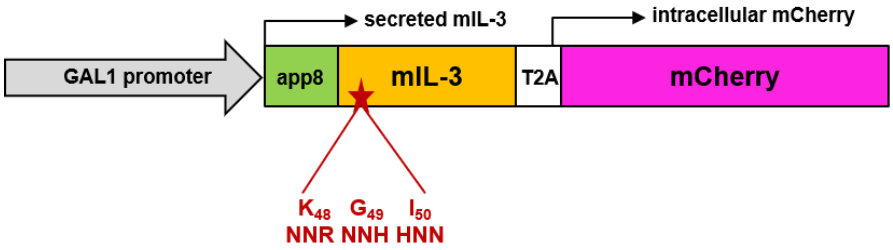

Figure 43. Randomization site in the mIL-3 E49G gene.

Randomization was performed by PCR and the library was transformed in *S. cerevisiae* (EBY100) using gap-repair cloning. Correct randomization was verified by Sanger sequencing, confirming desired distribution of the mutations (Figure S5A). Functional screening was performed in the same manner as the mixing experiments, by co-encapsulation of the library-secreting yeast cells together with the Ba/F3-CIS-d2EGFP reporter cells in agarose containing microdroplets (Fig. 29), followed by incubation overnight and FACS sorting of double-fluorescent agarose microbeads (Figure S5B). Although four consecutive selection rounds were performed, no significant enrichment of reporter cells-activating yeast in the expanded populations could be observed (Fig. 44A). Moreover, testing reporter cell activation with supernatants of 50 single clones after the third selection round did not reveal GFP expression induction by any of the tested clones (Fig. 44B). Functional

selection, using the randomized library was repeated in three more rounds, starting with the initial library, however again without success in enrichment of biologically active mIL-3 variants.

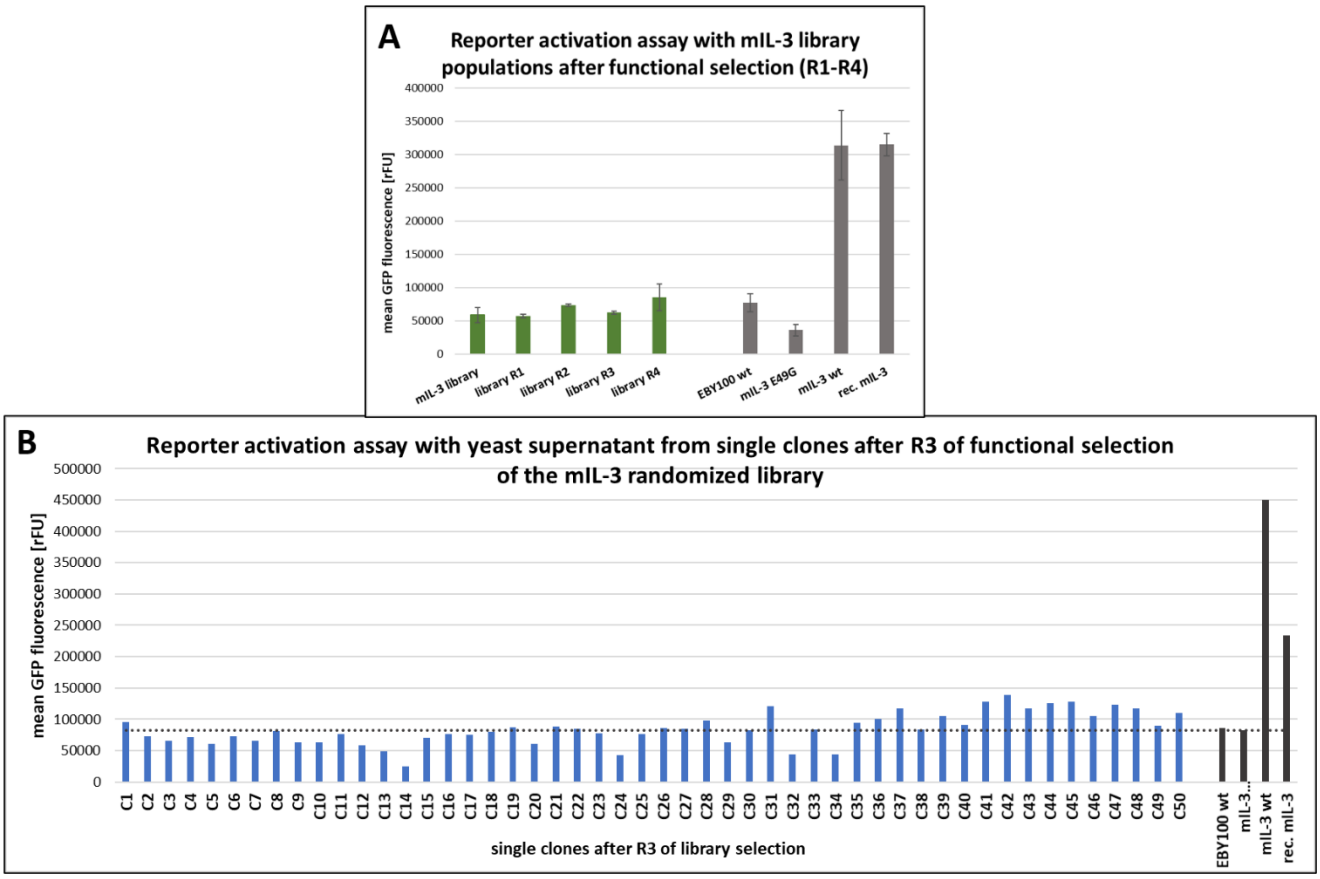

Figure 44. **Analysis of enrichment of reporter cell-activating yeast after four consecutive functional screening rounds with yeast cells secreting the randomized mIL-3 library. (A)** Reporter cell activation assay with supernatants from bulk yeast populations from each selection round (R1 – R4). **(B)** Reporter activation assay with supernatants from 50 randomly picked single yeast clones after R3 of functional selection.

5.3.9. Next generation sequencing

In order to gain an insight into the composition of the randomized library and to investigate the possible reasons for the failed enrichment of biologically active interleukin-3 variants, next generation sequencing (NGS) of the initial library, as well as of the yeast populations after selection rounds one to three was performed. For comparison, NGS of the 1:10,000 mIL-3 wt + mIL-3 E49G mixing experiments and of the corresponding enriched populations was performed, as well. To this end, barcoded primer were designed for each yeast population (chapter 3.5.3) consisting of a partial Illumina sequence (capital letters), a specific barcode (bold letters) and a gene complementary region (small letters). Plasmids were isolated from each sample and PCR was performed for amplification of the randomized region with the specific NGS primer. PCR products were mixed and sent for next generation sequencing.

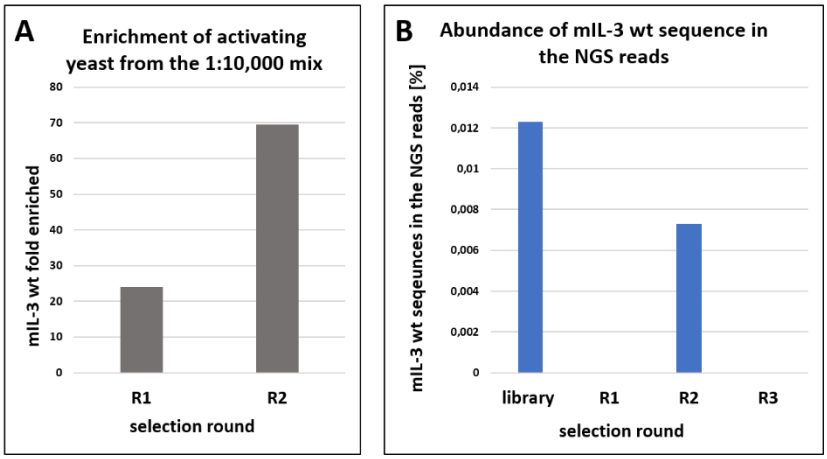

Figure 45. Analysis of NGS results. (A) Fold enrichment of mIL-3 wt NGS reads in the populations of the first and second rounds of functional screening of the 1 to 10,000 mixture of mIL-3 wt- and mIL-3 E49G-secreting yeast. **(B)** Relative abundance of wildtype mIL-3 sequence in the initial randomized mIL-3 library and in the yeast populations after functional selection rounds one to three. Sequence analysis was performed with Geneious 2020.0.5.

Over 120,000 NGS reads were obtained for the samples of both mIL-3 library and 1:10,000 mixing experiment. Analysis of the obtained sequences confirmed the gradual increase of wildtype mIL-3 sequences following each functional screening cycle of the 1:10,000 mixing experiment (Fig. 45A). However, in case of the randomized library, no enrichment of wildtype mIL-3 sequences could be observed (Fig. 45B). Although, statistically the frequency of wildtype cytokine clones should be 1 of 4,000 (0.025 %), the abundance of mIL-3 wt sequences in the initial library is only 0.012 % of all NGS reads, meaning the biologically active cytokine variant was twice as rare, as assumed. Furthermore, no significant enrichment of specific amino acid (aa) residues could be observed after detailed analysis of the NGS results (Fig. 46). Investigation of the relative frequency of all amino acid residues at the randomized positions (aa48, aa49, and aa50) revealed only minimal variation in the aa abundance between the selection rounds. Gradual enrichment of a specific residue throughout the selection process could only be observed for serine at position 49. However, in this case a fold enrichment of only 0.4 times could be achieved within the three consecutive selection rounds, which is too low to interpret as significant. After R2, valine is approx. 8 times more abundant at position 50 than in the initial library, however the relative frequency of this amino acid residue increased from 0.01 % to 0.08 % and dropped again to 0.01 % after the third selection cycle, indicating this result more likely as a sequencing artefact.

NGS analysis of the randomized library enabled a deep investigation of the library composition before and during the functional selection process. The abundance of wt mIL-3 clones in the initial library was lower than expected, which could represent one explanation for the unsuccessful enrichment of biologically active cytokine variants from the randomized library. Nevertheless, even if the frequency of the wildtype clone was only 0.012 % (meaning 1 of 8,000 yeast clones), it is still higher than the wildtype frequency in the 1:10,000 mixing experiment. Since the applicability of the functional screening procedure was demonstrated using the same yeast and reporter cells for a row of mixing experiments, which all resulted in a rapid enrichment of the functional wildtype cytokine, the low mIL-3 wt frequency in the initial library should not represent a huge limitation for the selection process, as long as enough yeast cells were used for the encapsulation procedure.

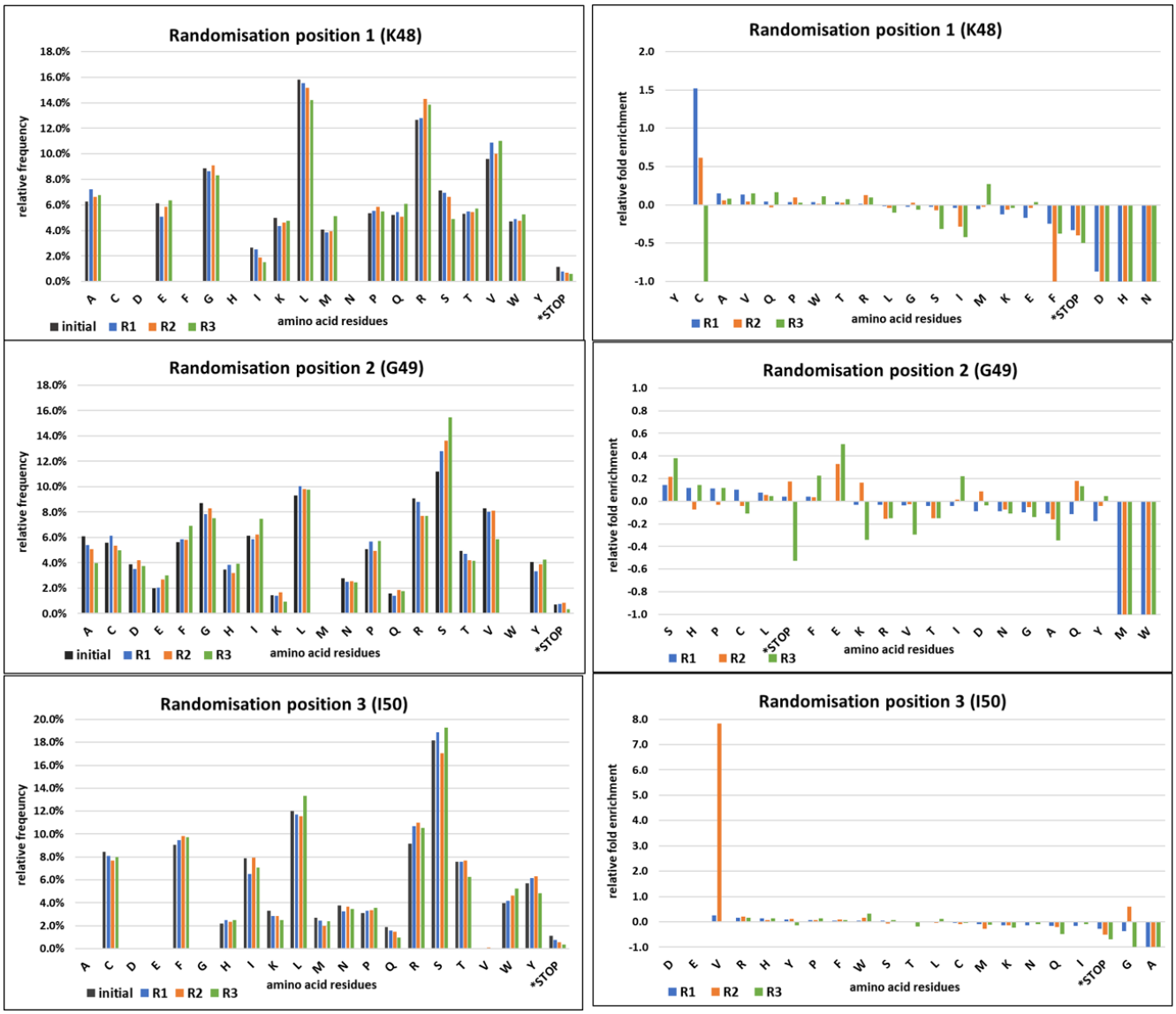

Figure 46. Next generation sequencing (NGS) analysis of sorted populations after rounds one to three of functional selection of the mIL-3 randomization library. On the left: frequencies (%) of amino acid (aa) residues at the corresponding randomized position (aa48, aa49 and aa50) for each selection round. Amino acids are sorted alphabetically. **On the right:** relative fold enrichment of the aa residue at the corresponding position. Residues are sorted, starting with the highest enrichment factor. Sequence analysis was performed with Geneious 2020.0.5.

Additionally, the randomization of the region which seems to be in high degree responsible for the functionality of the cytokine, could have unexpected negative effects on the properties of the molecules. On the one side, it was expected that additional amino acid combinations would also retain functionality of the cytokine. Klein *et al.* (1997) demonstrated that in the human IL-3 ortholog, the amino acid before the knockout position (D21) is involved in the interaction with the α subunit of the hIL-3 receptor, whereas the E22 is responsible for binding to the common β subunit (β_c)[234]. This means that both positions are sensitive to amino acid exchange and a random combination of amino acid side chains would rarely result in a functional protein. Furthermore, a mutational analysis of hIL-3 performed by Lambert *et al.* (1991), identified a row of cytokine mutants with significantly increased binding affinity to the IL-3 receptor, but with reduced stimulation activity[237]. High binding affinity of some mIL-3 variants in combination with co-encapsulation of multiple yeast cells in one droplet could

have led to false negative sorting events due to competition of the different mIL-3 mutants for the receptors on the reporter cell surface, which did not represent an issue during the mixing experiments. In this case if a mutant possesses a higher receptor binding affinity, but does not activate reporter response, a biologically active cytokine variant secreted by a yeast cell in the same droplet would not be capable of sufficient reporter induction.

However, since the human and mouse interleukin-3 and the associated receptors share relatively low homology, no direct extrapolation of hIL-3 mutation sites and their effects on the cytokine functionality could be performed. Unfortunately, no studies regarding the binding mechanism of murine IL-3 to its receptors are available, thus the influence of the two E49-neighboring amino acids on the functionality of mIL-3 could only be speculated. Further deep investigation would be necessary in order to identify the reason why the functional selection of the randomized library did not result in enrichment of reporter-activating yeast cells. However, since the mIL-3 cytokine in combination with the Ba/F3-CIS-d2EGFP reporter cells was used as a proof-of-concept system, and the performance of the functional screening approach was validated with help of the mixing experiments, screening of the randomized library was not further pursued.

5.4. Functional Selection of Agonistic anti-CD3 Antibodies

As described in chapter 5.3, the functional screening approach proved suitable for the enrichment of yeast cells secreting a biologically active wildtype mIL-3 cytokine. However, the feasibility of this novel approach could not be directly extrapolated for applications involving much more complex and larger molecules such as antibodies. Since the long-term aim of this study is to establish a system for selection of functional antibodies (agonistic, antagonistic, or cytosol-penetrating antibodies), the functional screening procedure needed to be validated also in the context of antibody molecules.

As a model system for selection of agonistic antibodies, a second reporter cell line – NF-κB/Jurkat/GFP, was used. This cell line is based on leukemic human T lymphocytes and expresses high levels of mature T cell receptor (TCR) and low levels of CD4, but no CD8 or MHC class II[238]. Due to its cancerous origin and easy propagation and expansion, Jurkat cells are often used as a T cell model system for testing of diverse immunomodulators and T cell activators[239]. *In vivo*, T cells are activated by interaction of the TCR (α and β domains) with an antigen bound to the major histo-compatible complex (MHC) on antigen-presenting cells. Signal transduction is carried out by the CD3 (T3) molecular complex, which is noncovalently associated with the TCR[240] (Fig. 47). Some CD3ε-specific antibodies have demonstrated T cell activation properties[241] by ligation of the TCR-CD3 complex with synergistic effects in combination with anti-CD28 antibodies. Stimulation of primary T cells in this manner leads to cell proliferation and has been utilized for cell expansion protocols[242, 243].

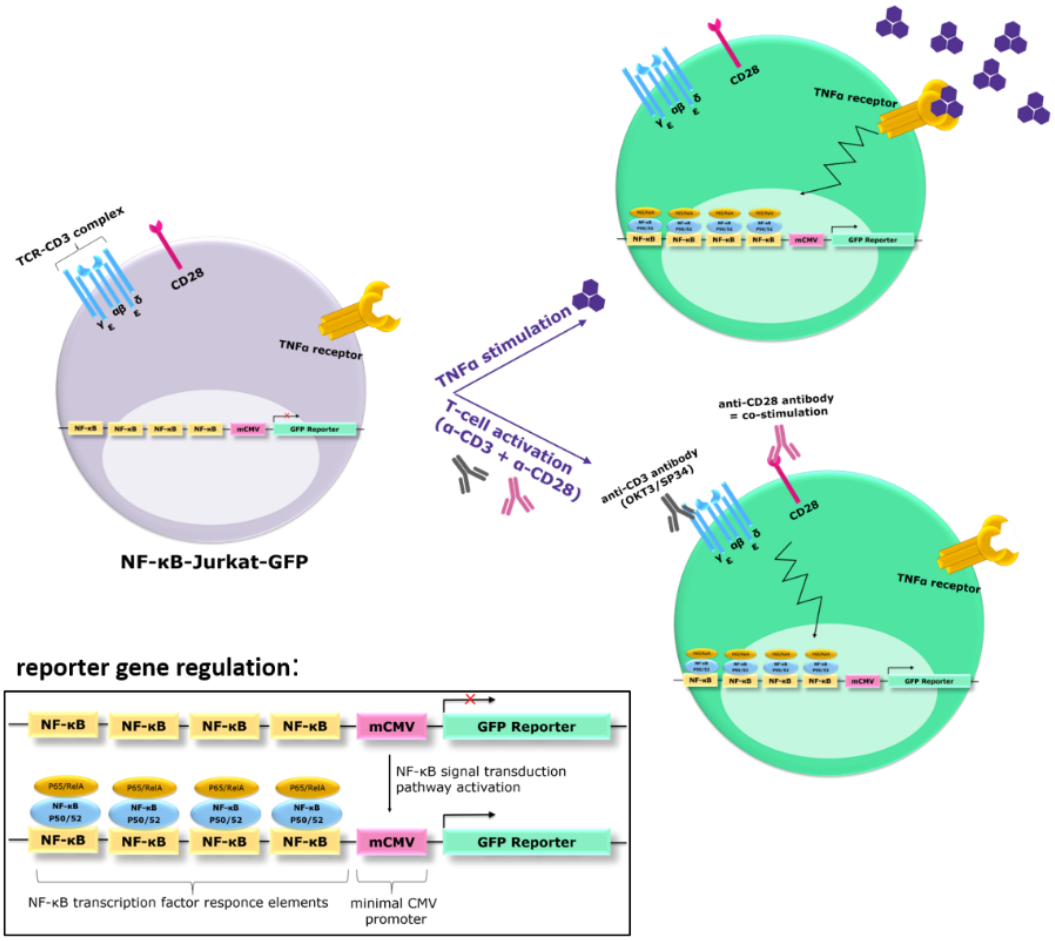

Figure 47. Activation of GFP expression in NF-κB/Jurkat/GFP reporter cell line.

5.4.1. NF-κB/Jurkat/GFP reporter cell line activation mechanisms

Signal transduction upon T cell activation results in initiation of a phosphorylation cascade involving phosphoinositide-3 kinase (PI-3 kinase)[244], leading to the activation of transcription factors (NF-AT, NF-κB, and AP-1)[245]. Regulation of reporter gene expression (GFP) in the NF-κB/Jurkat/GFP cell line is mediated by multiple NF-κB response elements (Fig. 47) resulting in GFP expression upon T cell activation by anti-CD3 antibodies. By co-stimulation with anti-CD28 antibodies, more transcription activators are released, leading to increased GFP expression and stronger fluorescence signal (Fig. 48). The NF-κB pathway is involved in signal transduction cascades induced by multiple receptors, under which tumor necrosis factor receptor 1 (TNFR1)[246]. Thus, activation of reporter gene expression can also be triggered by stimulation with the cytokine TNFα (Fig. 47), resulting in GFP fluorescence with medium intensity (Fig. 48).

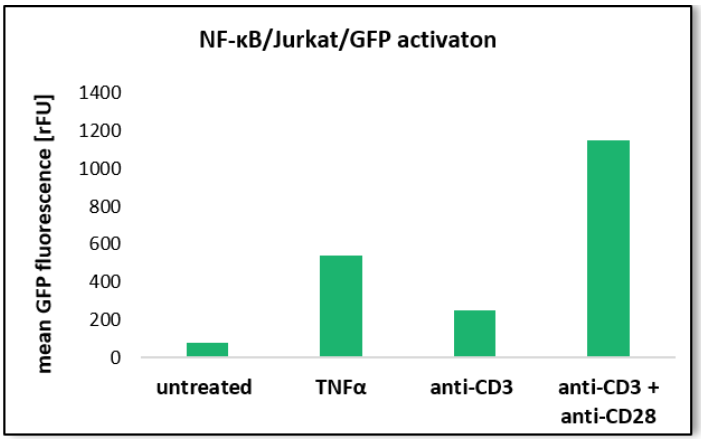

Figure 48. Mean GFP fluorescence intensity upon stimulation of NF-κB/Jurkat/GFP reporter cells. Cells were stimulated with 50 ng/mL rec. hTNFα, 1 µg/mL anti-CD3 monoclonal antibody (OKT3), or a mix of 1 µg/mL OKT3 + 1 µg/mL anti-CD28 monoclonal antibody. Cells were analysed by flow cytometry after 24 h of treatment.

5.4.2. Reporter cell line activation using secreted hTNFα from yeast

For investigation of NF-κB/Jurkat/GFP fluorescence signal intensity in dependence to the hTNFα-concentration, reporter cells were incubated with a dilution series of recombinant cytokine (0.15 – 10 ng/mL). Mean GFP fluorescence of the reporter cells increased in a dose-dependent manner with increasing hTNFα-concentration (Fig. 49A) and the reporter cells exhibited strong GFP signal after treatment with cytokine in the range of 5-10 ng/mL.

A gene construct for expression and secretion of hTNFα from *S. cerevisiae* yeast was generated (Fig. 50A) with the same composition as the construct for secretion of mIL-3 (secretion signal (app8), followed by the gene sequence of the cytokine, ribosomal skipping peptide (T2A) and intracellular expression control (mCherry)). Expression and secretion of hTNFα by the yeast cells was validated by reporter cell activation assay with yeast culture supernatant. A significant increase in the GFP fluorescence of Jurkat reporter cells, incubated with the supernatant from hTNFα-secreting yeast could be observed (Fig. 49B) in comparison to untreated reporter cells. As positive control, the reporter cells were treated with 10 ng/mL rec. hTNFα and exhibited slightly stronger but still comparable GFP fluorescence intensity than the cells treated with the yeast supernatant.

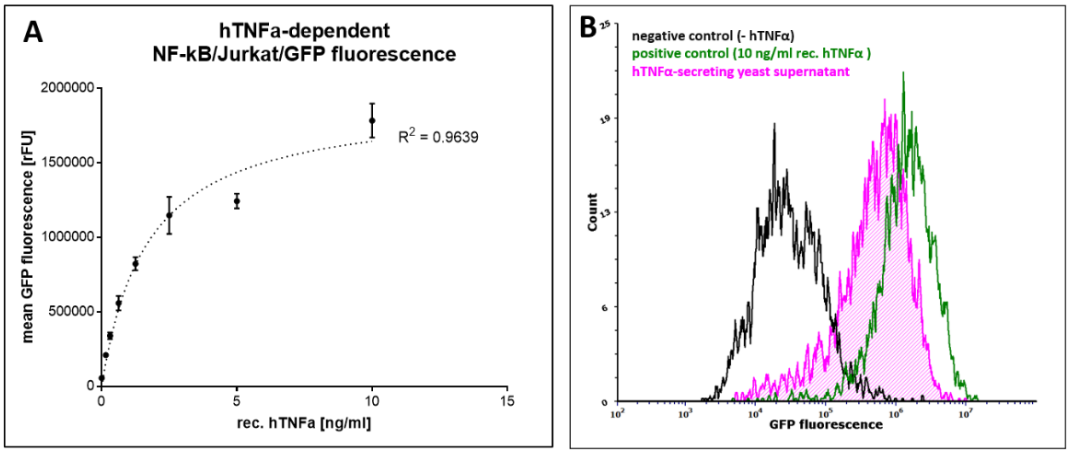

Figure 49. (A) Reporter activation in NF-κB/Jurkat/GFP cell line in dependency to the hTNFα concentration. Mean GFP fluorescence intensity determined by flow cytometry after incubation overnight of reporter cells in a 96-well plate with a dilution row (156 pg/mL – 10 ng/mL) of recombinant hTNFα in standard cultivation medium (RPMI-1640). Dashed line represents a logarithmic trendline. **(B) Flow cytometry histograms of NF-κB/Jurkat/GFP reporter cells incubated with yeast supernatant after expression**

and secretion of from hTNFα from *S. cerevisiae*. Controls represent the GFP fluorescence signals of cells incubated with or without addition of rec. hTNFα.

5.4.3. Generation of OKT3-antibody secreting yeast

Gene constructs for expression and secretion of anti-CD3 antibody (OKT3) from *S. cerevisiae* were generated in order to test *in vitro* T cell activation in the context of functional screening using the NF-κB/Jurkat/GFP reporter cell line. Two plasmids carrying the gene sequences for the humanized OKT3 heavy (Fig. 11) and humanized OKT3 light chain (Fig. 12) were generated and yeast cells were co-transformed with both plasmids. Intracellular expression control was enabled by genetic fusion of a T2A ribosomal skipping peptide and mCherry fluorescent protein C-terminally to the heavy chain of the antibody (Fig. 50).

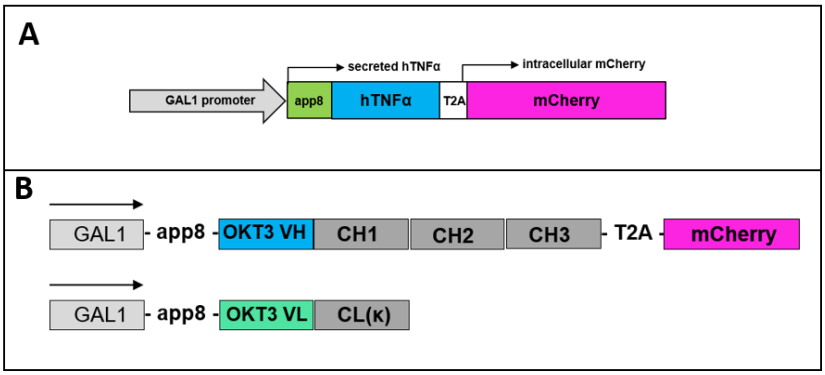

Figure 50. Gene constructs for expression and secretion from *S. cerevisiae*. (A) Construct for secretion of human tumor necrosis factor alpha (hTNFα). **(B)** Constructs for the heavy and light chains of humanized anti-CD3 antibody muromonab (OKT3).

Secretion of functional OKT3 mAb was verified by treatment of Jurkat cells with supernatant from induced yeast cells, carrying the plasmids for OKT3 mAb. Bound OKT3 antibodies were detected using specific fluorescently labeled detection antibodies against the κ-light chain and the Fc domain of the antibody (Fig. 51). A significant shift of the Jurkat cells treated with the supernatant from OKT3-secreting yeast could be observed upon detection of the light chain of the antibody (Fig. 51A) indicating successful secretion of the antibody and binding to the target cells. Detection of the heavy chain with anti-Fc antibody resulted in a slight fluorescence shift compared to the negative control (cells treated only with the detection antibody) (Fig. 51B). Overall, these results indicate successful secretion of the anti-CD3 antibody from the yeast cells. However, the marginal shift in case of anti-human Fc-PE detection antibody implies low concentration of the antibody in the yeast supernatant.

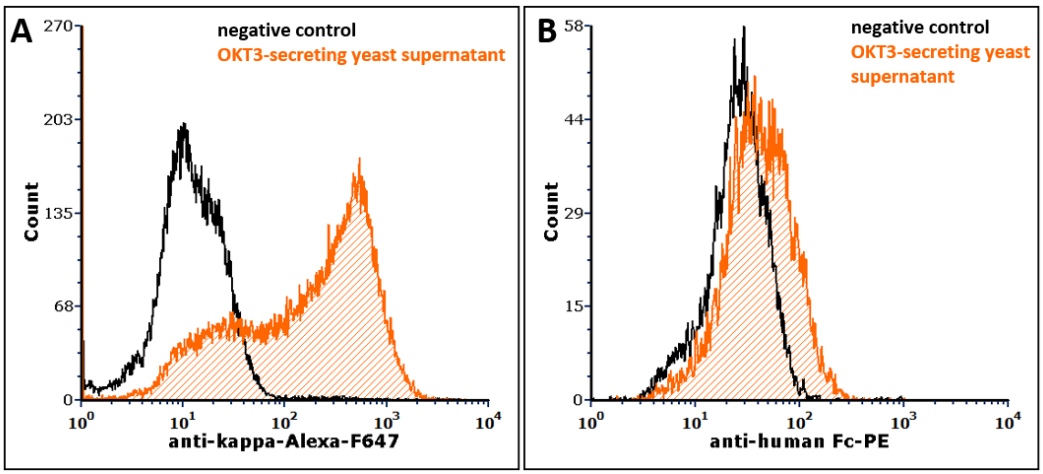

Figure 51. Analysis of secretion and binding of anti-CD3 mAb OKT3 from *S. cerevisiae*. NF-κB/Jurkat/GFP cells were treated with supernatant from OKT3-secreting yeast (after 24 h of expression at 30 °C, 180 rpm) for 2 h on ice. Bound OKT3 antibody was detected with **(A)** anti-κ light chain-Alexa Fluor647 conjugate and **(B)** anti-human Fc-PE (phycoerythrin) conjugate. As negative control, NF-κB/Jurkat/GFP cells were treated with the corresponding detection antibody.

Next, in vitro T cell activation using supernatant from OKT3-secreting yeast was tested. Secreted hTNFα from yeast cells at identical conditions (cell density etc.) was used as a control. Supernatants from both yeast cell cultures producing TNFα or OKT3, respectively, were harvested and the same volume supernatant was added to the NF-κB/Jurkat/GFP reporter cells. While reporter cell activation was detectable in case of the yeast supernatant from hTNFα-secreting yeast cells (Fig. 52), very low increase of the GFP fluorescence signal was observable after treatment with supernatant from OKT3-secreting yeast in comparison to the negative control (untreated reporter cells). Again, this result points out a very low concentration of the secreted antibody in the yeast supernatant, insufficient to induce significant reporter cell activation.

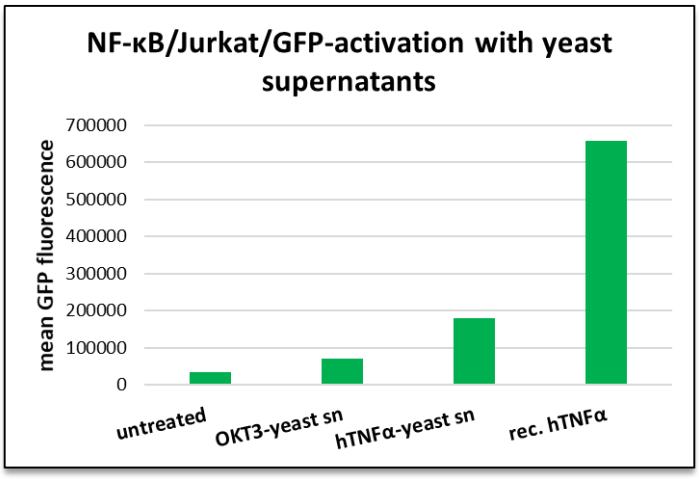

Figure 52. Reporter cell activation assay with yeast culture supernatants from OKT3 mAb- and hTNFα-expressing yeast cells. Protein expression and secretion was carried out for 48 h at 30 °C, 180 rpm. Cell supernatant was harvested and 25 µL were added to 100 µL reporter cell suspension (1×10^5 cells) in RPMI-1640 medium. Positive control represents reporter cells treated with 50 ng/mL rec. hTNFα.

5.4.4. Cocultivation of yeast and reporter cells in test tubes

Reporter cells were cocultured with hTNFα- and OKT3-secreting cells in order to investigate GFP expression rate under the coculturing conditions optimized for the Ba/F3-CIS-d2EGFP reporter cell line in combination with mIL-3-secreting yeast cells. Reporter cells cocultured with hTNFα-secreting yeast cells exhibited strong GFP fluorescence signal, which was comparable to the positive control (Fig. 53A). However, *in vitro* T cell activation by secreted OKT3 antibody from yeast cells was unsuccessful and no increase in the GFP fluorescence signal of the treated cells could be observed (Fig. 53B), although the cells were co-stimulated with anti-CD28 mAb. On the other side using 1 µg/mL commercially available OKT3 antibody in combination with the anti-CD28 mAb, resulted in an efficient T cell activation of the reporter cells, detected in form of increased GFP fluorescence intensity. This indicates that the culturing conditions under which the experiment was carried out are suitable for activation of the reporter cells both *via* the TNFR1 and CD3-receptors. Failed reporter cell activation by OKT3-secreting yeast cells most probably result from insufficient expression and/or secretion of the full-length antibody in *S. cerevisiae*. Furthermore, while in case of the cytokine, concentration of only 0.5 nM (10 ng/mL) is

sufficient to induce strong GFP expression, in case of the antibody-mediated T cell activation by anti-CD3 mAb, a concentration of 6 nM (1 µg/mL) was required for moderate reporter cell activation.

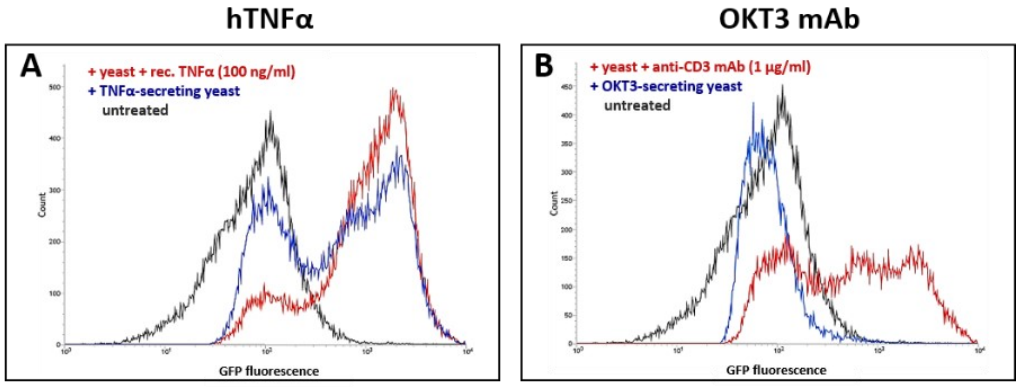

Figure 53. Cocultivation of live NF-κB-Jurkat-GFP reporter reporter cells and *S. cerevisiae* cells secreting (A) hTNFα or (B) anti-CD3 mAb (OKT3). Both cell types were suspended in 1 mL medium mix (50 % RPMI-1640 + 50 % DMEM-F12 Ham), supplemented with 2 % w/v galactose and 1 % Pen/Strep and were cocultured in 50 mL reaction tubes. Negative control represents untreated reporter cells. As positive controls rec. hTNFα (100 ng/mL) or a commercially available OKT3 antibody (1 µg/mL) were mixed to the cell medium. In case of antibody-mediated reporter cell activation assay, a co-stimulation was performed by addition 1 µg/mL anti-CD28 antibody to all samples. Flow cytometry analysis was performed after 20 h of cocultivation. Histograms depict the GFP fluorescence signal of the mammalian reporter cells only

5.4.5. Cocultivation of anti-CD3 antibody-producing Expi293F cells and reporter cells

To investigate, whether the observed low level of T cell activation was due to very low yeast secretion levels, we used Expi293F mammalian secretor cells which are known to produce and secrete significant amounts of antibodies. Hence, *in vitro* T cell activation by coculturing was further examined using a stably transfected Expi293F cell line which secretes another anti-CD3 antibody (SP34). In order to exclude false positive effects induced by the Expi293 cell line or the cultivation medium, a negative control with Expi293F cells stably expressing cetuximab (Expi-C225) was analysed. The stably transfected antibody-secreting Expi293F cells carry an intracellular mCherry fluorescent marker for transfection control and appear in the mCherry fluorescence channel as a separate population (Fig. 54). T cell activation of the reporter cells was observed by cocultivation with the SP34-secreting Expi293F cells (Expi-SP34) with about 9 % GFP positive Jurkat reporter cells. Co-stimulation with the anti-CD28 antibody further increased the fraction of activated reporter cells to about 32 %, while positive control with yeast cells secreting hTNFα resulted in approx. 36 % NF-κB/Jurkat/GFP cells expressing the reporter protein (Fig. 54).

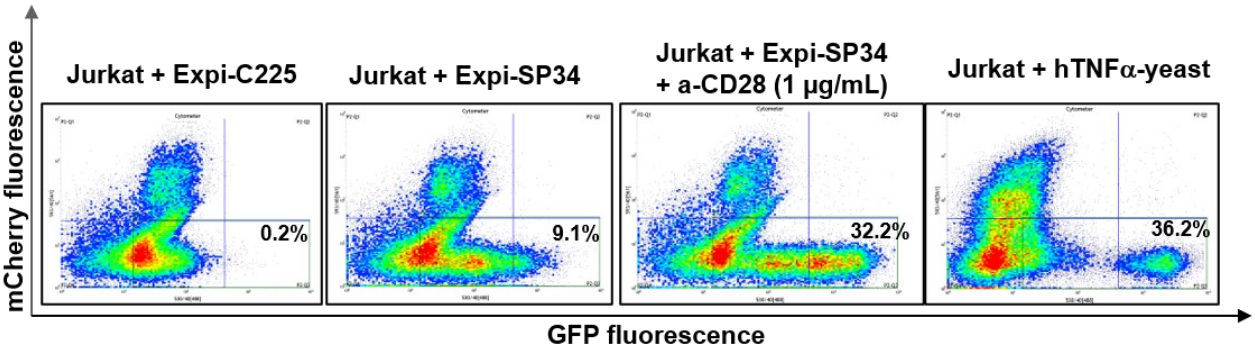

Figure 54. Reporter cell activation by cocultivation with anti-CD3 antibody (SP34)-secreting Expi293F cells. NF-κB/Jurkat/GFP cells were resuspended in 1 mL of a medium mix, consisting of 50 % RPMI-1640 + 50 % Expi293 Expression medium. Expi293F cell stably expressing and secreting either anti-EGFR mAb cetuximab (C225) or anti-CD3 mAb (SP34) were added to the cell suspension. Anti-CD28 antibody was added at concentration at 1 µg/mL for co-stimulation of the T cell activation. As a positive control, reporter cells were cocultured with hTNFα-secreting yeast cells as described above.

5.4.6. Co-encapsulation experiments with NF-κB/Jurkat/GFP reporter cells

Activation of reporter cells in droplets was investigated by co-encapsulation with OKT3- and hTNFα-secreting yeast cells, as well as with SP34-secreting Expi293F and hTNFα-secreting CHO cells. Since the NF-κB/Jurkat/GFP cell line demonstrated strong reduction of the cell viability by addition of hydrogel-forming polymers (alginate or agarose) to the encapsulation medium (Fig. 27B), these experiments were performed by encapsulation in droplets without addition of hydrogel-forming polymers.

While no GFP expression could be observed in reporter cells co-encapsulated with the OKT3-secreting *S. cerevisiae* cells, a low induction level of GFP fluorescence of the NF-κB/Jurkat/GFP cells co-encapsulated with hTNFα-secreting yeast was observed (Fig. 55A). Notably, the positive control consisting of reporter cells co-encapsulated with hTNFα-secreting yeast in presence of recombinant hTNFα, also resulted in a comparable low level of GFP production. This indicates that not the co-encapsulation efficiency of yeast and reporter cells is the reason for the limited reporter cell activation, but rather reduced reporter cell viability under the tested conditions may account for this finding. Interestingly, when NF-κB/Jurkat/GFP cells were encapsulated alone in droplets in absence of any activator of reporter response, a fraction of the reporter cells still exhibited induced GFP expression, while this was not the case during the cocultivation experiments in test tubes (Fig. 53 and Fig. 54). Activation of the NF-κB pathway under stress conditions in the microdroplets could be an explanation for this phenomenon, since NF-κB upregulation was reported in relation to serum deprivation and oxidative stress[247].

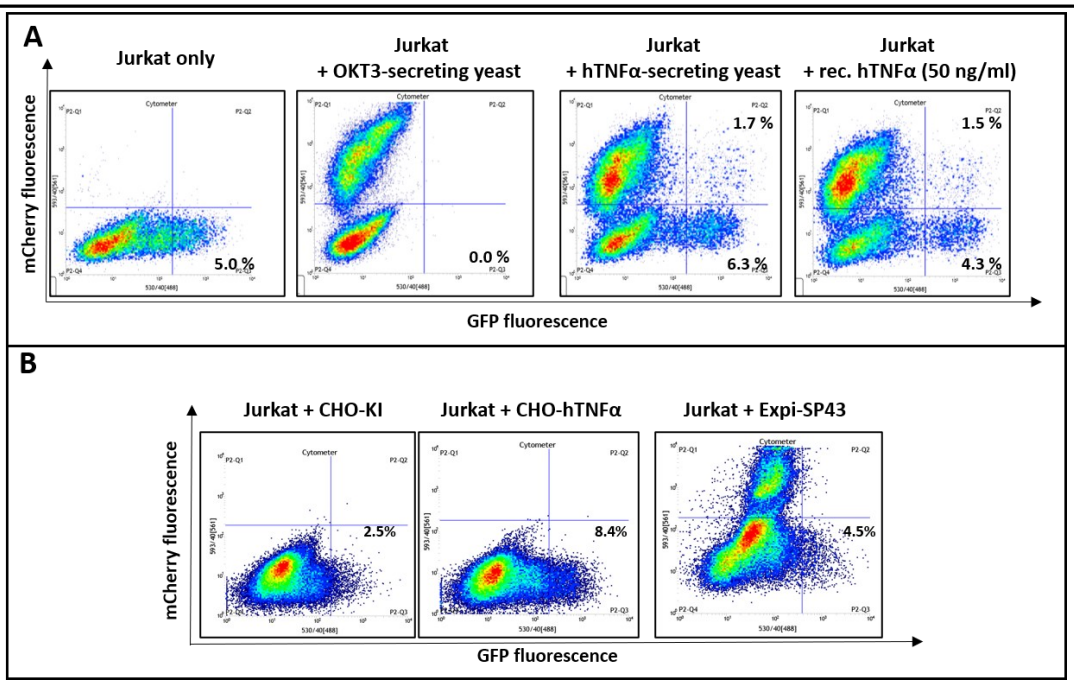

Figure 55. Co-encapsulation experiments with NF-κB/Jurkat/GFP reporter cells in microdroplets. **(A)** Reporter cells were co-encapsulated in droplets without hydrogel with yeast cells secreting anti-CD3 antibody (OKT3) or hTNFα. As negative control, reporter cells were encapsulated alone in microdroplets. As positive control, reporter cells were co-encapsulated with hTNFα-secreting yeast and 50 ng/mL rec. hTNFα were added to the encapsulation medium. Following a 20 h incubation at 37 °C, 8 % CO_2, 110 rpm, the emulsion was broken, cells were resuspended in PBS and analysed by flow cytometry. **(B)** Reporter cells were co-encapsulated in droplets together with stably transfected mammalian cells secreting either hTNFα (CHO-hTNFα) or anti-CD3 antibody (Expi-SP34). Following a 20 h incubation at 37 °C, 8 % CO_2, 110 rpm, the emulsion was broken, cells were resuspended in PBS and analysed by flow cytometry. As negative control, reporter cells were co-encapsulated with CHO-KI (wt) cells.

Co-encapsulation with CHO cells stably expressing and secreting hTNFα resulted in the strongest activation of the reporter cells (Fig. 55B) in this row of experiments. In case of co-encapsulation with SP34-secreting Expi293F cells, a fraction of the Jurkat reporter cells also exhibited elevated GFP signal. Nevertheless, the negative control (reporter cells co-encapsulated with wt CHO-KI cells) revealed induced GFP expression in some Jurkat cells as well. This hampers the estimation of the activation grade of the reporter cells in the context of functional selection of agonistic anti-CD3 antibodies. Therefore, further optimizations regarding the coculturing conditions in microdroplets and the secretion host for the anti-CD3 antibodies need to be carried out to enable the implementation of the NF-κB/Jurkat/GFP cell line for functional selection purposes by encapsulation in microdroplets.

6. Conclusion and Outlook

With the rapid expansion of the biopharmaceutical market, the demand for straightforward, cost-effective and time-saving discovery technologies for the generation of potent functional biologics has increased tremendously. The interest in the establishment of novel high-throughput functional screening methods, which surpass the limitations of the current state of the art technologies has raised, leading to the development of commercial platforms like Cyto-Mine® from Sphere Fluidics[248], Beacon® Optofluidic Platform from Berkeley Light, and xPloration™ Screening Platform from xCella Biosciences[249]. All three systems exploit different compartmentalization strategies and aim to perform sophisticated single-cell screening and selection.

In case of Cyto-Mine®, a microfluidic system is utilized for generation of picolitre-volume droplets and encapsulation of up to 40 million mammalian cells per day. The platform is optimized for detection of B cells or hybridomas, secreting an antibody of interest, which binds with high affinity to a soluble antigen and selection occurs in the same device by fluorescence-activated droplet-sorting (FADS). While easy to handle and with a user-friendly interface, this platform also brings certain disadvantages regarding detection only in a single fluorescence channel and limited incubation time of the emulsified cells. Furthermore, any kind of processing of the w/o emulsion off-chip is not possible, which limits the implementation of the device for some applications.

The Beacon® Optofluidics System is developed for a broader spectrum of applications including antibody discovery, cell line development, cell therapy development (by selection, validation and characterisation of CAR T cells), as well as for synthetic biology and gene editing. The platform is based on compartmentalization of single cells into nanocavities (250 pL) by light impulses (optofluidics). Isolated single cells in NanoPen chambers can be cultured, expanded, assayed and exported for further analysis. Comprehensive fluorescent imaging of each cell enables the analysis and selection of desired cells, based as well on binding affinity of secreted immunoglobulins, as on biological functionality[250]. Although the Beacon® Optofluidics System promises to reduce drastically the development time and costs for cell-based therapies and antibody discovery and development, it comes with a high price tag both for the device and the consumables. Hence, the platform is mainly oriented on the big pharma industry, with Pfizer, Novartis, Roche, Amgen, and Sanofi, being some of the first customers which purchased the technology[251].

Another player in the field of single-cell functional screening is xCella Biosciences. The xPloration™ Screening Platform aims at complete coverage of the immune repertoire with screening throughput of 10^6 B cells in less than 4 hours. The system should enable selection of rare antibodies against challenging targets like GPCRs (G-protein coupled receptors) and ion channels. B cells are compartmentalised in 40-µm-wide microcapillaries together with the target of interest (immobilized on beads) or with target/reporter cells. Antibody-target interaction and functionality are assayed over a period of time by time-lapse imaging[249]. Furthermore, the platform can be directly coupled to a next-generation sequencing (NGS) workflow for genotype analysis of hits.

Although the described platforms operate with high precision and are optimized for specific applications, they remain unreachable for academic purposes due to very high device and material costs. Furthermore, these systems comprise integrated devices with no or limited modularity, making an alteration of the system and adaptation to alternative applications not readily achievable. Nevertheless, with the advantages of sample

miniaturization and encapsulation in distinct microdroplets, microfluidic-assisted screening has emerged as a promising next-generation approach. Fortunately, alternative, module-based microfluidic systems have become commercially available for reasonable price. Modular microfluidic systems enable controlled and efficient cell encapsulation under flexible conditions, allowing for a broader application range.

In search of a screening approach for selection of cytoplasm-penetrating molecules in the scope of this doctoral research, a novel strategy for mammalian cell-based functional screening was developed by co-encapsulation of viable mammalian reporter cells with yeast secretor cells in millions of agarose-containing microdroplets. Encapsulation of cells in picolitre-volume droplets combines sample miniaturization and compartmentalization for phenotype-genotype coupling. Furthermore, the implementation of hydrogel-building polymers (e.g. agarose and alginate) makes the approach compatible with an ultra-high-throughput selection using a commercially available FACS device.

S. cerevisiae was chosen as a secretion host since it combines the advantages of a microbial expression system, characterized by high-transformation efficiencies and fast growth, with those of eukaryotes which possess an unfolded protein response machinery for elimination of misfolded proteins prior to secretion[252]. In addition, in our lab both immune and combinatorial libraries have been generated in *S. cerevisiae* with high efficiency enabling the specific selection of desired proteins[37, 253]. As the glycosylation pattern has proven to have a significant influence upon the bioactivity, physicochemical properties, and pharmacokinetics of the majority of biologics[254-256], *S. cerevisiae* brings further advantages in the context of functional screening, because human like N-glycosylation could successfully be engineered in this yeast[257]. Lastly, during this study *S. cerevisiae* has proven as a robust organism, capable of fast expansion after encapsulation in w/o emulsion and sorting of agarose microbeads. This enables functional screening in multiple rounds or different setups without risk of losing desired candidates due to low cell viability.

While yeast surface display in combination with FACS represents a powerful technology for fast and efficient isolation of protein variants with desired specificities, secretion of the molecules of interest was inevitable for the purposes of functional screening of cell-penetrating antibodies. However, secretion of a library of molecules in the culture medium brings up challenges regarding the phenotype-genotype coupling, as well as makes sorting by FACS not feasible for pre-selection of the library in an affinity-based format, which would be necessary for selection of agonistic or antagonistic antibodies. Nevertheless, this limitation can be surpassed by simultaneous secretion and display of the library variants on the yeast surface by utilizing an inefficient ribosomal skipping motif (F2A) as described by Cruz-Teran *et al.* (2017)[258]. This strategy could enable alternating affinity-based and functional selection. Since it utilizes live mammalian cells, our system could also be applicable for selection of molecules with defined biological function against non-soluble membrane-associated targets like GPCRs and ion channels. The screening process in this case could consist of an initial pre-selection of the variants displayed on the yeast surface using a biopanning procedure with the target mammalian cells as demonstrated by Yang *et al*. (2019)[259] for enrichment of target-specific variants. The enriched library would then be subjected to an ultra-high-throughput phenotypic screening by co-encapsulation with the reporter cells, followed by FACS of hydrogel microbeads for isolation of hits with desired biological function.

In comparison, several similar screening approaches have been published recently, which once again emphasizes the high demand in the field of high-throughput functional selection. In 2017, Fang *et al.* proposed an affinity-based antibody screening platform, based on co-encapsulation of antibody-secreting *Pichia pastoris* and fixed mammalian target cells in agarose microdroplets[225]. This study demonstrated that GMD-FACS is a reliable selection method and classical antibody staining procedures can be applied for the specific fluorescent detection of target-bound antibodies in the agarose microbeads. However, since this procedure was not optimized for viable mammalian cells, functional antibody screening would not be feasible.

Another system for microfluidic-based functional antibody selection was introduced by Zheng *et al.* in 2018. In this study, the authors co-encapsulated phage-secreting *E. coli* and mammalian reporter cells in medium-containing aqueous droplets and were able to detect reporter cell activation by agonist antibody fragment (scFv) presented on the phage surface[260]. This work expands the compatibility of droplet-based functional screening towards one of the best-established screening approaches, phage display[261]. However, the authors have not performed selection of agonistic antibodies in w/o emulsion and discussed the necessity of establishing a double emulsion-generation protocol to combine the procedure with FACS selection. We are convinced that in combination with a straightforward ultra-high-throughput GMD-FACS (by addition of agarose to the encapsulation medium) this approach would be feasible for phage display-based selection of agonistic antibody variants, bypassing the need of double emulsion generation, addressed by the authors.

A further example, demonstrating the versatility of droplet-based functional screening utilizing mammalian reporter cells is the study of Yaginuma *et al.* (2019). In a similar to our system fashion, they co-encapsulated peptide-secreting *S. cerevisiae* with mammalian reporter cells, responding to activation of the G-protein coupled receptor hGLP1R[262]. The fluorescence readout, in this case, was achieved by expression and secretion of β-galactosidase (LacZ) as a reporter enzyme, which converts a non-fluorogenic substrate, added to the droplets, into a fluorescent molecule. Selection of agonistic peptide variants from a randomized peptide library was performed by co-encapsulation of the peptide-secreting yeast with the reporter cells and manual microscopical observation of the droplets, followed by isolation of the highly fluorescent droplets by a micromanipulator. This study illustrates the applicability of droplet-based cocultivation screens utilizing viable mammalian cells for addressing challenging targets as GPCRs, where the generation of reliable soluble protein for standard affinity-based screens is not trivial. However, the throughput of this system is mainly limited by the microscope-assisted isolation of fluorescent droplets.

6.1. Summary

A novel functional screening procedure was developed based on co-encapsulation of viable mammalian reporter cells with yeast secretor cells in millions of agarose-containing microdroplets. This generic approach is compatible with an ultra-high-throughput screening utilizing a commercially available FACS device without need of extensive optimization and adaptation and may be implemented for selection of new functional biologics, including cytokines, agonistic or internalizing antibodies, and soluble receptors.

During this doctoral research, commonly used emulsification strategies (bulk emulsification and microfluidic-assisted droplet generation) were tested and resulting hydrogel microbeads were compared. Droplet generation utilizing a microfluidic system showed superiority for production of monodispersed and homogeneous droplets with desired size. Microdroplet generation was optimized using a µEncapsulator microfluidic system and fast and efficient encapsulation of cells in a high number of hydrogel microbeads was achieved. Furthermore, gelation conditions of three different hydrogel-forming substances (agarose, Matrigel and alginate) were tested. Thermal gelation of agarose and Matrigel was possible resulting in stable microbeads, which could readily be recovered in an aqueous buffer. However, upon cultivation of mammalian cells in Matrigel-containing droplets, no hydrogel gelation took place, suggesting degradation of the matrix by secreted proteases. External and internal crosslinking of alginate was tested and resulting calcium alginate microbeads were compared. Internal gelation by addition of chelated Ca^{2+} to the encapsulation solution and following Ca^{2+}-release under acidic conditions yielded uniform and homogeneous alginate microbeads. Reporter cell viability in the hydrogel microbeads was investigated revealing enhanced reporter cell mortality in presence of hydrogel-forming polymers, especially in case of alginate. Expression of reporter protein (GFP) upon stimulation of reporter cells was highly dependent on the cell viability in the microdroplets, being high in medium-only droplets and strongly impaired in alginate-containing microdroplets. Hence, agarose was used as a hydrogel-of-choice, since it enabled sufficient cell viability and reporter cell activation.

In a proof-of-concept model study the functional selection procedure was validated. Therefore, activation of a murine reporter cell line (Ba/F3-CIS-d2EGFP) by murine interleukin-3 secreted by yeast cells, was extensively characterized and a non-functional mIL-3 mutant was designed and secreted from yeast cells. Mixing experiments with different ratios of “activating” mIL-3 wt-secreting yeast in an excess of yeast cells secreting the non-functional (E49G) mutant resulted in rapid enrichment of the biologically active cytokine after functional selection by co-encapsulation with the reporter cells and FACS. Selection progress in each screening round was monitored by reporter cell activation assays using supernatants from the enriched yeast populations, revealing gradual enrichment of functional cytokine after each functional selection cycle. A randomized library was generated for regain-of-function screening experiments. NGS analysis of the generated library confirmed the presence of wt-mIL-3 sequence, however it was twice as rare in the yeast population, as expected. No enrichment of reporter cell-activating yeast variants could be observed after four consecutive cycles of functional selection, raising uncertainty whether the randomization of the protein site have had unexpected negative effects.

For adaptation of the functional selection system towards screening of agonistic antibodies, an immortalized T cell reporter cell line was used. Induction of reporter protein expression (GFP) was possible using secreted hTNFα from yeast cells, but was not successful by secretion of agonistic anti-CD3 antibody (OKT3). Secretion of another anti-CD3 antibody variant (SP34) from stably transfected mammalian cells resulted in strong T cell activation of the reporter cells after co-stimulation with an anti-CD28 antibody in cell suspension, but was limited in w/o emulsion. Furthermore, unspecific activation of the reporter cell line was observed after encapsulation in microdroplets, implying reporter gene expression under stress conditions and nutrient deprivation.

6.2. Outlook

In conclusion, a novel concept for selection of biomolecules, based on their biological function in an ultra-high-throughput manner was developed and validated. Co-encapsulation and cocultivation of reporter mammalian cells and secretor yeast cells in picolitre-volume droplets containing hydrogel-forming polymers was challenging with respect to retaining the viability and functionality of both cell types. Reduced reporter cell viability was observed in presence of alginate and agarose polymers, hence, further optimization of the composition of the encapsulation medium would be beneficial. Since the co-encapsulation efficiency of both cell types plays an important role for the throughput of the system, and flocculation of the yeast demonstrated negative effects upon the distribution of the yeast cells in the generated droplets, a deeper investigation of the encapsulation medium composition and its effects on yeast cell flocculation should be performed. Additives like EDTA or sugars (mannose)[263] should be tested for dispersion of yeast flocs and their influence on the protein secretion rate of the yeast and reporter cell viability should be carefully evaluated.

Using a murine reporter cell line (Ba/F3-CIS-d2EGFP) which expresses GFP upon stimulation with murine interleukin-3, the functional selection approach was validated. Mixing experiments in different ratios (1:10, 1:100, 1:1,000, and 1:10,000) using a non-functional mIL-3 mutant resulted in rapid enrichment of yeast cells secreting the biologically active mIL-3 wildtype cytokine. The extent of mIL-3 wt-enrichment was limited to 15-25 % in the yeast population, which was sufficient to identify multiple positive clones by testing single yeast clones. However, further efforts of optimizing the screening conditions should be invested aimed at improving the enrichment factor by performing additional selection rounds with decreased yeast cell density in the encapsulation medium during droplet generation, since this would minimize sorting of false positive yeast clones.

Since the aim of the research was to establish a screening platform for functional antibodies (e.g. cell-internalizing, agonistic or antagonistic properties), the functional selection concept should be optimized for selection of antibody-secreting yeast cells. Initial experiments using anti-CD3 agonistic antibody (OKT3), secreted from *S. cerevisiae* revealed new critical aspects, which need to be addressed.

Firstly, secretion of the OKT3 antibody could be verified by specific binding to the target cells (NF-κB/Jurkat/GFP), performed by staining with detection antibodies. However, the concentration of the antibody in the yeast supernatant was very low and only a slight shift in the fluorescence signal of the target

cells with bound antibodies could be observed. This implies very low antibody secretion levels from *S. cerevisiae*, and has been previously reported as an issue in case of large and complex proteins, such as full-length antibodies[264]. For this reason, we envisaged adaptation of the functional screening system to an alternative microbial secretion host, which is known for secretion of high amounts of full-length antibodies – *Komagataella Phaffii* (*Pichia pastoris*)[265]. As demonstrated by Fang *et al.* (2017), *P. pastoris* is a suitable secretion host compatible with encapsulation procedures in agarose microbeads and following GMD-FACS selection[225]. Therefore, we are confident that our functional screening approach could be adapted for co-encapsulation with antibody-secreting *P. pastoris*.

Nevertheless, even very low amounts of secreted OKT3 antibody should be sufficient for induction of T cell activation in the microdroplets. In a droplet volume of only 45 pL, secretion of as few as 1.6×10^5 antibody molecules would be sufficient to reach a concentration required for T cell activation (6 nM). While anti-CD3 antibodies in soluble form have demonstrated immunosuppressive properties by blocking the TCR-CD3 complex for interaction with antigen-MHC complexes, T cell activation relies on crosslinking of the anti-CD3 antibody by Fc-receptors on accessory cells (monocytes)[266] which induces T cell proliferation and systemic release of cytokines. Multiple reports have evidenced that proliferative effects of OKT3 on T cells depend on the antibody subclass and on its affinity to human Fcγ-receptors[267, 268]. Furthermore, humanization of OKT3 by CDR-grafting onto human IgG1 resulted in reduced mitogenic activity compared to the wildtype OKT3[269]. In our case, a humanized IgG1 OKT3 antibody was secreted from the yeast cells after grafting of the mouse CDRs to a human IgG1 framework, whereas recombinant mouse IgG2a OKT3 antibody (wt) was used as a positive control. In order to exclude possible decrease in the T cell activation levels due to the format alteration, the humanized OKT3 variant should be recombinantly produced and reporter cell activation with the purified antibody should be tested. Additionally, secretion of the mouse IgG2a-OKT3 variant from yeast cells and reporter cell activation by coculturing with the reporter cells should be examined.

A second aspect, which needs further investigation is the unspecific activation of the NF-κB/Jurkat/GFP reporter cells after overnight culturing in microdroplets. Enhanced GFP fluorescence signal in approx. 5-10 % of all Jurkat cells was detected, although the cells were not treated either with hTNFα, nor with anti-CD3 antibodies. Nuclear translocation of NF-κB was described in Jurkat cells under stress conditions (nutrient deficiency)[270] and could explain the unspecific GFP expression in the microdroplets, where the nutritional supply is limited. Thus, further optimization of the medium composition for droplet formation, as well as of the culturing conditions in the w/o emulsion would be necessary in order to increase the reporter cell viability and to reduce the unspecific GFP fluorescent signal in the agarose microbeads.

7. References

(1) Rick, N. G. *Drugs: From Discovery to Approval*, John Wiley & Sons (2015).

(2) Pina, A. S., Hussain, A., and Roque, A. C. A. An historical overview of drug discovery. In *Ligand-Macromolecular Interactions in Drug Discovery*, pp 3-12, Springer (2010).

(3) Dailey, J. W. (2018) Pharmaceutical industry. In *Encyclopædia Britannica*, Encyclopædia Britannica, inc.

(4) Brook, K., Bennett, J., and Desai, S. P. The chemical history of morphine: an 8000-year journey, from resin to de-novo synthesis. *Journal of Anesthesia History* **3**, 50-55 (2017).

(5) Meshnick, S. R., and Dobson, M. J. The history of antimalarial drugs. In *Antimalarial chemotherapy*, pp 15-25, Springer (2001).

(6) Ruetsch, Y. A., Boni, T., and Borgeat, A. From cocaine to ropivacaine: the history of local anesthetic drugs. *Current Topics in Medicinal Chemistry* **1**, 175-182 (2001).

(7) Pray, L. Discovery of DNA structure and function: Watson and Crick. *Nature Education* **1**, 100 (2008).

(8) Morange, M. *A history of molecular biology*, Harvard University Press (2000).

(9) Quianzon, C. C., and Cheikh, I. History of insulin. *Journal of Community Hospital Internal Medicine Perspectives* **2** (2012).

(10) Shoeib, S. A., Elshebini, E. M., and AbdAlla, A. N. Biologics: a target therapy of lupus nephritis: a systematic review. *Menoufia Med. J.* **32**, 1208 (2019).

(11) Boyle, R. M. The Use of Biologics in Cancer Therapy. *U. S. Pharmacist* **35**, 4-7 (2010).

(12) G de la Torre, B., and Albericio, F. The pharmaceutical industry in 2018. An analysis of FDA drug approvals from the perspective of molecules. *Molecules* **24**, 809 (2019).

(13) Grand View Research. (2017) Biologics Market Size Worth $399.5 Billion By 2025. https://www.grandviewresearch.com/press-release/global-biologics-market, accessed at 21.01.2020.

(14) European Medicines Agency (EMA). Biosimilar medicines: Overview. https://www.ema.europa.eu/en/human-regulatory/overview/biosimilar-medicines-overview, accessed at 22.03.2020.

(15) U.S. Food and Drug Administration (FDA). What Are "Biologics" Questions and Answers. https://www.fda.gov/about-fda/center-biologics-evaluation-and-research-cber/what-are-biologics-questions-and-answers, accessed at 22.03.2020.

(16) Mazzeo, A., and Carpenter, P. Stability studies for biologics. In *Handbook of stability testing in pharmaceutical development*, pp 353-369, Springer (2009).

(17) Köhler, G., and Milstein, C. Continuous cultures of fused cells secreting antibody of predefined specificity. *Nature* **256**, 495-497 (1975).

(18) Mordor Intelligence. (2019) BIOLOGICS MARKET - GROWTH, TRENDS, AND FORECAST (2020 - 2025). https://www.mordorintelligence.com/industry-reports/biologics-market, accessed at 23.03.2020.

(19) Palm, A.-K. E., and Henry, C. Remembrance of things past: long-term B cell memory after infection and vaccination. *Frontiers in Immunology* **10**, 1787 (2019).

(20) Zaroff, S., and Tan, G. Hybridoma technology: the preferred method for monoclonal antibody generation for in vivo applications. *BioTechniques* **67**, 90-92 (2019).

(21) Liu, J. K. The history of monoclonal antibody development–progress, remaining challenges and future innovations. *Annals of Medicine and Surgery* **3**, 113-116 (2014).

(22) Cervino, C., Weber, E., Knopp, D., et al. Comparison of hybridoma screening methods for the efficient detection of high-affinity hapten-specific monoclonal antibodies. *Journal of Immunological Methods* **329**, 184-193 (2008).

(23) Ecker, D. M., Jones, S. D., and Levine, H. L. The therapeutic monoclonal antibody market. *mAbs* **7**, 9-14 (2015).

(24) Rodgers, K. R., and Chou, R. C. Therapeutic monoclonal antibodies and derivatives: Historical perspectives and future directions. *Biotechnology Advances* **34**, 1149-1158 (2016).

(25) Pierpont, T. M., Limper, C. B., and Richards, K. L. Past, present, and future of rituximab—the world's first oncology monoclonal antibody therapy. *Frontiers in Oncology* **8**, 163 (2018).

(26) Zhang, C. Hybridoma technology for the generation of monoclonal antibodies. In *Antibody Methods and Protocols*, pp 117-135, Springer (2012).

(27) Foote, J., and Winter, G. Antibody framework residues affecting the conformation of the hypervariable loops. *Journal of Molecular Biology* **224**, 487-499 (1992).

(28) Etches, R. The OmniAb® Platform: Human Sequence Antibodies from Mouse, Rat and Chicken. *Genetic Engineering & Biotechnology News* **39**, 27-29 (2019).

(29) McCafferty, J., Griffiths, A. D., Winter, G., et al. Phage antibodies: filamentous phage displaying antibody variable domains. *Nature* **348**, 552-554 (1990).

(30) Boder, E. T., and Wittrup, K. D. Yeast surface display for screening combinatorial polypeptide libraries. *Nature Biotechnology* **15**, 553-557 (1997).

(31) Ståhl, S., and Uhlén, M. Bacterial surface display: trends and progress. *Trends in Biotechnology* **15**, 185-192 (1997).

(32) Hanes, J., and Plückthun, A. In vitro selection and evolution of functional proteins by using ribosome display. *Proceedings of the National Academy of Sciences* **94**, 4937-4942 (1997).

(33) Persson, M. A. Twenty years of combinatorial antibody libraries, but how well do they mimic the immunoglobulin repertoire? *Proceedings of the National Academy of Sciences* **106**, 20137-20138 (2009).

(34) Barbas, C. F., Bain, J., Hoekstra, D. M., et al. Semisynthetic combinatorial antibody libraries: a chemical solution to the diversity problem. *Proceedings of the National Academy of Sciences* **89**, 4457-4461 (1992).

(35) Mondon, P., Dubreuil, O., Bouayadi, K., et al. Human antibody libraries: a race to engineer and explore a larger diversity. *Frontiers in Bioscience* **13**, 1117-1129 (2008).

(36) Zahra, D. G., Vancov, T., Dunn, J. M., et al. Selectable in-vivo recombination to increase antibody library size—an improved phage display vector system. *Gene* **227**, 49-54 (1999).

(37) Grzeschik, J., Yanakieva, D., Roth, L., et al. Yeast surface display in combination with fluorescence-activated cell sorting enables the rapid isolation of antibody fragments derived from immunized chickens. *Biotechnology Journal* **14** (2019).

(38) Carmen, S., and Jermutus, L. Concepts in antibody phage display. *Briefings in Functional Genomics* **1**, 189-203 (2002).

(39) Pande, J., Szewczyk, M. M., and Grover, A. K. Phage display: concept, innovations, applications and future. *Biotechnology Advances* **28**, 849-858 (2010).

(40) Benatuil, L., Perez, J. M., Belk, J., et al. An improved yeast transformation method for the generation of very large human antibody libraries. *Protein Engineering Design and Selection* **23**, 155-159 (2010).

(41) Cherf, G. M., and Cochran, J. R. Applications of yeast surface display for protein engineering. In *Yeast Surface Display*, pp 155-175, Springer (2015).

(42) Colby, D. W., Kellogg, B. A., Graff, C. P., et al. Engineering antibody affinity by yeast surface display. In *Methods in Enzymology*, pp 348-358, Elsevier (2004).

(43) Bradbury, A. R., Sidhu, S., Dübel, S., et al. Beyond natural antibodies: the power of in vitro display technologies. *Nature Biotechnology* **29**, 245 (2011).

(44) Lu, R.-M., Hwang, Y.-C., Liu, I.-J., et al. Development of therapeutic antibodies for the treatment of diseases. *Journal of Biomedical Science* **27**, 1-30 (2020).

(45) Bahara, N. H. H., Tye, G. J., Choong, Y. S., et al. Phage display antibodies for diagnostic applications. *Biologicals* **41**, 209-216 (2013).

(46) Sormanni, P., Aprile, F. A., and Vendruscolo, M. Third generation antibody discovery methods: in silico rational design. *Chemical Society Reviews* **47**, 9137-9157 (2018).

(47) OPIG. (2019) Structural Information to Aid in silico Therapeutic Antibody Design from Next-Generation Sequencing Repertoires. In *American Pharmaceutical Review*, Oxford Protein Informatics Group.

(48) Norman, R. A., Ambrosetti, F., Bonvin, A. M., et al. Computational approaches to therapeutic antibody design: established methods and emerging trends. *Briefings in Bioinformatics* **bbz095** (2019).

(49) Scott, A. M., Allison, J. P., and Wolchok, J. D. Monoclonal antibodies in cancer therapy. *Cancer Immunity Archive* **12**, 14 (2012).

(50) Suzuki, M., Kato, C., and Kato, A. Therapeutic antibodies: their mechanisms of action and the pathological findings they induce in toxicity studies. *Journal of Toxicologic Pathology* **28**, 133-139 (2015).

(51) Kawaguchi, Y., Kono, K., Mimura, K., et al. Targeting EGFR and HER-2 with cetuximab-and trastuzumab-mediated immunotherapy in oesophageal squamous cell carcinoma. *British Journal of Cancer* **97**, 494-501 (2007).

(52) Ferrara, N., Hillan, K. J., and Novotny, W. Bevacizumab (Avastin), a humanized anti-VEGF monoclonal antibody for cancer therapy. *Biochemical and Biophysical Research Communications* **333**, 328-335 (2005).

(53) Biswas, S., Nyman, J. S., Alvarez, J., et al. Anti-transforming growth factor β antibody treatment rescues bone loss and prevents breast cancer metastasis to bone. *PloS One* **6** (2011).

(54) Narayan, M., Wilken, J. A., Harris, L. N., et al. Trastuzumab-induced HER reprogramming in "resistant" breast carcinoma cells. *Cancer Research* **69**, 2191-2194 (2009).

(55) Ducry, L., and Stump, B. Antibody− drug conjugates: linking cytotoxic payloads to monoclonal antibodies. *Bioconjugate Chemistry* **21**, 5-13 (2010).

(56) Bourgeois, M., Bailly, C., Frindel, M., et al. Radioimmunoconjugates for treating cancer: recent advances and current opportunities. *Expert Opinion on Biological Therapy* **17**, 813-819 (2017).

(57) Huehls, A. M., Coupet, T. A., and Sentman, C. L. Bispecific T-cell engagers for cancer immunotherapy. *Immunology and Cell Biology* **93**, 290-296 (2015).

(58) Feltes, T. F., Cabalka, A. K., Meissner, H. C., et al. Palivizumab prophylaxis reduces hospitalization due to respiratory syncytial virus in young children with hemodynamically significant congenital heart disease. *The Journal of Pediatrics* **143**, 532-540 (2003).

(59) Ferrara, N., Hillan, K. J., Gerber, H.-P., et al. Discovery and development of bevacizumab, an anti-VEGF antibody for treating cancer. *Nature Reviews Drug Discovery* **3**, 391-400 (2004).

(60) Tan, S., Liu, K., Chai, Y., et al. Distinct PD-L1 binding characteristics of therapeutic monoclonal antibody durvalumab. *Protein & Cell* **9**, 135-139 (2018).

(61) Bain, B., and Brazil, M. Adalimumab. *Nature Reviews Drug Discovery* **2**, 693-694 (2003).

(62) Markham, A., and Lamb, H. M. Infliximab. *Drugs* **59**, 1341-1359 (2000).

(63) Carter, P. J., and Lazar, G. A. Next generation antibody drugs: pursuit of the'high-hanging fruit'. *Nature Reviews Drug Discovery* **17**, 197 (2018).

(64) Clark, E. A., and Ledbetter, J. A. Amplification of the immune response by agonistic antibodies. *Immunology Today* **7**, 267-270 (1986).

(65) Mayes, P. A., Hance, K. W., and Hoos, A. The promise and challenges of immune agonist antibody development in cancer. *Nature Reviews Drug Discovery* **17**, 509-527 (2018).

(66) Vonderheide, R. H., and Glennie, M. J. Agonistic CD40 antibodies and cancer therapy. *American Association for Cancer Research* (2013).

(67) Aspeslagh, S., Postel-Vinay, S., Rusakiewicz, S., et al. Rationale for anti-OX40 cancer immunotherapy. *European Journal of Cancer* **52**, 50-66 (2016).

(68) Knee, D. A., Hewes, B., and Brogdon, J. L. Rationale for anti-GITR cancer immunotherapy. *European Journal of Cancer* **67**, 1-10 (2016).

(69) Amatore, F., Gorvel, L., and Olive, D. Inducible Co-Stimulator (ICOS) as a potential therapeutic target for anti-cancer therapy. *Expert Opinion on Therapeutic Targets* **22**, 343-351 (2018).

(70) Sanmamed, M. F., Pastor, F., Rodriguez, A., et al. Agonists of co-stimulation in cancer immunotherapy directed against CD137, OX40, GITR, CD27, CD28, and ICOS. *Seminars in Oncology* **42**, 640-655 (2015).

(71) Carter, P., Smith, L., and Ryan, M. Identification and validation of cell surface antigens for antibody targeting in oncology. *Endocrine-Related Cancer* **11**, 659-687 (2004).

(72) Gonzalez-Munoz, A. L., Minter, R. R., and Rust, S. J. Phenotypic screening: the future of antibody discovery. *Drug Discovery Today* **21**, 150-156 (2016).

(73) Lazo, J. S., and Sharlow, E. R. Drugging undruggable molecular cancer targets. *Annual Review of Pharmacology and Toxicology* **56**, 23-40 (2016).

(74) Cox, A. D., Fesik, S. W., Kimmelman, A. C., et al. Drugging the undruggable RAS: mission possible? *Nature Reviews Drug Discovery* **13**, 828-851 (2014).

(75) Dang, C. V., Reddy, E. P., Shokat, K. M., et al. Drugging the'undruggable'cancer targets. *Nature Reviews Cancer* **17**, 502 (2017).

(76) Klepsch, V., Hermann-Kleiter, N., Do-Dinh, P., et al. Nuclear receptor NR2F6 inhibition potentiates responses to PD-L1/PD-1 cancer immune checkpoint blockade. *Nature Communications* **9**, 1-13 (2018).

(77) Slastnikova, T. A., Ulasov, A. V., Rosenkranz, A. A., et al. Targeted intracellular delivery of antibodies: The state of the art. *Frontiers in Pharmacology* **9**, 1208 (2018).

(78) Ritchie, M., Tchistiakova, L., and Scott, N. Implications of receptor-mediated endocytosis and intracellular trafficking dynamics in the development of antibody drug conjugates. *mAbs* **5**, 13-21 (2013).

(79) Zhao, Y., Lou, D., Burkett, J., et al. Chemical engineering of cell penetrating antibodies. *Journal of Immunological Methods* **254**, 137-145 (2001).

(80) Masuda, R., Yamamoto, K., and Koide, T. Cellular uptake of IgG using collagen-like cell-penetrating peptides. *Biological and Pharmaceutical Bulletin* **39**, 130-134 (2016).

(81) Herrmann, A., Nagao, T., Zhang, C., et al. An effective cell-penetrating antibody delivery platform. *JCI Insight* **4** (2019).

(82) Courtête, J., Sibler, A.-P., Zeder-Lutz, G., et al. Suppression of cervical carcinoma cell growth by intracytoplasmic codelivery of anti-oncoprotein E6 antibody and small interfering RNA. *Molecular Cancer Therapeutics* **6**, 1728-1735 (2007).

(83) Tian, X., Nyberg, S., Sharp, P. S., et al. LRP-1-mediated intracellular antibody delivery to the Central Nervous System. *Scientific Reports* **5**, 11990 (2015).

(84) Amornwachirabodee, K., Tantimekin, N., Pan-In, P., et al. Oxidized carbon black: preparation, characterization and application in antibody delivery across cell membrane. *Scientific Reports* **8**, 1-11 (2018).

(85) Abraham, A., Natraj, U., Karande, A. A., et al. Intracellular delivery of antibodies by chimeric Sesbania mosaic virus (SeMV) virus like particles. *Scientific Reports* **6**, 21803 (2016).

(86) Hansen, J. E., Chan, G., Liu, Y., et al. Targeting cancer with a lupus autoantibody. *Science Translational Medicine* **4**, 157ra142-157ra142 (2012).

(87) Douglas, J. N., Gardner, L., and Levin, M. Antibodies to an intracellular antigen penetrate neuronal cells and cause deleterious effects. *Journal of Clinical and Cellular Immunology* **4**, 134 (2013).

(88) Foster, M. H., Kieber-Emmons, T., Ohliger, M., et al. Molecular and structural analysis of nuclear localizing anti-DNA lupus antibodies. *Immunologic Research* **13**, 186-206 (1994).

(89) Chen, Z., Patel, J. M., Noble, P. W., et al. A lupus anti-DNA autoantibody mediates autocatalytic, targeted delivery of nanoparticles to tumors. *Oncotarget* **7**, 59965 (2016).

(90) Hansen, J. E., Sohn, W., Kim, C., et al. Antibody-mediated Hsp70 protein therapy. *Brain Research* **1088**, 187-196 (2006).

(91) Choi, D.-K., Bae, J., Shin, S.-M., et al. A general strategy for generating intact, full-length IgG antibodies that penetrate into the cytosol of living cells. *mAbs* **6**, 1402-1414 (2014).

(92) Kim, J.-S., Choi, D.-K., Shin, J.-Y., et al. Endosomal acidic pH-induced conformational changes of a cytosol-penetrating antibody mediate endosomal escape. *Journal of Controlled Release* **235**, 165-175 (2016).

(93) Kim, J.-s., Park, J.-Y., Shin, S.-M., et al. Engineering of a tumor cell–specific, cytosol-penetrating antibody with high endosomal escape efficacy. *Biochemical and Biophysical Research Communications* **503**, 2510-2516 (2018).

(94) Egan, T. J., Diem, D., Weldon, R., et al. Novel multispecific heterodimeric antibody format allowing modular assembly of variable domain fragments. *mAbs* **9**, 68-84 (2017).

(95) Min, S. E., Lee, K. H., Park, S. W., et al. Cell-free production and streamlined assay of cytosol-penetrating antibodies. *Biotechnology and Bioengineering* **113**, 2107-2112 (2016).

(96) Beck, A. Biosimilar, biobetter and next generation therapeutic antibodies. *mAbs* **3**, 107-110 (2011).

(97) Zheng, W., Thorne, N., and McKew, J. C. Phenotypic screens as a renewed approach for drug discovery. *Drug Discovery Today* **18**, 1067-1073 (2013).

(98) Beck, A., Wurch, T., Bailly, C., et al. Strategies and challenges for the next generation of therapeutic antibodies. *Nature Reviews Immunology* **10**, 345-352 (2010).

(99) Ljungars, A., Mårtensson, L., Mattsson, J., et al. A platform for phenotypic discovery of therapeutic antibodies and targets applied on Chronic Lymphocytic Leukemia. *NPJ Precision Oncology* **2**, 1-4 (2018).

(100) Boutros, M., Heigwer, F., and Laufer, C. Microscopy-based high-content screening. *Cell* **163**, 1314-1325 (2015).

(101) Schirle, M., Bantscheff, M., and Kuster, B. Mass spectrometry-based proteomics in preclinical drug discovery. *Chemistry & Biology* **19**, 72-84 (2012).

(102) Terstappen, G. C., Schlüpen, C., Raggiaschi, R., et al. Target deconvolution strategies in drug discovery. *Nature Reviews Drug Discovery* **6**, 891-903 (2007).

(103) Shih, H. H. Discovery process for antibody-based therapeutics. In *Development of Antibody-Based Therapeutics* (Tabrizi M., B. G., Klakamp S. , Ed.), pp 9-32, Springer New York (2012).

(104) Chodorge, M., Züger, S., Stirnimann, C., et al. A series of Fas receptor agonist antibodies that demonstrate an inverse correlation between affinity and potency. *Cell Death & Differentiation* **19**, 1187-1195 (2012).

(105) Ho, S. K., Xu, Z., Thakur, A., et al. Epitope and Fc-mediated Crosslinking, but not High Affinity, Are Critical for Antitumor Activity of CD137 Agonist Antibody with Reduced Liver Toxicity. *Molecular Cancer Therapeutics* (2020).

(106) Almagro, J. C., Pedraza-Escalona, M., Arrieta, H. I., et al. Phage Display Libraries for Antibody Therapeutic Discovery and Development. *Antibodies* **8**, 44 (2019).

(107) Goodnow, J., Guba, W., and Haap, W. Library design practices for success in lead generation with small molecule libraries. *Combinatorial Chemistry & High Throughput Screening* **6**, 649-660 (2003).

(108) Joslin, J., Gilligan, J., Anderson, P., et al. A fully automated high-throughput flow cytometry screening system enabling phenotypic drug discovery. *SLAS Discovery* **23**, 697-707 (2018).

(109) Yadav, S., Liu, J., Scherer, T. M., et al. Assessment and significance of protein–protein interactions during development of protein biopharmaceuticals. *Biophysical Reviews* **5**, 121-136 (2013).

(110) Vainshtein, I., Roskos, L. K., Cheng, J., et al. Quantitative measurement of the target-mediated internalization kinetics of biopharmaceuticals. *Pharmaceutical research* **32**, 286-299 (2015).

(111) Schreiber, A. B., Libermann, T., Lax, I., et al. Biological role of epidermal growth factor-receptor clustering. Investigation with monoclonal anti-receptor antibodies. *Journal of Biological Chemistry* **258**, 846-853 (1983).

(112) Weiner, G. J. Rituximab: mechanism of action. *Seminars in Hematology* **47**, 115-123 (2010).

(113) Zanella, F., Lorens, J. B., and Link, W. High content screening: seeing is believing. *Trends in Biotechnology* **28**, 237-245 (2010).

(114) Rabal, O., Link, W., Serelde, B. G., et al. An integrated one-step system to extract, analyze and annotate all relevant information from image-based cell screening of chemical libraries. *Molecular BioSystems* **6**, 711-720 (2010).

(115) Loo, L.-H., Wu, L. F., and Altschuler, S. J. Image-based multivariate profiling of drug responses from single cells. *Nature Methods* **4**, 445-453 (2007).

(116) Starkuviene, V., and Pepperkok, R. The potential of high-content high-throughput microscopy in drug discovery. *British Journal of Pharmacology* **152**, 62-71 (2007).

(117) Wu, G., and Doberstein, S. K. HTS technologies in biopharmaceutical discovery. *Drug Discovery Today* **11**, 718-724 (2006).

(118) Szymański, P., Markowicz, M., and Mikiciuk-Olasik, E. Adaptation of high-throughput screening in drug discovery—toxicological screening tests. *International Journal of Molecular Sciences* **13**, 427-452 (2012).

(119) Yang, L., and Nolan, J. P. High-throughput screening and characterization of clones selected from phage display libraries. *Cytometry Part A: The Journal of the International Society for Analytical Cytology* **71**, 625-631 (2007).

(120) Cronk, D. Chapter 8 - High-throughput screening. In *Drug Discovery and Development (Second Edition)* (Hill, R. G., and Rang, H. P., Eds.), pp 95-117, Churchill Livingstone (2013).

(121) Brandish, P. E., Chiu, C.-S., Schneeweis, J., et al. A cell-based ultra-high-throughput screening assay for identifying inhibitors of D-amino acid oxidase. *Journal of Biomolecular Screening* **11**, 481-487 (2006).

(122) Pereira, S. A. P., Dyson, P. J., and Saraiva, M. L. M. F. S. Miniaturized technologies for high-throughput drug screening enzymatic assays and diagnostics – A review. *Trends in Analytical Chemistry* **126**, 115862 (2020).

(123) Ríos, Á., and Zougagh, M. Modern qualitative analysis by miniaturized and microfluidic systems. *Trends in Analytical Chemistry* **69**, 105-113 (2015).

(124) Smith, A. How small should you go? *Nature* **418**, 457-457 (2002).

(125) Howbrook, D. N., van der Valk, A. M., O'Shaughnessy, M. C., et al. Developments in microarray technologies. *Drug Discovery Today* **8**, 642-651 (2003).

(126) MacBeath, G., and Schreiber, S. L. Printing proteins as microarrays for high-throughput function determination. *Science* **289**, 1760-1763 (2000).

(127) Stoll, D., Bachmann, J., Templin, M. F., et al. Microarray technology: an increasing variety of screening tools for proteomic research. *Drug Discovery Today: TARGETS* **3**, 24-31 (2004).

(128) Syahir, A., Usui, K., Tomizaki, K.-y., et al. Label and label-free detection techniques for protein microarrays. *Microarrays* **4**, 228-244 (2015).

(129) Chen, H., and Li, J. Nanotechnology. In *Microarrays*, pp 411-436, Springer (2007).

(130) Convery, N., and Gadegaard, N. 30 years of microfluidics. *Micro and Nano Engineering* (2019).

(131) Qin, D., Xia, Y., Rogers, J. A., et al. Microfabrication, microstructures and microsystems. In *Microsystem Technology in Chemistry and Life Science*, pp 1-20, Springer (1998).

(132) Whitesides, G. M. The origins and the future of microfluidics. *Nature* **442**, 368-373 (2006).

(133) Gao, Y., Li, P., and Pappas, D. A microfluidic localized, multiple cell culture array using vacuum actuated cell seeding: integrated anticancer drug testing. *Biomedical Microdevices* **15**, 907-915 (2013).

(134) Huh, D., Hamilton, G. A., and Ingber, D. E. From 3D cell culture to organs-on-chips. *Trends in Cell Biology* **21**, 745-754 (2011).

(135) Marsano, A., Conficconi, C., Lemme, M., et al. Beating heart on a chip: a novel microfluidic platform to generate functional 3D cardiac microtissues. *Lab on a Chip* **16**, 599-610 (2016).

(136) Guo, M. T., Rotem, A., Heyman, J. A., et al. Droplet microfluidics for high-throughput biological assays. *Lab on a Chip* **12**, 2146-2155 (2012).

(137) Teh, S.-Y., Lin, R., Hung, L.-H., et al. Droplet microfluidics. *Lab on a Chip* **8**, 198-220 (2008).

(138) Rosen, M. J., and Kunjappu, J. T. *Surfactants and Interfacial Phenomena*, John Wiley & Sons (2012).

(139) Brouzes, E., Medkova, M., Savenelli, N., et al. Droplet microfluidic technology for single-cell high-throughput screening. *Proceedings of the National Academy of Sciences* **106**, 14195-14200 (2009).

(140) Kaltenbach, M., Devenish, S. R., and Hollfelder, F. A simple method to evaluate the biochemical compatibility of oil/surfactant mixtures for experiments in microdroplets. *Lab on a Chip* **12**, 4185-4192 (2012).

(141) Holtze, C., Rowat, A., Agresti, J., et al. Biocompatible surfactants for water-in-fluorocarbon emulsions. *Lab on a Chip* **8**, 1632-1639 (2008).

(142) Tran, T., Lan, F., Thompson, C., et al. From tubes to drops: droplet-based microfluidics for ultrahigh-throughput biology. *Journal of Physics D: Applied Physics* **46**, 114004 (2013).

(143) Sphere Fluidics. (10.04.2020) Pico-Surf(TM) Surfactant. https://spherefluidics.com/store/pico-surf-1-5-w-w-in-novec-7500/?v=3a52f3c22ed6, accessed at 10.04.2020.

(144) Damiati, S., Kompella, U. B., Damiati, S. A., et al. Microfluidic devices for drug delivery systems and drug screening. *Genes* **9**, 103 (2018).

(145) Utada, A. S., Fernandez-Nieves, A., Stone, H. A., et al. Dripping to jetting transitions in coflowing liquid streams. *Physical Review Letters* **99**, 094502 (2007).

(146) Garstecki, P., Fuerstman, M. J., Stone, H. A., et al. Formation of droplets and bubbles in a microfluidic T-junction—scaling and mechanism of break-up. *Lab on a Chip* **6**, 437-446 (2006).

(147) Abate, A., Poitzsch, A., Hwang, Y., et al. Impact of inlet channel geometry on microfluidic drop formation. *Physical Review E* **80**, 026310 (2009).

(148) Collins, D. J., Neild, A., DeMello, A., et al. The Poisson distribution and beyond: methods for microfluidic droplet production and single cell encapsulation. *Lab on a Chip* **15**, 3439-3459 (2015).

(149) Kim, H. S., Devarenne, T. P., and Han, A. A high-throughput microfluidic single-cell screening platform capable of selective cell extraction. *Lab on a Chip* **15**, 2467-2475 (2015).

(150) Tang, D. G. Understanding cancer stem cell heterogeneity and plasticity. *Cell Research* **22**, 457-472 (2012).

(151) Yin, H., and Marshall, D. Microfluidics for single cell analysis. *Current Opinion in Biotechnology* **23**, 110-119 (2012).

(152) Frenz, L., Blank, K., Brouzes, E., et al. Reliable microfluidic on-chip incubation of droplets in delay-lines. *Lab on a Chip* **9**, 1344-1348 (2009).

(153) Link, D., Anna, S. L., Weitz, D., et al. Geometrically mediated breakup of drops in microfluidic devices. *Physical Review Letters* **92**, 054503 (2004).

(154) Mazutis, L., Baret, J.-C., and Griffiths, A. D. A fast and efficient microfluidic system for highly selective one-to-one droplet fusion. *Lab on a Chip* **9**, 2665-2672 (2009).

(155) Mazutis, L., and Griffiths, A. D. Selective droplet coalescence using microfluidic systems. *Lab on a Chip* **12**, 1800-1806 (2012).

(156) Ahn, K., Agresti, J., Chong, H., et al. Electrocoalescence of drops synchronized by size-dependent flow in microfluidic channels. *Applied Physics Letters* **88**, 264105 (2006).

(157) Abate, A. R., Hung, T., Mary, P., et al. High-throughput injection with microfluidics using picoinjectors. *Proceedings of the National Academy of Sciences* **107**, 19163-19166 (2010).

(158) Sciambi, A., and Abate, A. R. Accurate microfluidic sorting of droplets at 30 kHz. *Lab on a Chip* **15**, 47-51 (2015).

(159) Mazutis, L., Gilbert, J., Ung, W. L., et al. Single-cell analysis and sorting using droplet-based microfluidics. *Nature Protocols* **8**, 870 (2013).

(160) Eastburn, D. J., Sciambi, A., and Abate, A. R. Identification and genetic analysis of cancer cells with PCR-activated cell sorting. *Nucleic Acids Research* **42**, e128-e128 (2014).

(161) Wang, B. L., Ghaderi, A., Zhou, H., et al. Microfluidic high-throughput culturing of single cells for selection based on extracellular metabolite production or consumption. *Nature Biotechnology* **32**, 473 (2014).

(162) Fidalgo, L. M., Whyte, G., Bratton, D., et al. From microdroplets to microfluidics: selective emulsion separation in microfluidic devices. *Angewandte Chemie International Edition* **47**, 2042-2045 (2008).

(163) Hulett, H. R., Bonner, W. A., Barrett, J., et al. Cell sorting: automated separation of mammalian cells as a function of intracellular fluorescence. *Science* **166**, 747-749 (1969).

(164) Becton Dickinson. BD Influx. https://www.bdbiosciences.com/en-us/instruments/research-instruments/research-cell-sorters/influx, accessed at 16.04.2020.

(165) Herzenberg, L. A., Parks, D., Sahaf, B., et al. The history and future of the fluorescence activated cell sorter and flow cytometry: a view from Stanford. *Clinical Chemistry* **48**, 1819-1827 (2002).

(166) Bonner, W., Hulett, H., Sweet, R., et al. Fluorescence activated cell sorting. *Review of Scientific Instruments* **43**, 404-409 (1972).

(167) Herzenberg, L. A., De Rosa, S. C., and Herzenberg, L. A. Monoclonal antibodies and the FACS: complementary tools for immunobiology and medicine. *Immunology Today* **21**, 383-390 (2000).

(168) Brown, M., and Wittwer, C. Flow cytometry: principles and clinical applications in hematology. *Clinical Chemistry* **46**, 1221-1229 (2000).

(169) Yang, G., and Withers, S. G. Ultrahigh-throughput FACS-based screening for directed enzyme evolution. *ChemBioChem* **10**, 2704-2715 (2009).

(170) Bernath, K., Magdassi, S., and Tawfik, D. S. In vitro compartmentalization (ivc): A high-throughput screening technology using emulsions and facs. *Discovery Medicine* **4**, 49-53 (2009).

(171) Aharoni, A., Amitai, G., Bernath, K., et al. High-throughput screening of enzyme libraries: thiolactonases evolved by fluorescence-activated sorting of single cells in emulsion compartments. *Chemistry & Biology* **12**, 1281-1289 (2005).

(172) Sukovich, D. J., Kim, S. C., Ahmed, N., et al. Bulk double emulsification for flow cytometric analysis of microfluidic droplets. *Analyst* **142**, 4618-4622 (2017).

(173) van der Graaf, S., Schroën, C., and Boom, R. Preparation of double emulsions by membrane emulsification—a review. *Journal of Membrane Science* **251**, 7-15 (2005).

(174) Mastrobattista, E., Taly, V., Chanudet, E., et al. High-throughput screening of enzyme libraries: in vitro evolution of a β-galactosidase by fluorescence-activated sorting of double emulsions. *Chemistry & Biology* **12**, 1291-1300 (2005).

(175) Kim, S.-H., Kim, J. W., Cho, J.-C., et al. Double-emulsion drops with ultra-thin shells for capsule templates. *Lab on a Chip* **11**, 3162-3166 (2011).

(176) Dolomite Bio. (2019) Cells in double emulsions for FACS sorting https://www.dolomite-microfluidics.com/support/downloads/, accessed at 17.04.2020.

(177) Cole, R. H., Tran, T. M., and Abate, A. R. Double emulsion generation using a polydimethylsiloxane (pdms) co-axial flow focus device. *JoVE (Journal of Visualized Experiments)*, e53516 (2015).

(178) Hua, T., Zhang, X., Tang, B., et al. Tween-20 transiently changes the surface morphology of PK-15 cells and improves PCV2 infection. *BMC Veterinary Research* **14**, 138 (2018).

(179) Han, D., Liu, K., Guo, S., et al. Dose-effect relationship of DMSO and Tween 80 influencing the growth and viability of murine bone marrow-derived cells in vitro. *Journal of Experimental Hematology* **16**, 377-380 (2008).

(180) Zinchenko, A., Devenish, S. R., Kintses, B., et al. One in a million: flow cytometric sorting of single cell-lysate assays in monodisperse picolitre double emulsion droplets for directed evolution. *Analytical Chemistry* **86**, 2526-2533 (2014).

(181) Zhang, Y., Ho, Y.-P., Chiu, Y.-L., et al. A programmable microenvironment for cellular studies via microfluidics-generated double emulsions. *Biomaterials* **34**, 4564-4572 (2013).

(182) Sukhorukov, G. B., Volodkin, D. V., Günther, A. M., et al. Porous calcium carbonate microparticles as templates for encapsulation of bioactive compounds. *Journal of Materials Chemistry* **14**, 2073-2081 (2004).

(183) Weaver, J. C., Bliss, J. G., Harrison, G. I., et al. Microdrop technology: a general method for separating cells by function and composition. *Methods* **2**, 234-247 (1991).

(184) Weaver, J. C., McGrath, P., and Adams, S. Gel microdrop technology for rapid isolation of rare and high producer cells. *Nature Medicine* **3**, 583-585 (1997).

(185) Tibbitt, M. W., and Anseth, K. S. Hydrogels as extracellular matrix mimics for 3D cell culture. *Biotechnology and Bioengineering* **103**, 655-663 (2009).

(186) Wang, Y., and Wang, J. Mixed hydrogel bead-based tumor spheroid formation and anticancer drug testing. *Analyst* **139**, 2449-2458 (2014).

(187) Yu, L., Chen, M. C., and Cheung, K. C. Droplet-based microfluidic system for multicellular tumor spheroid formation and anticancer drug testing. *Lab on a Chip* **10**, 2424-2432 (2010).

(188) Yoon, S., Kim, J. A., Lee, S. H., et al. Droplet-based microfluidic system to form and separate multicellular spheroids using magnetic nanoparticles. *Lab on a Chip* **13**, 1522-1528 (2013).

(189) Peppas, N. Fundamentals, preparation method and structure of hydrogels, Vol. I. In *Hydrogels in Medicine and Pharmacy*, Boca Raton: CRS Press, Florida (1986).

(190) Mahinroosta, M., Farsangi, Z. J., Allahverdi, A., et al. Hydrogels as intelligent materials: A brief review of synthesis, properties and applications. *Materials Today Chemistry* **8**, 42-55 (2018).

(191) Tirella, A., Magliaro, C., Penta, M., et al. Sphyga: a multiparameter open source tool for fabricating smart and tunable hydrogel microbeads. *Biofabrication* **6**, 025009 (2014).

(192) Liang, Y., Kashdan, T., Sterner, C., et al. Algal biorefineries. In *Industrial Biorefineries & White Biotechnology*, pp 35-90, Elsevier (2015).

(193) Lee, P., and Rogers, M. Effect of calcium source and exposure-time on basic caviar spherification using sodium alginate. *International Journal of Gastronomy and Food Science* **1**, 96-100 (2012).

(194) Tønnesen, H. H., and Karlsen, J. Alginate in drug delivery systems. *Drug Development and Industrial Pharmacy* **28**, 621-630 (2002).

(195) Pasparakis, G., and Bouropoulos, N. Swelling studies and in vitro release of verapamil from calcium alginate and calcium alginate–chitosan beads. *International Journal of Pharmaceutics* **323**, 34-42 (2006).

(196) Griffith, L. Polymeric biomaterials. *Acta Materialia* **48**, 263-277 (2000).

(197) Poojari, R., and Srivastava, R. Composite alginate microspheres as the next-generation egg-box carriers for biomacromolecules delivery. *Expert Opinion on Drug Delivery* **10**, 1061-1076 (2013).

(198) Håti, A. G., Bassett, D. C., Ribe, J. M., et al. Versatile, cell and chip friendly method to gel alginate in microfluidic devices. *Lab on a Chip* **16**, 3718-3727 (2016).

(199) Quong, D., Neufeld, R., Skjåk-Bræk, G., et al. External versus internal source of calcium during the gelation of alginate beads for DNA encapsulation. *Biotechnology and Bioengineering* **57**, 438-446 (1998).

(200) Huang, K.-S., Lai, T.-H., and Lin, Y.-C. Manipulating the generation of Ca-alginate microspheres using microfluidic channels as a carrier of gold nanoparticles. *Lab on a Chip* **6**, 954-957 (2006).

(201) Wang, N., Adams, G., Buttery, L., et al. Alginate encapsulation technology supports embryonic stem cells differentiation into insulin-producing cells. *Journal of Biotechnology* **144**, 304-312 (2009).

(202) Koch, S., Schwinger, C., Kressler, J., et al. Alginate encapsulation of genetically engineered mammalian cells: comparison of production devices, methods and microcapsule characteristics. *Journal of Microencapsulation* **20**, 303-316 (2003).

(203) Kim, C., Lee, K. S., Kim, Y. E., et al. Rapid exchange of oil-phase in microencapsulation chip to enhance cell viability. *Lab on a Chip* **9**, 1294-1297 (2009).

(204) Liu, H., Li, G., Sun, X., et al. Microfluidic generation of uniform quantum dot-encoded microbeads by gelation of alginate. *RSC Advances* **5**, 62706-62712 (2015).

(205) Utech, S., Prodanovic, R., Mao, A. S., et al. Microfluidic generation of monodisperse, structurally homogeneous alginate microgels for cell encapsulation and 3D cell culture. *Advanced Healthcare Materials* **4**, 1628-1633 (2015).

(206) Kleinman, H. K., and Martin, G. R. Matrigel: basement membrane matrix with biological activity. *Seminars in Cancer Biology* **15**, 378-386 (2005).

(207) Hughes, C. S., Postovit, L. M., and Lajoie, G. A. Matrigel: a complex protein mixture required for optimal growth of cell culture. *Proteomics* **10**, 1886-1890 (2010).

(208) Molina-Jimenez, F., Benedicto, I., Thi, V. L. D., et al. Matrigel-embedded 3D culture of Huh-7 cells as a hepatocyte-like polarized system to study hepatitis C virus cycle. *Virology* **425**, 31-39 (2012).

(209) Dolega, M. E., Abeille, F., Picollet-d'Hahan, N., et al. Controlled 3D culture in Matrigel microbeads to analyze clonal acinar development. *Biomaterials* **52**, 347-357 (2015).

(210) Laperrousaz, B., Porte, S., Gerbaud, S., et al. Direct transfection of clonal organoids in Matrigel microbeads: a promising approach toward organoid-based genetic screens. *Nucleic Acids Research* **46**, e70-e70 (2018).

(211) Zhang, W. Encapsulation of transgenic cells for gene therapy. In *Gene Therapy-Principles and Challenges*, IntechOpen (2015).

(212) Arnott, S., Fulmer, A., Scott, W., et al. The agarose double helix and its function in agarose gel structure. *Journal of Molecular Biology* **90**, 269-284 (1974).

(213) Wang, N., and Wu, X. S. Preparation and characterization of agarose hydrogel nanoparticles for protein and peptide drug delivery. *Pharmaceutical Development and Technology* **2**, 135-142 (1997).

(214) Li, R. H., Altreuter, D. H., and Gentile, F. T. Transport characterization of hydrogel matrices for cell encapsulation. *Biotechnology and Bioengineering* **50**, 365-373 (1996).

(215) WANG, J.-l., ZAHNG, X.-q., YE, J., et al. Preparation and characterization of agarose with low gelling temperature. *Modern Chemical Industry*, 27 (2017).

(216) Velasco, D., Tumarkin, E., and Kumacheva, E. Microfluidic encapsulation of cells in polymer microgels. *Small* **8**, 1633-1642 (2012).

(217) Snap Gene. (07.04.2020) GAL1 promoter. https://www.snapgene.com/resources/plasmid-files/?set=basic_cloning_vectors&plasmid=GAL1_promoter, accessed at 07.04.2020.

(218) Rakestraw, J. A., Sazinsky, S. L., Piatesi, A., et al. Directed evolution of a secretory leader for the improved expression of heterologous proteins and full-length antibodies in Saccharomyces cerevisiae. *Biotechnology and Bioengineering* **103**, 1192-1201 (2009).

(219) Grzeschik, J., Hinz, S. C., Könning, D., et al. A simplified procedure for antibody engineering by yeast surface display: Coupling display levels and target binding by ribosomal skipping. *Biotechnology Journal* **12**, 1600454 (2017).

(220) Kamiyama, D., Sekine, S., Barsi-Rhyne, B., et al. Versatile protein tagging in cells with split fluorescent protein. *Nature Communications* **7**, 1-9 (2016).

(221) Austin, C. D., De Mazière, A. M., Pisacane, P. I., et al. Endocytosis and sorting of ErbB2 and the site of action of cancer therapeutics trastuzumab and geldanamycin. *Molecular Biology of the Cell* **15**, 5268-5282 (2004).

(222) Kaesberg, P. R., Ershler, W. B., Esko, J. D., et al. Chinese hamster ovary cell adhesion to human platelet thrombospondin is dependent on cell surface heparan sulfate proteoglycan. *The Journal of Clinical Investigation* **83**, 994-1001 (1989).

(223) Cabantous, S., Terwilliger, T. C., and Waldo, G. S. Protein tagging and detection with engineered self-assembling fragments of green fluorescent protein. *Nature Biotechnology* **23**, 102-107 (2005).

(224) Kent, K. P., Childs, W., and Boxer, S. G. Deconstructing green fluorescent protein. *Journal of the American Chemical Society* **130**, 9664-9665 (2008).

(225) Fang, Y., Chu, T. H., Ackerman, M. E., et al. Going native: Direct high throughput screening of secreted full-length IgG antibodies against cell membrane proteins. *mAbs* **9**, 1253-1261 (2017).

(226) Duarte, J. M., Barbier, I. v., and Schaerli, Y. Bacterial microcolonies in gel beads for high-throughput screening of libraries in synthetic biology. *ACS Synthetic Biology* **6**, 1988-1995 (2017).

(227) Kuwahara, K., Zhu, D., Humayun, M., et al. Evaluation of Matrigel Degradation by MMP Secretion of hESC-RPE. *Investigative Ophthalmology & Visual Science* **53**, 5916-5916 (2012).

(228) Zhang, J.-M., and An, J. Cytokines, inflammation and pain. *International Anesthesiology Clinics* **45**, 27 (2007).

(229) del Peso, L., González-Garcıa, M., Page, C., et al. Interleukin-3-induced phosphorylation of BAD through the protein kinase Akt. *Science* **278**, 687-689 (1997).

(230) Reddy, E. P., Korapati, A., Chaturvedi, P., et al. IL-3 signaling and the role of Src kinases, JAKs and STATs: a covert liaison unveiled. *Oncogene* **19**, 2532-2547 (2000).

(231) Robin, C., and Durand, C. The roles of BMP and IL-3 signaling pathways in the control of hematopoietic stem cells in the mouse embryo. *International Journal of Developmental Biology* **54**, 1189-1200 (2010).

(232) Li, X., Zhao, X., Fang, Y., et al. Generation of destabilized green fluorescent protein as a transcription reporter. *Journal of Biological Chemistry* **273**, 34970-34975 (1998).

(233) Danhier, P., Krishnamachary, B., Bharti, S., et al. Combining optical reporter proteins with different half-lives to detect temporal evolution of hypoxia and reoxygenation in tumors. *Neoplasia* **17**, 871-881 (2015).

(234) Klein, B. K., Feng, Y., McWherter, C. A., et al. The receptor binding site of human interleukin-3 defined by mutagenesis and molecular modeling. *Journal of Biological Chemistry* **272**, 22630-22641 (1997).

(235) Salari, R., and Salari, R. Investigation of the best Saccharomyces cerevisiae growth condition. *Electronic Physician* **9**, 3592 (2017).

(236) Jin, Y.-L., and Speers, R. A. Flocculation of Saccharomyces cerevisiae. *Food Research International* **31**, 421-440 (1998).

(237) Dorssers, L., Mostert, M., Burger, H., et al. Receptor and antibody interactions of human interleukin-3 characterized by mutational analysis. *Journal of Biological Chemistry* **266**, 21310-21317 (1991).

(238) Roose, J. P., Diehn, M., Tomlinson, M. G., et al. T cell receptor-independent basal signaling via Erk and Abl kinases suppresses RAG gene expression. *PLoS Biology* **1** (2003).

(239) Abraham, R. T., and Weiss, A. Jurkat T cells and development of the T-cell receptor signalling paradigm. *Nature Reviews Immunology* **4**, 301-308 (2004).

(240) Smith-Garvin, J. E., Koretzky, G. A., and Jordan, M. S. T cell activation. *Annual Review of Immunology* **27**, 591-619 (2009).

(241) Tsoukas, C. D., Landgraf, B., Bentin, J., et al. Activation of resting T lymphocytes by anti-CD3 (T3) antibodies in the absence of monocytes. *The Journal of Immunology* **135**, 1719-1723 (1985).

(242) Trickett, A., and Kwan, Y. L. T cell stimulation and expansion using anti-CD3/CD28 beads. *Journal of Immunological Methods* **275**, 251-255 (2003).

(243) Nijhuis, E. W., Figdor, C. G., and van Lier, R. A. Activation and expansion of tumour-infiltrating lymphocytes by anti-CD3 and anti-CD28 monoclonal antibodies. *Cancer Immunology, Immunotherapy* **32**, 245-250 (1990).

(244) Kane, L. P., and Weiss, A. The PI-3 kinase/Akt pathway and T cell activation: pleiotropic pathways downstream of PIP3. *Immunological Reviews* **192**, 7-20 (2003).

(245) Nel, A. E. T-cell activation through the antigen receptor. Part 1: signaling components, signaling pathways, and signal integration at the T-cell antigen receptor synapse. *Journal of Allergy and Clinical Immunology* **109**, 758-770 (2002).

(246) Hayden, M. S., and Ghosh, S. Shared principles in NF-κB signaling. *Cell* **132**, 344-362 (2008).

(247) Imran, M., and Lim, I. K. Regulation of Btg2/TIS21/PC3 expression via reactive oxygen species–protein kinase C–NFκB pathway under stress conditions. *Cellular Signalling* **25**, 2400-2412 (2013).

(248) Josephides, D., Davoli, S., Whitley, W., et al. Cyto-Mine: An Integrated, Picodroplet System for High-Throughput Single-Cell Analysis, Sorting, Dispensing, and Monoclonality Assurance. *SLAS Technology*, 2472630319892571 (2020).

(249) Roberts, J. P. Single-Cell Analysis Deepens Antibody Discovery: High-throughput single-cell techniques are revealing the genotype-phenotype relationships that enrich immune repertoires. *Genet. Eng. Biotechn. N.* **40**, 23-25 (2020).

(250) Jorgolli, M., Nevill, T., Winters, A., et al. Nanoscale integration of single cell biologics discovery processes using optofluidic manipulation and monitoring. *Biotechnology and Bioengineering* **116**, 2393-2411 (2019).

(251) Cross, R. (2018) Berkeley Lights raises $95 million for its automated cell therapy manufacturing machines. https://cen.acs.org/business/investment/Berkeley-Lights-raises-95-million/96/i42, accessed at 17.05.2020.

(252) Welihinda, A. A., and Kaufman, R. J. The Unfolded Protein Response Pathway in Saccharomyces cerevisiae oligomerization and trans-phosphorylation of Ire1P (Ern1p) are required for kinase activation. *Journal of Biological Chemistry* **271**, 18181-18187 (1996).

(253) Deweid, L., Neureiter, L., Englert, S., et al. Directed Evolution of a Bond-Forming Enzyme: Ultrahigh-Throughput Screening of Microbial Transglutaminase Using Yeast Surface Display. *Chemistry–A European Journal* **24**, 15195-15200 (2018).

(254) Arnold, J. N., Wormald, M. R., Sim, R. B., et al. The impact of glycosylation on the biological function and structure of human immunoglobulins. *Annual Review of Immunology* **25**, 21-50 (2007).

(255) Delorme, E., Lorenzini, T., Giffin, J., et al. Role of glycosylation on the secretion and biological activity of erythropoietin. *Biochemistry* **31**, 9871-9876 (1992).

(256) Lingg, N., Zhang, P., Song, Z., et al. The sweet tooth of biopharmaceuticals: importance of recombinant protein glycosylation analysis. *Biotechnology Journal* **7**, 1462-1472 (2012).

(257) Nasab, F. P., Aebi, M., Bernhard, G., et al. A combined system for engineering glycosylation efficiency and glycan structure in Saccharomyces cerevisiae. *Applied and Environental Microbiology* **79**, 997-1007 (2013).

(258) Cruz-Teran, C. A., Tiruthani, K., Mischler, A., et al. Inefficient ribosomal skipping enables simultaneous secretion and display of proteins in Saccharomyces cerevisiae. *ACS Synthetic Biology* **6**, 2096-2107 (2017).

(259) Yang, Z., Wan, Y., Tao, P., et al. A cell–cell interaction format for selection of high-affinity antibodies to membrane proteins. *Proceedings of the National Academy of Sciences* **116**, 14971-14978 (2019).

(260) Zheng, T., Xie, J., Yang, Z., et al. Antibody selection using clonal cocultivation of Escherichia coli and eukaryotic cells in miniecosystems. *Proceedings of the National Academy of Sciences* **115**, E6145-E6151 (2018).

(261) Schmitz, U., Versmold, A., Kaufmann, P., et al. Phage display: a molecular tool for the generation of antibodies—a review. *Placenta* **21**, S106-S112 (2000).

(262) Yaginuma, K., Aoki, W., Miura, N., et al. High-throughput identification of peptide agonists against GPCRs by co-culture of mammalian reporter cells and peptide-secreting yeast cells using droplet microfluidics. *Scientific Reports* **9**, 1-11 (2019).

(263) Soares, E. V. Flocculation in Saccharomyces cerevisiae: a review. *Journal of Applied Microbiology* **110**, 1-18 (2011).

(264) de Ruijter, J. C., Koskela, E. V., and Frey, A. D. Enhancing antibody folding and secretion by tailoring the Saccharomyces cerevisiae endoplasmic reticulum. *Microbial Cell Factories* **15**, 87 (2016).

(265) Ogunjimi, A. A., Chandler, J. M., Gooding, C. M., et al. High-level secretory expression of immunologically active intact antibody from the yeast Pichia pastoris. *Biotechnology Letters* **21**, 561-567 (1999).

(266) Palacios, R. Mechanisms by which accessory cells contribute in growth of resting T lymphocytes initiated by OKT3 antibody. *European Journal of Immunology* **15**, 645-651 (1985).

(267) Cole, M. S., Anasetti, C., and Tso, J. Y. Human IgG2 variants of chimeric anti-CD3 are nonmitogenic to T cells. *The Journal of Immunology* **159**, 3613-3621 (1997).

(268) Choi, I., De Ines, C., Kürschner, T., et al. Recombinant chimeric OKT3 scFv IgM antibodies mediate immune suppression while reducing T cell activation in vitro. *European Journal of Immunology* **31**, 94-106 (2001).

(269) Li, J., Davis, J., Bracht, M., et al. Modulation of antigen-specific T cell response by a non-mitogenic anti-CD3 antibody. *International Immunopharmacology* **6**, 880-891 (2006).

(270) Rodriguez-Melendez, Schwab, and Zempleni. Jurkat cells respond to biotin deficiency with increased nuclear translocation of NF-kB, mediating cell survival. *International Journal for Vitamin and Nutrition Research* **74**, 209-216 (2004).

8. Appendix

8.1. Supplementary Figures

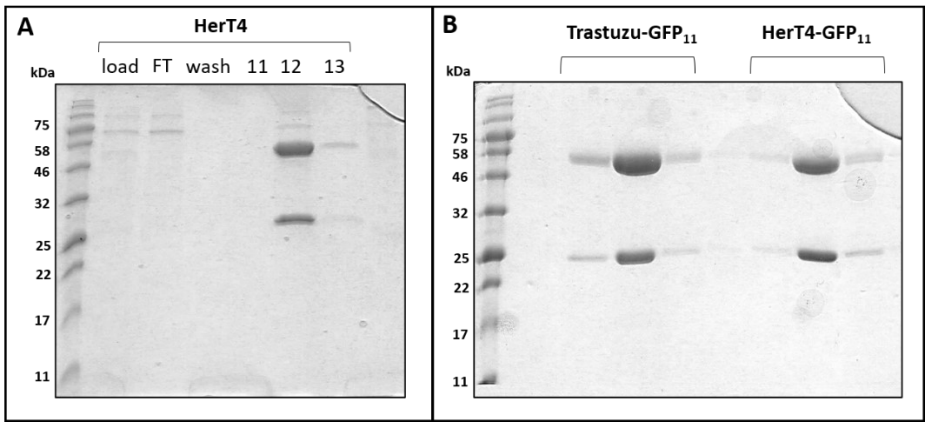

Figure S1. SDS-PAGE after antibody expression in Expi293F cells and purification by Protein A chromatography. (A) HerT4 cytotransmab was generated by substitution of the trastuzumab VL by the VL of an autoantibody hT4. **(B)** Production of antibody constructs carrying a triple GFP_{11} tandem tag for detection of cytoplasmic localization by GFP complementation.

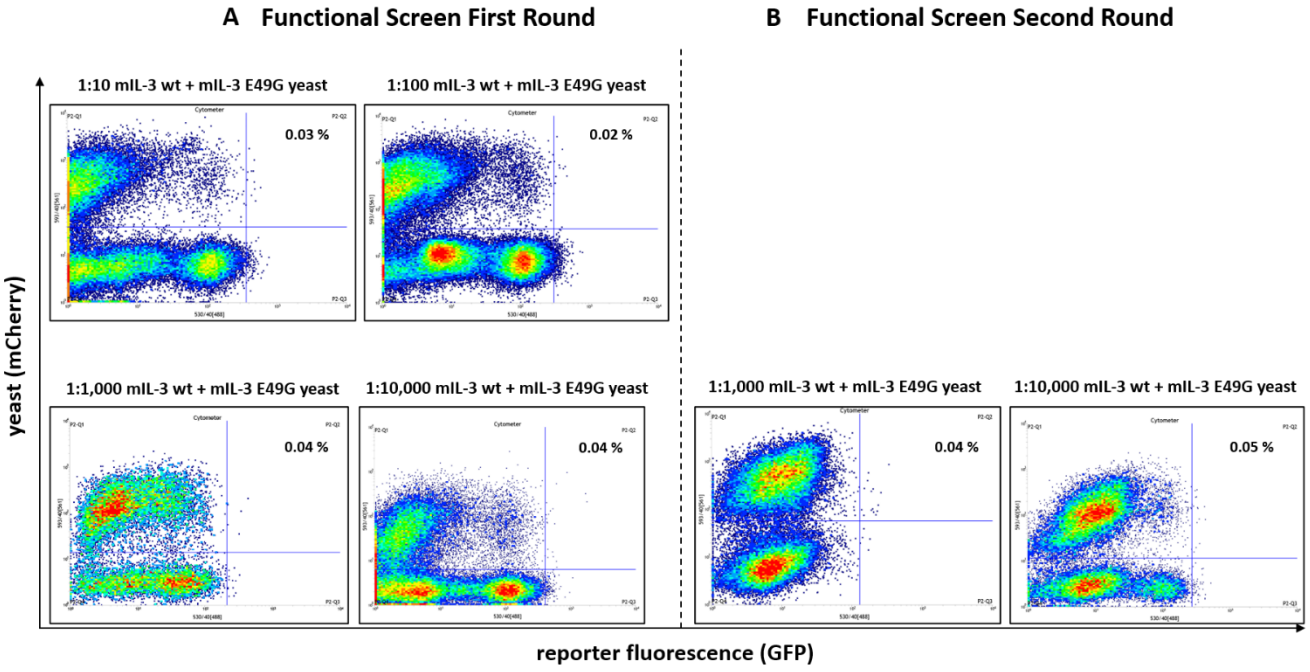

Figure S2. FACS plots of first and second selection rounds of the 1:10, 1:100, 1:1,000, and 1:10,000 mIL-3 wt + mIL-3 E49G yeast mixtures, co-encapsulated with mammalian reporter cells.

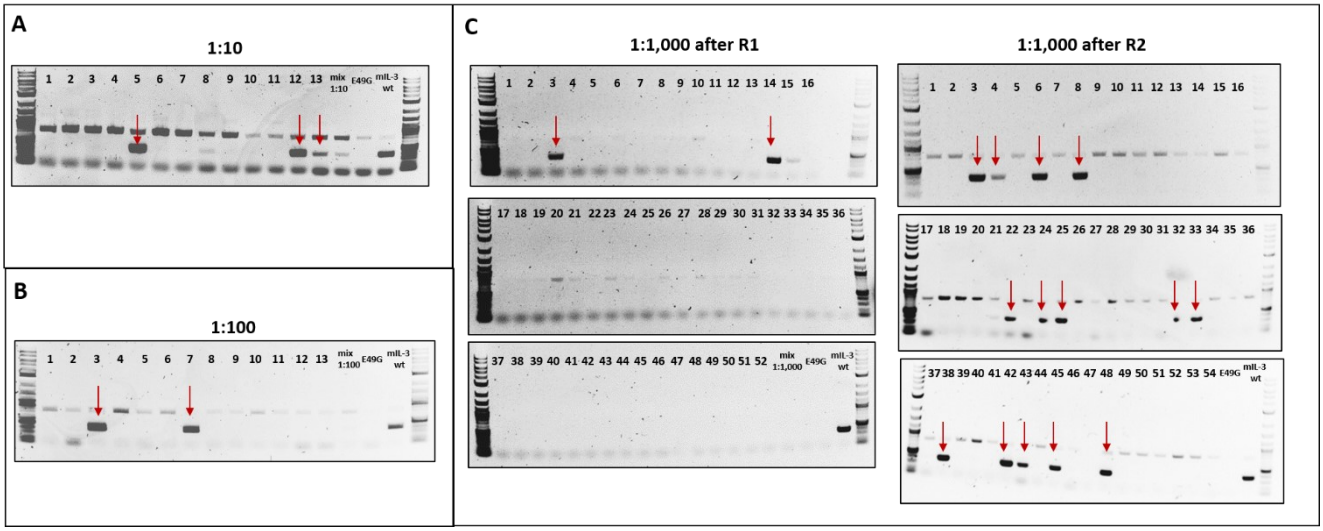

Figure S3. PCR screen of single clones after functional screening of 1:10, 1:100, and 1:1,000 mIL-3 wt + mIL-3 E49G mixtures. (A) and (B) Colony PCR with 13 random single clones after R1 of functional selection of 1:10 and 1:100 mixtures, respectively. **(C)** Colony PCR with 52 or 54 random single clones after the first (left side) and second (right side) functional selection round, respectively, with 1:1,000 mixed mIL-3 wt and mIL-3 E49G yeast cells. Colony PCR was performed using a primer specific for the wildtype mIL-3, resulting in specific band at approx. 400 bp. Positive single clones are marked with a red arrow.

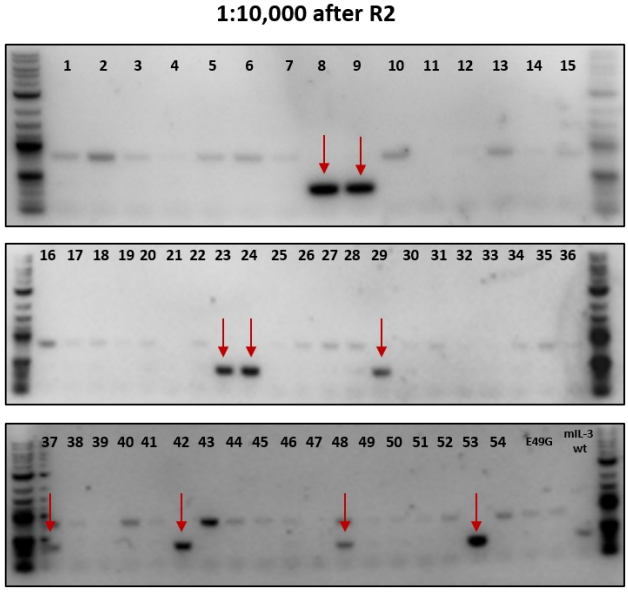

Figure S4. PCR screen of single clones after second round of functional screening of a 1:10,000 mIL-3 wt + mIL-3 E49G mixture. Colony PCR with a mIL-3 wt-specific primer was performed on 54 random single clones. PCR product corresponding to the wildtype mIL-3 sequence is marked with a red arrow.

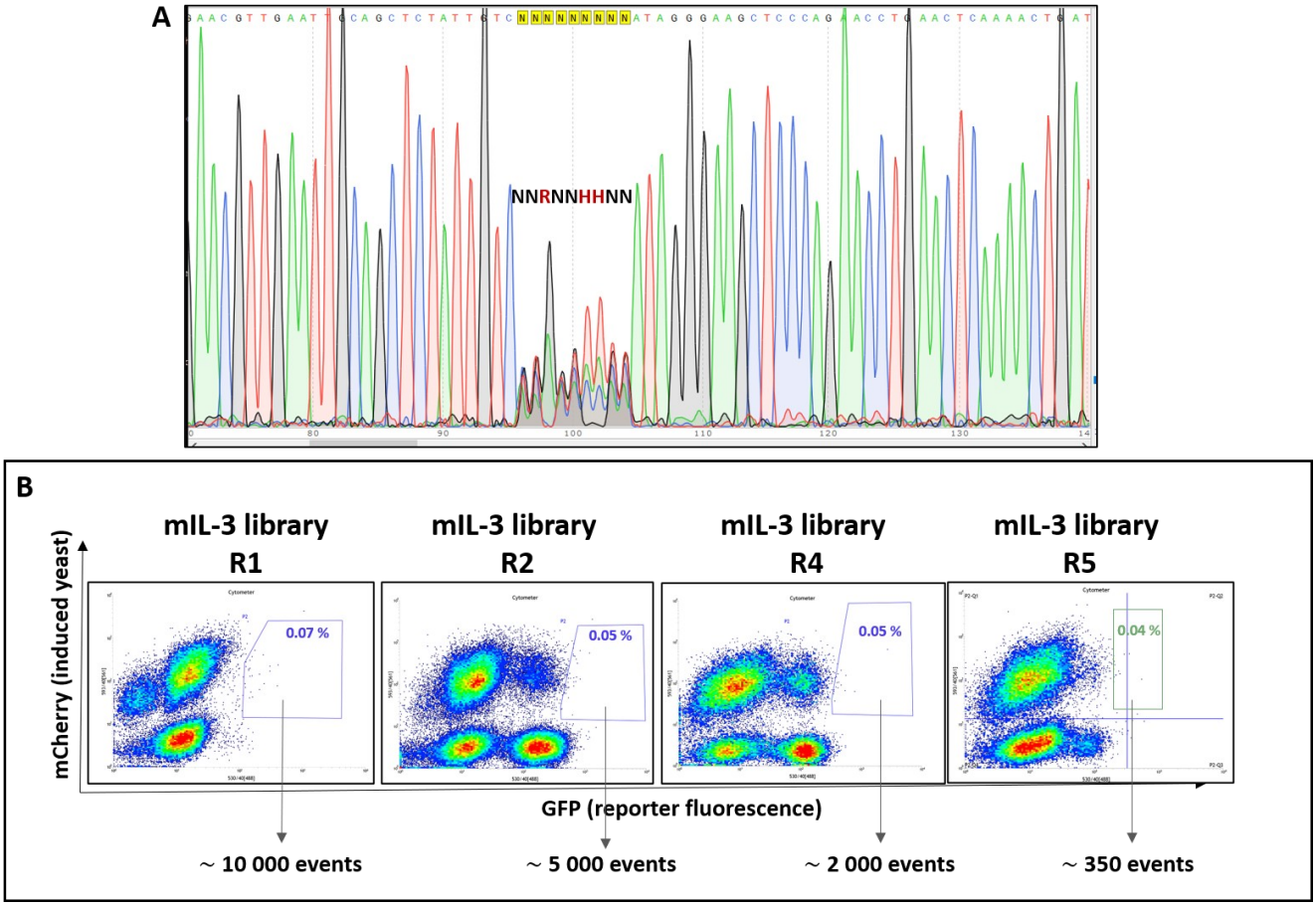

Figure S5. Generation and selection of randomized mIL-3 library. (A) Sequencing of the randomized region by Sanger sequencing. Plasmids from the yeast library populations were extracted and PCR was performed using primer outside the randomized region and PCR product was sent for sanger sequencing. **(B)** Functional selection of the mIL-3 library secreted by yeast cells using co-encapsulation of Ba/F3-CIS-d2EGFP reporter cells in agarose microbeads. Functional screening was performed in four consecutive selection rounds comprised of co-encapsulation, incubation, FACS sorting and yeast expansion.

8.2. Protein Sequences

Trastuzumab heavy chain:
EVQLVESGGGLVQPGGSLRLSCAASGFNIKDTYIHWVRQAPGKGLEWVARIYPTNGYTRYADSVKGRFTISADTSKNTAYLQM
NSLRAEDTAVYYCSRWGGDGFYAMDYWGQGTLVTVSSASTKGPSVFPLAPSSKSTSGGTAALGCLVKDYFPEPVTVSWNSGA
LTSGVHTFPAVLQSSGLYSLSSVVTVPSSSLGTQTYICNVNHKPSNTKVDKKVEPPKSCDKTHTCPPCPAPELLGGPSVFLFPPKP
KDTLMISRTPEVTCVVVDVSHEDPEVKFNWYVDGVEVHNAKTKPREEQYNSTYRVVSVLTVLHQDWLNGKEYKCKVSNKALP
APIEKTISKAKGQPREPQVYTLPPSRDELTKNQVSLTCLVKGFYPSDIAVEWESNGQPENNYKTTPPVLDSDGSFFLYSKLTVDKS
RWQQGNVFSCSVMHEALHNHYTQKSLSLSPGLLQG

Trastuzumab light chain:
DIQMTQSPSSLSASVGDRVTITCRASQDVNTAVAWYQQKPGKAPKLLIYSASFLYSGVPSRFSGSRSGTDFTLTISSLQPEDFATY
YCQQHYTTPPTFGQGTKVEIKRTVAAPSVFIFPPSDEQLKSGTASVVCLLNNFYPREAKVQWKVDNALQSGNSQESVTEQDSK
DSTYSLSSTLTLSKADYEKHKVYACEVTHQGLSSPVTKSFNRGEC

hT4 light chain:
DLVMTQSPSSLSASVGDRVTITCKSSQSLFNSRTRKNYLAWYQQKPGKAPKLLIYWASTRESGVPSRFSGSGSGTDFTLTISSLQP
EDFATYYCQQYYYHMYTFGQGTKVEIKRTVAAPSVFIFPPSDEQLKSGTASVVCLLNNFYPREAKVQWKVDNALQSGNSQESV
TEQDSKDSTYSLSSTLTLSKADYEKHKVYACEVTHQGLSSPVTKSFNRGEC

Trastuzumab heavy chain- 3×(GFP_{11}):
EVQLVESGGGLVQPGGSLRLSCAASGFNIKDTYIHWVRQAPGKGLEWVARIYPTNGYTRYADSVKGRFTISADTSKNTAYLQM
NSLRAEDTAVYYCSRWGGDGFYAMDYWGQGTLVTVSSASTKGPSVFPLAPSSKSTSGGTAALGCLVKDYFPEPVTVSWNSGA
LTSGVHTFPAVLQSSGLYSLSSVVTVPSSSLGTQTYICNVNHKPSNTKVDKKVEPPKSCDKTHTCPPCPAPELLGGPSVFLFPPKP
KDTLMISRTPEVTCVVVDVSHEDPEVKFNWYVDGVEVHNAKTKPREEQYNSTYRVVSVLTVLHQDWLNGKEYKCKVSNKALP
APIEKTISKAKGQPREPQVYTLPPSRDELTKNQVSLTCLVKGFYPSDIAVEWESNGQPENNYKTTPPVLDSDGSFFLYSKLTVDKS
RWQQGNVFSCSVMHEALHNHYTQKSLSLSPGGGGRDHMVLHEYVNAAGITGGGGSGGGGSGGGSSRDHMVLHEYVNAA
GITGGGGSGGGGSGGGSSRDHMVLHEYVNAAGITGGGGSGGKFM

Split turbo GFP_{1-10} fragment:
MVSKGEELFTGVVPILVELDGDVNGHKFSVRGEGEGDATIGKLTLKFICTTGKLPVPWPTLVTTLTYGVQCFSRYPDHMKQHDF
FKSAMPEGYVQERTISFKDDGKYKTRAVVKFEGDTLVNRIELKGTDFKEDGNILGHKLEYNFNSHNVYITADKQKNGIKANFTVR
HNVEDGSVQLADHYQQNTPIGDGPVLLPDNHYLSTQTVLSKDPVGLVRLINGSGIPPLSLPPP

Split turbo GFP_{11} fragment:
RDHMVLHEYVNAAGIT

app8 secretion signal:
MRFPSIFTAVLFAASSALAAPANTTTEDETAQIPAEAVIDYSDLEGDFDAAALPLSNSTNNGLSSTNTTIASIAAKEEGVQLDKR

T2A ribosomal skipping motif:
EGRGSLLTCGDVEENPGP

mCherry red fluorescent protein:
MCVSKGEEDNMAIIKEFMRFKVHMEGSVNGHEFEIEGEGEGRPYEGTQTAKLKVTKGGPLPFAWDILSPQFMYGSKAYVKHP
ADIPDYLKLSFPEGFKWERVMNFEDGGVVTVTQDSSLQDGEFIYKVKLRGTNFPSDGPVMQKKTMGWEASSERMYPEDGAL
KGEIKQRLKLKDGGHYDAEVKTTYKAKKPVQLPGAYNVNIKLDITSHNEDYTIVEQYERAEGRHSTGGMDELYK

mIL-3 wildtype:
DTHRLTRTLNCSSIVK**E**IIGKLPEPELKTDDEGPSLRNKSFRRVNLSKFVESQGEVDPEDRYVIKSNLQKLNCCLPTSANDSALPGV
FIRDLDDFRKKLRFYMVHLNDLETVLTSRPPQPASGSVSPNRGTVEC

mIL-3 E49G:
DTHRLTRTLNCSSIVK**G**IIGKLPEPELKTDDEGPSLRNKSFRRVNLSKFVESQGEVDPEDRYVIKSNLQKLNCCLPTSANDSALPGV
FIRDLDDFRKKLRFYMVHLNDLETVLTSRPPQPASGSVSPNRGTVEC

hTNFα:
VRSSSRTPSDKPVAHVVANPQAEGQLQWLNRRANALLANGVELRDNQLVVPSEGLYLIYSQVLFKGQGCPSTHVLLTHTISRIA
VSYQTKVNLLSAIKSPCQRETPEGAEAKPWYEPIYLGGVFQLEKGDRLSAEINRPDYLDFAESGQVYFGIIAL

OKT3 heavy chain (humanized, CDRs marked in bold):
QVQLVQSGGGVVQPGRSLRLSCKASGYTFT**RYTMH**WVRQAPGKGLEWIG**YINPSRGYTNYNQKVKD**RFTISRDNSKNTAFL
QMDSLRPEDTGVYFCAR**YYDDHYCLDY**WGQGTPVTVSSASTKGPSVFPLAPSSKSTSGGTAALGCLVKDYFPEPVTVSWNSG
ALTSGVHTFPAVLQSSGLYSLSSVVTVPSSSLGTQTYICNVNHKPSNTKVDKRVEPKSCDKTHTCPPCPAPELLGGPSVFLFPPKP
KDTLMISRTPEVTCVVVDVSHEDPEVKFNWYVDGVEVHNAKTKPREEQYQSTYRVVSVLTVLHQDWLNGKEYKCKVSNKALP
APIEKTISKAKGQPREPQVYTLPPSREEMTKNQVSLTCLVKGFYPSDIAVEWESNGQPENNYKTTPPVLDSDGSFFLYSKLTVDK
SRWQQGNVFSCSVMHEALHNHYTQKSLSLSPGK

OKT3 light chain (humanized, CDRs are marked in bold):
DIQMTQSPSSLSASVGDRVTITC**SASSSVSYMN**WYQQTPGKAPKRWIY**DTSKLAS**GVPSRFSGSGSGTDYTFTISSLQPEDIAT
YYC**QQWSSNPFT**FGQGTKLQITRTVAAPSVFIFPPSDEQLKSGTASVVCLLNNFYPREAKVQWKVDNALQSGNSQESVTEQDS
KDSTYSLSSTLTLSKADYEKHKVYACEVTHQGLSSPVTKSFNRGEC

8.3. List of Figures

8.4. List of Tables

8.5. Abbreviations

Abbreviation	*Meaning*
aa	amino acid
AP-1	activator protein 1
CD28	T cell surface receptor for CD80 and CD86 proteins
CD3	cluster of differentiation 3
CDR	complementarity determining region
CH1	antibody constant domain 1 of the heavy chain
CL	antibody constant domain of the light chain
EGFR, Her1	epidermal growth factor receptor
Fab	fragment variable
Fab	fragment antigen binding of an antibody
FACS	fluorescence activated cell sorter
FBS	fetal bovine serum
Fc	fragment cristallizable of an antibody
GMD-FACS	gel microdroplet fluorescence-activated cell sorting
GPCR	G-protein coupled receptor
HC	antibody heavy chain
Her2	human epidermal growth factor receptor 2
hIL-3	human interleukin-3
HSPG	heparan sulfate proteoglycan
IL-3	interleukin-3
LC	antibody light chain
mAb	monoclonal antibody
mIL-3	murine interleukin-3
NF-AT	nuclear factor of activated T cells
NF-κB	nuclear factor “kappa-light-chain-enhancer” of activated B-cells
PDMS	poly-di-methyl-siloxane
Pen/Strep	Penicillin – Streptomycin
rec. mIL-3	recombinant interleukin-3
scFv	single chain variable fragment
scFv	single chain variable fragment
sn	supernatant
TCR	T cell receptor
VH	antibody variable domain of the heavy chain
VL	antibody variable domain of the light chain
w/o	water-in-oil
w/o/w	water-in-oil-in-water

8.6. Danksagung

Zum Schluss dieser Arbeit möchte ich meinen aufrichtigen Dank den folgenden Personen aussprechen:

Herrn **Prof. Harald Kolmar** möchte ich für die Betreuung meiner Doktorarbeit herzlich danken. Danke für die ständige Unterstützung, die Flut an neuen, zum Teil verrückten Ideen und Dein Vertrauen in mich. Danke, dass Du trotz vielen, nicht erwarteten Hürden im Laufe dieses Projektes, ständig positiv geblieben bist und mich motiviert hast weiter daran zu arbeiten.

Prof. Siegfried Neumann gilt meine Dankbarkeit für die sofortige Übernahme der Rolle des Korreferenten bei meiner Disputation und für die nette und herzliche Antwort meiner Anfrage.

Prof. Katja Schmitz danke ich ebenfalls für die kurzfristige Übernahme der Vorsitzende der Prüfungskommission bei meiner Promotionsprüfung.

Dr. Tobias Meckel möchte ich für die unentbehrliche Hilfe am konfokalen Mikroskop im Laufe meiner gesamten Promotion danken, für sein Enthusiasmus das zu entdecken, wonach man sucht und die korrekte wissenschaftliche Interpretation von den Aufnahmen. Außerdem, danke für Deine freundliche Art und, dass Du die Position des zweiten Fachprüfers bei meiner Disputation übernommen hast.

Adrian Elter möchte ich ganz besonders für die bedingungslose Unterstützung als Partner, wie auch als Arbeitskollege danken. Ohne Deine Hilfe im Labor und am FACS, unsere stundenlangen Diskussionen und Deine Überzeugung, dass die Experimente irgendwann klappen werden, hätte ich es nie geschafft. Danke, dass Du mich in den schwierigsten Zeiten immer unterstützt und versorgt hast, meine Freude sowie Trauer im Alltag geteilt hast, immer für mich da warst und das gemeinsam mit mir durchgezogen hast!

Dr. Julius Grzeschik danke ich für die gemeinsame Publikation, den sarkastischen Humor und die unzähligen lustigen Stunden verbracht mit Bier in der Hand auf unserer heiligen Dachterrasse, die wir alle so sehr vermissen.

Dr. Hendrik Schneider, **Steffen Hinz**, **Simon Englert**, **Bastian Becker**, **Arturo Macarron**, **Ataurehman Ali, Jan Bogen, Dr. Lukas Deweid, Valentina Hilberg, Dominic Happel, Jan Habermann, Sebastian Bitsch** und allen aktuellen Mitgliedern des Arbeitskreises danke ich für die tollen gemeinsamen 4 Jahre, die gute Zusammenarbeit und die Hilfe und Unterstützung bei Allem. Wir sind alle durch schwierige Perioden gegangen und waren füreinander da. Ich danke Euch herzlich dafür und bin mir sicher, dass unsere Freundschaft für immer erhalten bleibt.

Sebastian Bitsch danke ich zusätzlich für die harte Klonierungs- und Etablierungsarbeit mit *P. pastoris*, welche (hoffentlich) die Fortsetzung des Projektes auf Antikörperebene ermöglichen wird.

Dr. Andreas Christmann und **Dr. Olga Avrutina** möchte ich für alle wichtigen Hinweise und Tipps im Labor danken. Andreas danke ich explizit auch für die Expertise bezüglich der FACS-Geräte und des Sortierungs-prozesses.

Des Weiteren möchte ich meine Dankbarkeit an **Dr. Stefan Becker**, **Dr. Simon Krah**, **Dr. Stefan Zielonka**, **Dr. Achim Dörner, Dr. Vanessa Siegmund** und allen anderen von Firma Merck in Darmstadt aussprechen, die an unserer tollen Kooperation teilgenommen haben. Ohne Eure Unterstützung wäre dieses Projekt nie so weit gekommen und ich freue mich sehr in der Zukunft noch näher mit Euch zusammenarbeiten zu dürfen!

Janna Sturm und **Carolin Dombrowsky** möchte ich für die fleißige und extrem selbständige Arbeit während ihrer Marsterarbeiten an einem sehr anspruchsvollen Projekt danken. Ihr habt es toll gemacht und ich bin glücklich, dass ich Euch betreuen durfte. Carolin, ich bin zuversichtlich, dass wir mithilfe Deiner konsistenten und extrem gut geplanten Arbeitsweise, das Projekt ziemlich weit bringen werden!

Allen Kollegen von Ferring Pharmaceuticals in Darmstadt (**Dr. David Fiebig**, **Dr. Benjamin Mattes**, **Jan Bogen**, **Stefania Carrara** und **Michael Ulitzka**) möchte ich für die schöne Zusammenarbeit und die lustige Zeit in Kleinwalsertal danken. David, Dir bin ich für immer schuldig, dass Du mich aus dem tiefen Schnee beim Skifahren ausgegraben hast!

Dr. Doreen Köning, **Janine Becker**, **Dr. Bernhard Valldorf**, **Dr. Stefan Dickgiesser, Dr. Christina Uth** und allen anderen ehemaligen Mitarbeiter und Alumni aus dem AK Kolmar danke ich für die Erfahrung und die riesige Hilfe im Labor während meiner Masterarbeit und am Anfang meiner Promotion. Ich freue mich jedes Jahr auf unsere schöne Weihnachtsfeier, wo wir uns mal wieder alle treffen.

Barbara Diestelmann danke ich für ihre ständige Hilfsbereitschaft und Freundlichkeit beim Erledigen jeglichen Bürokratie-Kramms und für die vielen netten Gespräche.

Dana Schmidt möchte ich für ihre Einsatzbereitschaft bei dringenden Bestellungen und anderen organisatorischen Angelegenheiten danken.

Selbstverständlich gilt ein riesiger Dank meiner Mutter, die mein gesamtes Studium ermöglicht und unterstützt hat. Danke für den Rückhalt, den Zuspruch und die mütterliche Liebe, die mir während der Promotion immer wieder Kraft und Motivation gegeben haben! Meiner Oma, meinem Onkel und allen anderen Familienmitgliedern möchte ich ebenfalls meiner Dankbarkeit aussprechen für die Unterstützung und das ständige Interesse an meiner Arbeit, obwohl sie für Euch immer noch unverständlich und kompliziert klingt.

Am Ende möchte ich einen großen Dank aller meiner Freunde, die sich in Deutschland, in Bulgarien oder egal wo auf der Welt gerade befinden, aussprechen. Ihr habt mein Leben während dieser recht anstrengenden 4 Jahren so viel besser gemacht! Danke für Eure Liebe und Hilfe und für die sehr schöne zusammenverbrachte Zeit, ihr könnt jetzt endlich Stolz auf mich sein :D

8.7. Curriculum vitae

PERSÖNLICHE DATEN

Name:	Desislava Yanakieva
Geburtsdatum:	25.08.1992
Geburtsort:	Varna, Bulgarien
Staatsangehörigkeit:	bulgarisch
Familienstand:	ledig

AUSBILDUNG UND WISSENSCHAFTLICHER WERDEGANG

10/2016 – present day	**TU Darmstadt – Promotion zum Dr. rer. nat.** Promotion am Clemens-Schöpf-Institut für Organische Chemie und Biochemie unter Prof. Dr. Harald Kolmar: *Establishment of an Ultra-High-Throughput Single-Cell Functional Screening by Combination of Microfluidics and GMD-FACS*
03/2017 – 04/2018	**TU Darmstadt – Merck Lab @ Technische Universität Darmstadt** Wissenschaftliche Mitarbeiterin Schwerpunkt: *Low-instrumental diagnostics and analytics*
10/2014 – 10/2016	**TU Darmstadt – Master of Science** Studiengang: Biomolecular Engineering Masterarbeit am Clemens-Schöpf-Institut für Organische Chemie und Biochemie unter Prof. Dr. Harald Kolmar: *Antibody-Mediated Cytoplasmic Payload Delivery*
10/2011 – 10/2014	**TU Darmstadt – Bachelor of Science** Studiengang: Biomolecular Engineering Bachelorarbeit am Paul-Ehrlich-Institut in Langen unter Prof. Dr. Eberhard Hildt: *Role of the Hepatitis B Virus-dependent Activation of the Nrf2 Transcription Factor for the Autophagy*
09/2003 – 06/2011	**Abitur am Gymnasium für Mathematik und Naturwissenschaften in Burgas, Bulgarien**

8.8. Affirmations

Desislava Yanakieva

Am Alten Friedhof 2

64287 Darmstadt

Darmstadt, 09.06.2020

Erklärung

Ich erkläre hiermit, dass ich meine Dissertation selbstständig und nur mit den angegebenen Hilfsmitteln angefertigt und noch keinen Promotionsversuch unternommen habe.

Desislava Yanakieva

Desislava Yanakieva

Am Alten Friedhof 2

64287 Darmstadt

Darmstadt, 09.06.2020

Erklärung

Ich erkläre hiermit, dass die elektronische Version der Doktorarbeit mit der schriftlichen Version übereinstimmt. Die elektronische Version liegt dem Prüfungssekretariat vor.

Desislava Yanakieva